PROCESSES CONTROLLING RADON-222 AND RADIUM-226 ON THE SOUTHEASTERN BERING SEA SHELF

RECOMMENDED:

D B Hawk

Richard J Stoffberg

David G. Shaw

George W Happhut

John J Goering

W. S. Reeburgh
Chairman, Advisory Committee

Director, Institute of Marine Science

Robert T Cooney
Head, Department of Marine Sciences and Limnology

APPROVED:

Dean, College of Natural Sciences

D B Hawk
Director of Graduate Programs

9/26/85
Date

PROCESSES CONTROLLING RADON-222 AND RADIUM-226 ON THE SOUTHEASTERN BERING SEA SHELF

A

THESIS

Presented to the Faculty of the University of Alaska

in Partial Fulfillment of the Requirements

for the Degree of

DOCTOR OF PHILOSOPHY

By

David M. Glover, B.S., M.S.

Fairbanks, Alaska

December 1985

ABSTRACT

An investigation was made into the use of radon-222 and radium-226 as tracers of air-sea gas exchange, water column mixing and sediment-water exchange on the southeastern Bering Sea shelf. Furthermore, a two-dimensional model was developed to unify these three processes into a coherent picture of radon-222 flux out of the sediments, through the water column and into the atmosphere. The best time period to average wind speeds when regressing them against gas transfer coefficients was found to be 3.3 days by a linear regression optimization, approximately the synoptic time scale of storms in the southeastern Bering Sea. A statistically significant relationship between averaged wind speed and transfer coefficients was found at the 80% confidence level. Gas transfer coefficients were found to be obscured in shallow waters by radon flux from the sediments. Two-dimensional mixing in these continental shelf waters rendered the traditional one-dimensional vertical mixing model of excess radon-222 unable to obtain reliable vertical eddy diffusivities. Exchange across the sediment-water interface was calculated from the deficiency of radon-222 measured in sediment cores, the standing crop of excess radon-222 in the overlying water column and the radon-222 production rate of sediment surface grab samples. The flux of radon-222 out of the sediments was found to increase in the onshore direction. Biological irrigation appears to be the primary exchange mechanism between the sediment and water columns on this shelf. Distributions in the water column show finestructure reported previously as well as

biological removal of radium-226. A chi-square hypersurface search found the optimal horizontal and vertical eddy diffusivities that explained the two-dimensional distribution of radon-222 provided from a kriging estimation exercise on the data measured in this study. This model was essentially a hybrid of a least squares surface fit and a numerical integration of the governing differential equation of radon-222. When considered as a two-dimensional system in the cross-shelf direction, the rates of gas exchange, water column mixing and sediment-water exchange agree with each other to an acceptable degree.

TABLE OF CONTENTS

	Page
ABSTRACT	3
TABLE OF CONTENTS	5
LIST OF FIGURES	8
LIST OF TABLES	14
ACKNOWLEDGMENTS	15
Chapter 1. INTRODUCTION	17
Scope and Purpose	17
Geochemistry of Radon-222 and Radium-226	19
Previous Work	22
Methods	25
Preliminary Results	26
Study Area	26
Chapter 2. DATA COLLECTION	35
Sampling Strategy	35
Radon-222 Analysis	36
Radium-226 Analysis	38
Sediment Radon and Radium Analysis	38
Alpha Scintillation Counting	39
Data Reduction and Error Analysis	39
Chapter 3. AIR-SEA GAS EXCHANGE	41
Introduction	41
Mathematical Methods	41
Results	43

Discussion 43

Chapter 4. SEDIMENT RADON FLUX 56

Introduction 56

Mathematical Methods 56

Results 59

Discussion 66

Grab samples 66

Standing crop 67

Core measurements 68

Chapter 5. ONE-DIMENSIONAL WATER MASS MIXING MODEL 73

Introduction 73

Mathematical Methods 73

Results 75

Discussion 77

Chapter 6. TWO-DIMENSIONAL WATER MASS MIXING MODEL 80

Introduction 80

Mathematical Methods 82

Measured-data 82

Kriged-data 84

Functional approximation of ^{222}Rn distribution 94

χ^2 hypersurface search for optimal K_H and K_v 96

Results 100

Discussion 106

Kriged-data 106

χ^2 hypersurface search for optimal K_H and K_v 113

Chapter 7. CONCLUSIONS 122

Appendix 1. MEASURED-DATA LISTING 125

Appendix 2. KRIGED-DATA MATRICES 135

2a. Total ^{222}Rn 136

2b. ^{226}Ra 138

2c. Sigma-t 140

2d. Temperature 142

2e. Kriging error estimate 144

REFERENCES CITED 146

LIST OF FIGURES

Page

Figure 1-1. Ideal ocean radon profile. Over most of the water column ^{222}Rn is in radioactive equilibrium with its parent ^{226}Ra. Near the surface the deficiency in ^{222}Rn is caused by evasion to the atmosphere. Near the bottom an excess of ^{222}Rn is caused by input from the sediments. A portion of the ^{238}U decay series and the important properties of the members is also shown. 20

Figure 1-2. Logarithm of bottom slope versus distance offshore. The breaks in shelf slope appear as peaks and are labeled with the corresponding hydrographic front. Critical slopes based on the eddy diffusivities of Coachman (1985) and this study are shown. 27

Figure 1-3. Idealized cross shelf hydrography (from Coachman, 1982). 29

Figure 1-4. Representative ^{222}Rn and ^{226}Ra depth distributions from each of the hydrographic domains in the PROBES area. Outer shelf: stations TT159-3115 and TT159-3119, 135 m. Middle shelf: station HX028-0041, 73 m. Inner shelf: station TT159-4021, 40 m. 31

Figure 1-5. Time scaling argument diagram. x_* and t_x^* are

characteristic horizontal mixing length and time; z_* and t_z^* are characteristic vertical mixing length and time. See text for explanation. 33

Figure 2-1a. Water column station locations from cruises in 1980 (O), 1981 (+) and 1982 (X). Several station locations overlay each other. 37

Figure 2-1b. Sediment sampling sites. Benthos corer samples are shown by (O), 1979 grab samples by (+) and 1981 grab samples by (X). 37

Figure 3-1. Transfer coefficients versus distance offshore calculated from profiles measured in 1980, 1981 and 1982. 45

Figure 3-2. Wind speed and transfer coefficients versus day of year, 1981 in the PROBES area. Wind speeds were averaged 96 hours prior to sampling. Wind speed is the solid line; transfer coefficients are the inverted triangles. 48

Figure 3-3. Optimum linear regression of averaged wind speed versus transfer coefficient. a) Winds were averaged 3.3 days prior to sampling; this was the optimal averaging period, the line shown is statistically significant at the 80% confidence level ($r = 0.50$, $n = 9$). b) Correlation coefficient spectra for averaging periods of 2 hours to 20 days. 49

Figure 4-1. Radon-222 production rate versus distance offshore. Radon-222 production rate was determined from ^{226}Ra secular equilibrium activities of grab samples collected in 1979 and 1981. 60

Figure 4-2. Molecular flux of ^{222}Rn from sediment versus distance offshore. Flux was estimated from the grab sample production rates and porosities. The unfrozen 1981 samples may have unreliable porosity estimates due to desiccation. 62

Figure 4-3. Excess ^{222}Rn standing crop versus distance offshore. The line shown is statistically significant at the 95% confidence level (r = 0.70, n = 20). 63

Figure 4-4. Radon-222 and ^{226}Ra depth distributions in sediment cores. The actual flux exceeds the molecular flux (atoms cm^{-2} sec^{-1}). a) Station HX028-0120, 110 m. b) Station HX048-0014, 129 m. Δ ^{222}Rn, 0 ^{226}Ra. 65

Figure 4-5. ln(^{210}Pb activities) versus cumulative mass. Samples for ^{210}Pb analysis were taken from the same cores in Figure 4-4. PRB-8.5 was station HX028-0120 and PRB-6 was station HX048-0014. Note the lack of an homogeneous ^{210}Pb layer near the surface of the sediments. 69

Figure 6-1. Comparison of measured-data and kriged-data profiles. The measured-data profiles were 392.1/462.8, 253.5 and 99.5 km offshore for the outer, middle and inner shelf domains; the kriged-data profiles were 396.05/441.75, 258.95 and 121.85 km offshore respectively. The middle shelf measured-data profile was measured in 1982 and therefore compares poorly with the kriged-data profile, which was based solely on 1981 data. 83

Figure 6-2. Total ^{222}Rn contour plot across the southeastern Bering Sea shelf. Prepared from kriged-data matrix (see Appendix 2); the actual measured-data points are shown as (+). 85

Figure 6-3. Excess ^{222}Rn contour plot across the southeastern Bering Sea shelf. Prepared from kriged-data matrix (see Appendix 2); the actual measured-data points are shown as (+). 86

Figure 6-4. Radium-226 contour plot across the southeastern Bering Sea shelf. Prepared from kriged-data matrix (see Appendix 2); the actual measured-data points are shown as (+). 87

Figure 6-5. Sigma-t contour plot across the southeastern Bering Sea shelf. Prepared from kriged-data matrix (see Appendix 2); the actual measured-data

points are shown as (+). 88

Figure 6-6. Temperature contour plot across the southeastern Bering Sea shelf. Prepared from kriged-data matrix (see Appendix 2); the actual measured-data points are shown as (+). 89

Figure 6-7. Two water column ^{222}Rn and ^{224}Ra profiles measured at non-tidal sampling intervals. The similarity between these two profiles is taken as further evidence that the southeastern Bering Sea shelf was in quasi-steady state during the summer of 1981. 91

Figure 6-8. Semivariogram of total ^{222}Rn versus distance offshore and depth. 101

Figure 6-9. Semivariogram of ^{224}Ra versus distance offshore and depth. 102

Figure 6-10. Semivariogram of sigma-t versus distance offshore and depth. 103

Figure 6-11. Comparison of profile and two-dimensional model estimates of transfer coefficients versus distance offshore. 107

Figure 6-12. Comparison of various estimates of sediment ^{222}Rn flux with two-dimensional model estimates versus distance offshore. 108

Figure 6-13. Kriging error contour plot across the southeastern Bering Sea shelf. Prepared from

kriged-data matrix (see Appendix 2); the actual measured-data points are shown as (+). 110

Figure 6-14. Radium-226 activity versus soluble silica concentrations in the PROBES area, 1981. A correlation coefficient of 0.66 obtained from 153 data points is statistically significant at the 95% confidence level. 114

LIST OF TABLES

		page
Table 3-1.	Gas transfer coefficients.	44
Table 3-2.	Comparison of linear regressed wind velocities verses transfer coefficients.	51
Table 3-3.	Comparison of methods of estimating CO_2 gas exchange.	55
Table 4-1.	Sediment ^{222}Rn production rate and molecular diffusive flux.	61
Table 4-2.	Standing crop of excess ^{222}Rn and implied sediment flux.	64
Table 5-1.	Near bottom vertical eddy diffusivities from one-dimensional model.	76
Table 6-1.	Two-dimensional model summary.	105
Table 6-2.	Transfer coefficients suggested by two-dimensional model.	109
Table 6-3.	Sediment flux suggested by two-dimensional model.	109

ACKNOWLEDGMENTS

There is an old cliché that is none the worse for the wear: I couldn't have done this alone. It is particularly true in my case and I think this is an appropriate place to thank all those people who have helped me to attain my doctoral degree.

First, I thank my major advisor William S. Reeburgh for all his wise guidance through my tenure as a Ph.D. candidate. By working with him and listening to him I learned a lot about being a good scientist and being a successful scientist. Best of all, I learned from Bill how to combine the two.

When I started graduate school, I thought that I was a reformed hacker. Daniel B. Hawkins changed all of that within the first week and for better or worse my enthusiasm towards the application of computer tools to the environment stems from his. My appreciation for the subtleties of statistics are due to the many in-depth conversations I have had with Dan.

I owe many thanks to the other members of my advisory committee. Richard J. Stolzberg polished my laboratory abilities as well as my analytical thinking. George W. Kipphut has kept me honest by carefully thinking about all the ideas I have put forth over the years. David G. Shaw and John J. Goering have been very supportive during the critical turning points of my graduate career.

Daniel W. Swift, Zygmunt Kowalik and Sister Juliana Lucey introduced me to and trained me in the application of finite numerical approximations to differential equations. Joan P. Gosink and my good

friend C. J. Beegle helped me toward a better understanding of hydrodynamics. Thomas C. Royer not only stood in for Bill Reeburgh while he was away on sabbatical but also infused me with a desire to explain the environment in terms of underlying physical principles.

I have spent many hours discussing problems in mathematics and science with David L. Musgrave, Marc J. Alperin, Susan F. Sugai, Susan Banahan, Jeffery Cornwell, Allen P. Doyle, Warren Lee and John Luick. Our conversations increased my appreciation of many of the problems within the environmental sciences. I also thank my colleagues in the PROBES project for all their help on deck during the sampling program.

To Dorothy A. and Benjamin H. Glover I extend my heartfelt thanks and appreciation for all their encouragement and support throughout my life.

Last, but not least in my heart, I thank Tina D. Balog for all her support, understanding and patience through some very rough times. It wasn't easy, but it would have been impossible without you; thank you very much Tina.

This work was supported by the National Science Foundation under Grant #DDP-76-23340, Division of Polar Programs. I also acknowledge the support of a fellowship from the Jesse Smith Noyes Foundation and thank them for the flexibility exhibited in the manner of its allocation.

Chapter 1: **INTRODUCTION**

This tale grew in the telling
J.R.R. Tolkien

Scope and Purpose

The main objective of this dissertation is to show how a two-dimensional model of ^{222}Rn distributions on the southeastern Bering Sea shelf unifies three transport processes into a coherent representation of ^{222}Rn transport on a continental shelf. This objective is accomplished by examining each process in terms of a traditional model, pointing out the limitations of these interpretations and drawing inferences about ^{222}Rn and ^{226}Ra on the southeastern Bering Sea shelf. In Chapter 3, I present my efforts to obtain unbiased gas transfer coefficients. It is shown how sediment ^{222}Rn flux can obscure the transfer rates in shallow near surface waters. Chapter 4 presents three methods to estimate sediment-water ^{222}Rn exchange rates. Upper and lower limits of sedimentary ^{222}Rn flux across the shelf will be derived. Chapter 5 primarily demonstrates the inadequacy of the one-dimensional, vertical eddy mixing model in this environment. The results of application of this model to excess ^{222}Rn profiles on the shelf suggest that assumptions of the one-dimensional model are being violated. In Chapter 6, I present a two-dimensional model that explains ^{222}Rn profiles as a function of horizontal as well as vertical net transport of ^{222}Rn in the water column. A component of this model then finds the optimal combination of horizontal and vertical eddy diffusivities that fit with the two-dimensional distribution of ^{222}Rn. Based on these eddy diffusivities, another part

of this model compares estimated transfer rates at the air-sea and sediment-water interfaces with unbiased estimates from regions of the shelf where the one-dimensional assumptions were not violated. Chapter 7 is a brief conclusion and summary of the interpretations of the features manifested in this study.

Radon-222 and its parent ^{226}Ra have been used to study physical processes in various environments, however, their application to a continental shelf has been relatively unsuccessful. As part of the PROBES (Processes and Resources of the Bering Sea shelf) project I measured ^{222}Rn and ^{226}Ra in the water column and sediments of the southeastern Bering Sea. The PROBES project was a focused study of the physical and biological interactions of the southeastern Bering Sea and the extensive sampling program on the shelf allowed the application of ^{222}Rn techniques. There were two major outcomes of this study: calculation of three rates of physical transport of ^{222}Rn and the construction of a two-dimensional model of ^{222}Rn distribution on the shelf. The three rate calculations were: 1) air-sea gas transfer, 2) water column mixing and 3) sediment-water column exchange. These three rates, in conjunction with the model, answered the following question, "Do these three rates of transport balance for ^{222}Rn on the southeastern Bering Sea shelf?".

Essentially, this dissertation has been an investigation into the application of ^{222}Rn and ^{226}Ra as tracers of physical processes on a continental shelf. The transfer rates of ^{222}Rn at either the air-sea or sediment-water interfaces or within the water column had the

following applications to the southeastern Bering Sea shelf. The air-sea gas transfer rate helped to constrain CO_2 budget calculations, it was used to investigate the relationship between wind speed and gas transfer rate and it was a useful boundary condition constraint on the model as the ultimate sink of ^{222}Rn on the shelf. The water column mixing rates were determined using the model developed within this dissertation. This mixing affects the rate regenerated nutrients are supplied from waters below the photic zone and they were an independent check of the horizontal and vertical eddy diffusivities obtained by the physical oceanography component of PROBES. The sediment-water column exchange rates affect the supply rate of regenerated nutrients to the water column beneath the photic zone; they were also used as boundary condition constraints for the supply of ^{222}Rn to the shelf waters.

Geochemistry of Radon-222 and Radium-226

Radon-222 is the inert gas, short-lived (half life = 3.83 d), radioactive daughter of ^{226}Ra (half life = 1620 yr), a partially soluble product from the decay of insoluble ^{230}Th (half life = 7.5×10^4 yr). These differences in chemical and radioactive properties and concentrations detectable at natural levels make ^{222}Rn and ^{226}Ra an attractive tracer pair for evaluating sediment chemical flux, near bottom mixing intensity and air-sea gas exchange rate. The ^{238}U (half life = 4.5×10^9 yr) decay series in Figure 1-1 shows the tendency of ^{226}Ra to be incorporated largely in the sediments (Broecker, 1974). About 10% of the ^{226}Ra in the sediment diffuses into the water column

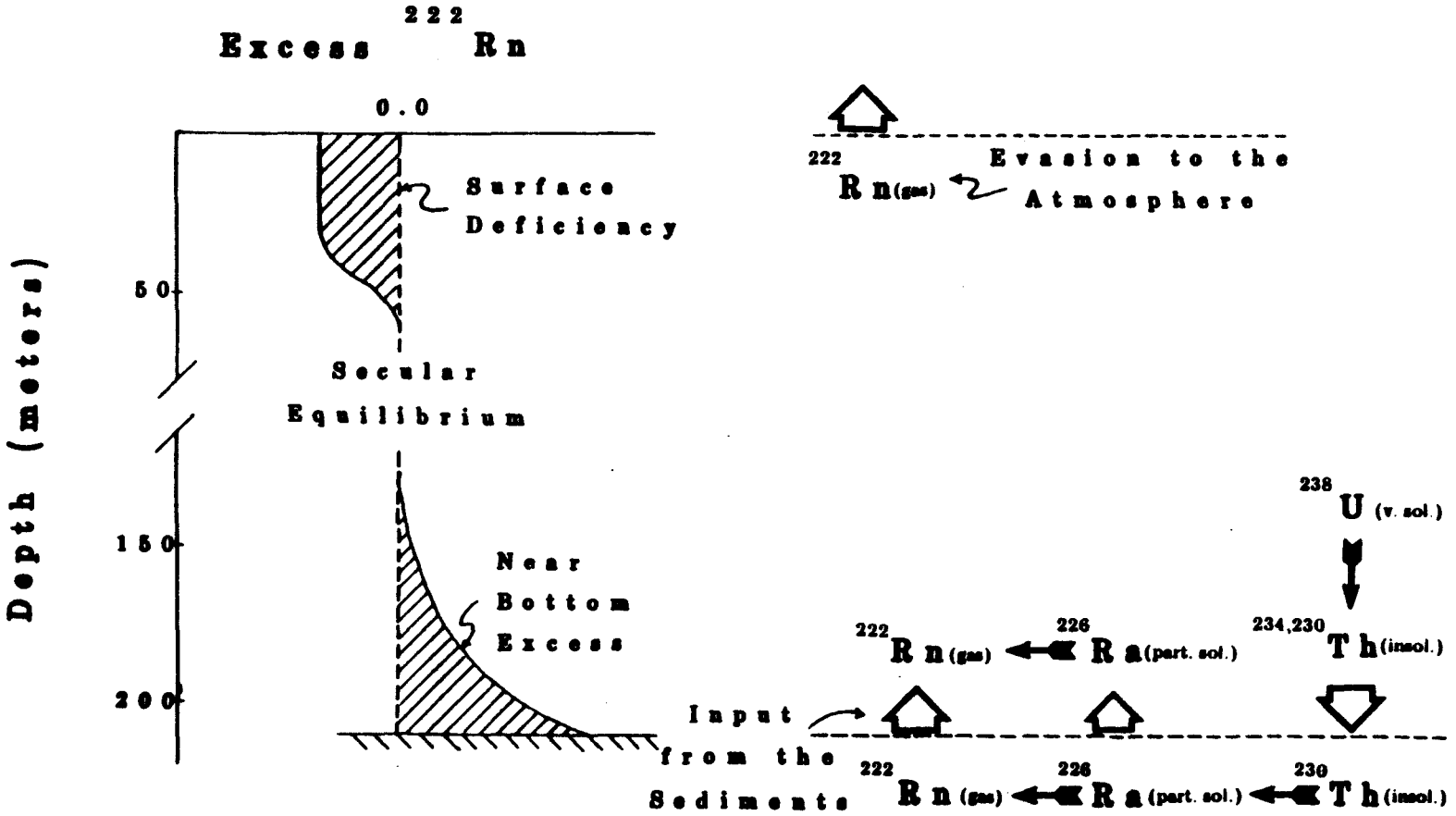

Figure 1-1. Ideal ocean radon profile. Over most of the water column ^{222}Rn is in radioactive equilibrium with its parent ^{226}Ra. Near the surface the deficiency in ^{222}Rn is caused by evasion to the atmosphere. Near the bottom an excess of ^{222}Rn is caused by input from the sediments. A portion of the ^{238}U decay series and the important properties of the members is also shown.

(Key et al., 1979a), giving rise to a supported level of ^{222}Rn. The ^{226}Ra remaining in the sediment decays to ^{222}Rn, which then engages in a unidirectional flux toward the atmosphere. Radium-226 radioactivities were subtracted from ^{222}Rn radioactivities to obtain ^{222}Rn excesses or deficits.

Radon-222 is in secular equilibrium with ^{226}Ra away from either the sediments or the atmosphere. Disequilibria between ^{222}Rn and ^{226}Ra at the sediment-seawater or air-sea interfaces lead to distributions similar to those shown in Fig. 1-1. Near the air-sea interface there is a deficiency of ^{222}Rn with respect to ^{226}Ra due to the escape of ^{222}Rn into the atmosphere. The rate of gas exchange (transfer coefficient) can be related to the integrated deficiency of ^{222}Rn in the near surface waters (Peng et al., 1979). Several different models have been offered to explain the mechanism of gas exchange (see Danckwerts, 1970), but the amount of ^{222}Rn missing in the upper water column gives the flux of ^{222}Rn directly. Near the sediment-seawater interface excess ^{222}Rn is present due to ^{222}Rn escaping from the interstitial waters of the sediment. The distribution of this excess ^{222}Rn above the bottom, in some environments, can be used to calculate vertical eddy diffusivities by fitting a one-dimensional exponential model to the distribution (Broecker, 1965). The flux of ^{222}Rn from the interstitial waters of the sediments causes a ^{222}Rn deficiency in the near surface sediments due to the unidirectional flux of ^{222}Rn. The sediment ^{222}Rn flux can be calculated from the sediment ^{222}Rn deficiency by equating the former to the latter (Smethie et al.,

1981).

Previous Work

Broecker (1965) outlined and gave examples of the use of ^{222}Rn as a tracer for three important physical processes in bodies of natural water. At the air-sea interface he demonstrated that the integrated ^{222}Rn deficiency could be used to calculate the transfer coefficient (or piston velocity) of gas exchange. The excess ^{222}Rn present in the near-bottom waters off the Bahama Banks was used to demonstrate the use and limitations of a one-dimensional, vertical, eddy diffusive flux model. Additionally, using the distribution of ^{222}Rn in the upper sediment column Broecker (1965) outlined the basic way in which sediment-seawater exchange rates are estimated. Although many of his techniques have been improved upon (Smethie et al., 1981, Greubel and Martens, 1984 and Hartman and Hammond, 1984) and the simple nature of his assumptions have disqualified their application in many environments, Broecker (1965) remains a landmark paper in the exploitation of ^{222}Rn as a tracer of gas exchange, vertical water column mixing and sediment chemical exchange.

Radon-222 has been used in gas exchange studies and film thickness values for a wide range of locations are reported (Emerson, 1975; Broecker and Peng, 1971; 1974 and Peng et al., 1974). These film thicknesses are summarized in Broecker and Peng (1982) and range from 10 microns to 120 microns in the oceans. The gas transfer coefficient can be related to the thickness of a hypothetical stagnant boundary film (Danckwerts, 1970). Elsinger and Moore (1983) report transfer

coefficients ranging from 2.1 to 4.1 m d^{-1} for a freshwater river while Emerson (1975) reports an average value of 0.2 m d^{-1} at ELA (Experimental Lakes Area). Transfer coefficients are less variable in seawater with an average transfer coefficient of 3.6 m d^{-1} at ocean station Papa (50° N, 145° W) (Peng et al., 1974) and 2.9 m d^{-1} for the Geosecs expedition (Peng et al., 1979) .

Although a relationship between wind speed and gas exchange rates has been found in laboratory experiments and theoretical considerations (Deacon, 1977; Liss, 1973; Broecker et al., 1978 and Kanwisher, 1963), a relationship is not always found in the field (Peng et al., 1979; Broecker and Peng, 1982; Hasse and Liss, 1980 and Liss, 1983). Empirical relationships are sometimes found (Hartman and Hammond, 1984; Wanninkhof et al., 1985 and Smethie et al., 1985) for a specific study area. The value of establishing an accurate relationship between wind speed and gas transfer rate cannot be denied. Attempts to elucidate the mechanism of gas exchange have been attempted using a variety of gases, including ^{222}Rn (Holmén and Liss, 1984 and Torgersen et al., 1982). Given that the mechanism of gas transfer is poorly understood partly due to uncertainties in the diffusion coefficients (Holmen and Liss, 1984) perhaps the empirical approach to the relationship between wind speed and transfer coefficient (Smethie et al., 1985) is the only approach likely to provide useful results.

Other workers have used ^{222}Rn to successfully obtain information about vertical eddy diffusivities in near bottom waters in fjords

(Smethie, 1981), offshore basins (Chung, 1973; Berelson et al., 1982) and lakes (Imboden and Emerson, 1978). The models employed have ranged from a simple one-dimensional model assuming no horizontal flux of ^{222}Rn to models assuming the ^{222}Rn is instantaneously mixed in the horizontal direction (Smethie, 1979). However, in nearshore environments, such as estuaries and continental shelves, the distributions of ^{222}Rn appear to vary widely with time and provide less clear results (Hammond et al., 1975, 1977). Biscaye et al. (1978) found that inhomogeneities in sediment ^{222}Rn production rates in the New York Bight make the interpretation of their profiles difficult. Lietzke and Lerman (1975) developed a two-dimensional diffusion-reaction model for steady state distributions of ^{222}Rn (in basins) and ^{226}Ra (on continental shelves) and found that bottom topography has a profound effect on the distributions in diffusionally anisotropic waters. Imboden and Emerson (1978) also developed a two-dimensional model of ^{222}Rn distribution in Greifensee, Switzerland, with good success. However, the application is to a closed basin not to an open shelf. Application of ^{222}Rn techniques to continental shelves has been limited by the lack of appropriate data and study site (ie. enough data points and a simple enough shelf). As will be discussed the southeastern Bering Sea has all the necessary attributes for a successful application of ^{222}Rn techniques.

The distributions of ^{222}Rn and ^{226}Ra in the sediments of the Washington continental shelf (Smethie et al., 1981) and the San Francisco Bay (Hartman and Hammond, 1984) have been used to

investigate sediment mixing processes. They found molecular diffusion is insufficient to explain the deficiency of ^{222}Rn present; consideration of bio-irrigation is needed. Gruebel and Martens (1984), however, find molecular diffusion explains the ^{222}Rn deficiency in the sediments of the White Oak River estuary. Many problems have arisen from the various procedures to measure fluxes of ^{222}Rn from sediments. Secular equilibrium between ^{222}Rn and ^{226}Ra has not been obtained in cores possibly due to lost ^{222}Rn (Gruebel and Martens, 1984) or the "slurry effect" (Key et al., 1979a and Smethie et al., 1981). Benthic flux chambers have been placed on the sediment surface, however, in some environments (Gruebel and Martens, 1984) there is no agreement between the chamber fluxes and the integrated core ^{222}Rn deficiency. Hartman and Hammond (1984) find agreement between their benthic flux chambers and core deficiency integrations suggesting that the nature of the environment (biological as well as physical) can affect the ^{222}Rn flux from sediments.

Methods

The analytical methods are a straight forward application of previously published techniques. The measurement of ^{222}Rn followed Mathieu (1977). The ^{226}Ra analysis are discussed by Moore (1976) and Key et al. (1979b). Basically ^{222}Rn was stripped out of a sealed vessel with a helium stream and collected on a charcoal trap, followed by alpha scintillation counting. The data reduction was accomplished through the application of Bateman solutions as discussed by Sarmiento et al. (1976) and Smethie (1979). The simple one-dimensional modeling

followed Broecker (1965) and the two-dimensional modeling was derived as part of this dissertation research.

Preliminary Results

Air-sea gas transfer rates were measured on the southeastern Bering Sea shelf during 1980, 1981 and 1982. Although gas transfer rates are highly dependent on local meteorological conditions the following range was observed. The lowest and highest unbiased transfer coefficients were observed during the cruise in 1981, 2.2 m d^{-1} and 4.9 m d^{-1}. The statistically significant (at the 95% confidence level) values of horizontal and vertical eddy diffusivities found for the upper water column of the middle shelf region were $\sim 6 \times 10^{6}$ and $\sim 5 \times 10^{-1}$ cm^2 sec^{-1} respectively. The estimates of sediment-water exchange rate varied over a wide range. This range covered from molecular diffusive fluxes ($\sim 10^{-3}$ atoms cm^{-2} sec^{-1}) to biologically mediated advective fluxes ($\sim 10^{-2}$ atoms cm^{-2} sec^{-1}).

Study Area

The southeastern Bering Sea shelf is unusually wide ($\sim$500 km) and relatively shallow ($\sim$50 m). The gradient of the bottom is distinguished only by two *steps* which are clearly visible on a plot of average bottom slope vs. distance offshore (Figure 1-2). The bottom of this shelf is described as a *flat and featureless* plane (Schumacher and Kinder, 1983). The other distinguishing physical characteristic of this shelf is the graded sediments. The average grain size of the bottom sediments becomes coarser in the onshore direction (Sharma, 1979).

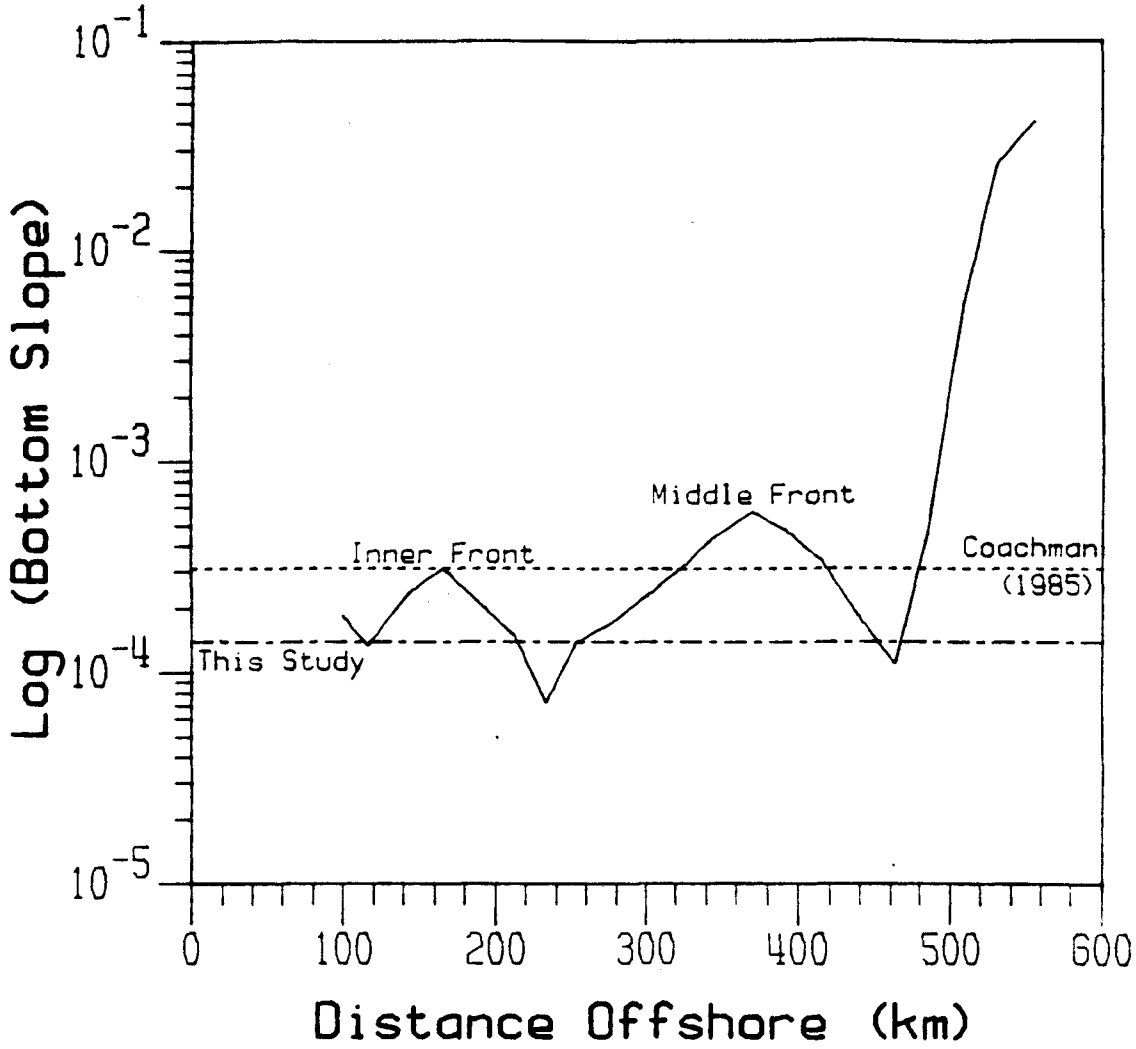

Figure 1-2. Logarithm of bottom slope versus distance offshore. The breaks in shelf slope appear as peaks and are labeled with the corresponding hydrographic front. Critical slopes based on the eddy diffusivities of Coachman (1985) and this study are shown.

Three hydrographic fronts divide the shelf waters into three shelf domains (Iverson et al., 1979). Front formation is poorly understood (Coachman, 1985), however, fronts are believed to be formed by the interaction of tidal and wind mixing, heating and cooling, freezing and melting and river runoff and lateral deep basin exchange (Kinder and Schumacher, 1981). The fronts are approximately located over breaks in the shelf bottom topography (Figure 1-2) and hence divide the shelf waters by depth (H) (Schumacher and Kinder, 1983 and Coachman, 1985) into: inner shelf ($H < 50$ m), middle shelf ($50 \text{ m} < H < 100$ m) and outer shelf ($100 \text{ m} < H < 150$ m). The outer and middle fronts can be identified as zones of enhanced horizontal gradients of properties; the inner front appears as a zone of transition in water column structure (Coachman, 1985). Figure 1-3 shows a generalized picture of the shelf water hydrography (from Coachman, 1982).

The circulation is reasonably well understood (Coachman and Charnell, 1979; Coachman and Walsh, 1981 and Coachman, 1985). Several current meters have been deployed on the southeastern Bering Sea shelf (Coachman and Charnell, 1979; Coachman, 1982; Schumacher and Kinder, 1983 and Coachman, 1985) and after removal of the tidal component small net flows have been found in some but not all shelf regimes. The inner shelf has a very small significant net flow (1 - 5 cm sec^{-1}) counterclockwise around Bristol Bay (Coachman, 1985). The middle shelf regime has no significant net flow and transport of properties across this regime is driven by *tidal diffusion* (Coachman, 1985). The outer shelf regime has a small ($\sim$5 cm sec^{-1}) net flow to the northwest with

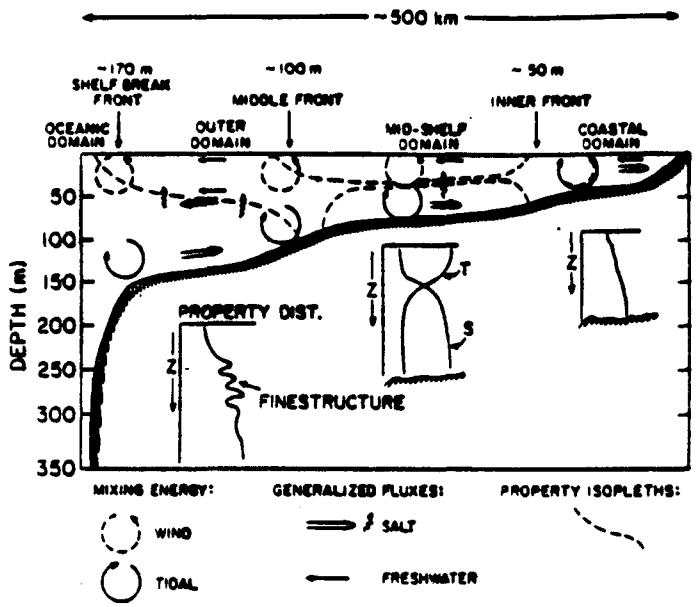

Figure 1-3. Idealized cross shelf hydrography (from Coachman, 1982).

a variable (1 - 5 cm sec^{-1}) cross-shelf component resulting in convergence or divergence at the middle front (Coachman, 1985). The driving mechanism for these flow regimes is related to the partitioning of kinetic energy within each shelf regime (Coachman, 1985). The very small net flow on the inner shelf is believed to be due to the difference between the mass field of the inner and middle shelf regimes and possibly to rectification of tidal currents (Schumacher and Kinder, 1983). The middle shelf waters are dominated by the tidal energy input (> 95% of the total kinetic energy) and the motion of these waters drives the *tidal diffusion* (Coachman, 1985). The along isobath flow on the outer shelf is probably driven by the horizontal pressure gradients generated by the upwelling occuring at the middle front (Coachman, 1985). The variable on- and offshore flows of the outer shelf drive the upwelling at the middle front through convergence and divergence, but the physics behind this process is poorly understood (Coachman, 1982, 1985).

Given that most of the kinetic energy on the southeastern Bering Sea shelf is in the tidal frequency band (Coachman, 1985) and that transport of properties on this shelf is largely diffusive (Coachman and Walsh, 1981), are two-dimensional fluxes important in this regime? The answer to this question affects whether one-dimensional models provide realistic values for vertical eddy diffusivity estimates. Figure 1-4 shows three representative profiles of ^{222}Rn and ^{226}Ra from each of the three shelf regimes. These profiles have distinct two-dimensional characteristics. A time scaling argument showed when two-

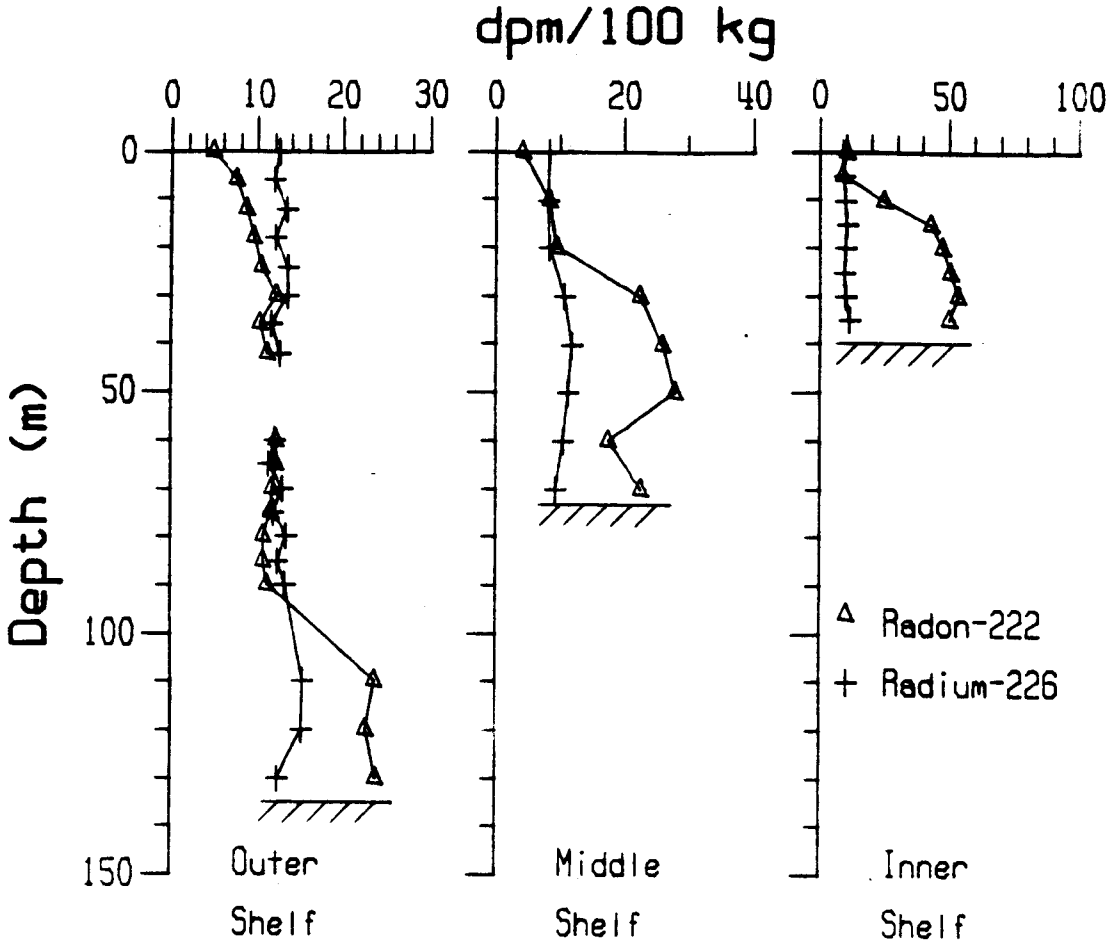

Figure 1-4. Representative ^{222}Rn and ^{226}Ra depth distributions from each of the hydrographic domains in the PROBES area. Outer shelf: stations TT159-3115 and TT159-3119, 135 m. Middle shelf: station HX028-0041, 73 m. Inner shelf: station TT159-4021, 40 m.

dimensional fluxes were important. Typical mixing scale lengths (horizontal and vertical) can be related to the slope of the bottom and to the eddy diffusivities through the characteristic mixing times. Let t_z^* and t_x^* be the characteristic mixing times in the vertical and horizontal directions, respectively. If horizontal mixing is as important as vertical mixing t_z^* and t_x^* will be approximately equal. These mixing times are given by:

$$t_z^* = \frac{z_*^2}{K_v} \quad \text{and} \quad t_x^* = \frac{x_*^2}{K_H} \tag{1-1}$$

where: z_* and x_* = typical mixing scale lengths,

K_v and K_H = vertical and horizontal eddy diffusivities.

Setting the characteristic mixing times equal obtains:

$$\frac{z_*^2}{K_v} = \frac{x_*^2}{K_H} \quad \text{or} \quad \frac{z_*^2}{x_*^2} = \frac{K_v}{K_H}. \tag{1-2}$$

The critical slope, m_*, of the bottom is defined as the slope below which the distance some property must travel horizontally (x) takes longer than it does to travel vertically (z) to the same point i.e.

$$m_* = \frac{z_*}{x_*}. \tag{1-3}$$

Substituting equation (1-3) into (1-2) yields:

$$m_*^2 = \frac{K_v}{K_H}. \tag{1-4}$$

This argument is shown diagramatically in Figure 1-5. Estimates of K_v and K_H can be taken from Coachman (1985) ($K_v \simeq 10^{-1}$ and $K_H \simeq 10^{4}$ cm^2 sec^{-1}). These approximations yield a critical slope of approximately 3.2×10^{-4}. The shelf has an average slope of approximately 3×10^{-4} (500 km wide and 150 m deep). This average slope would imply a ratio

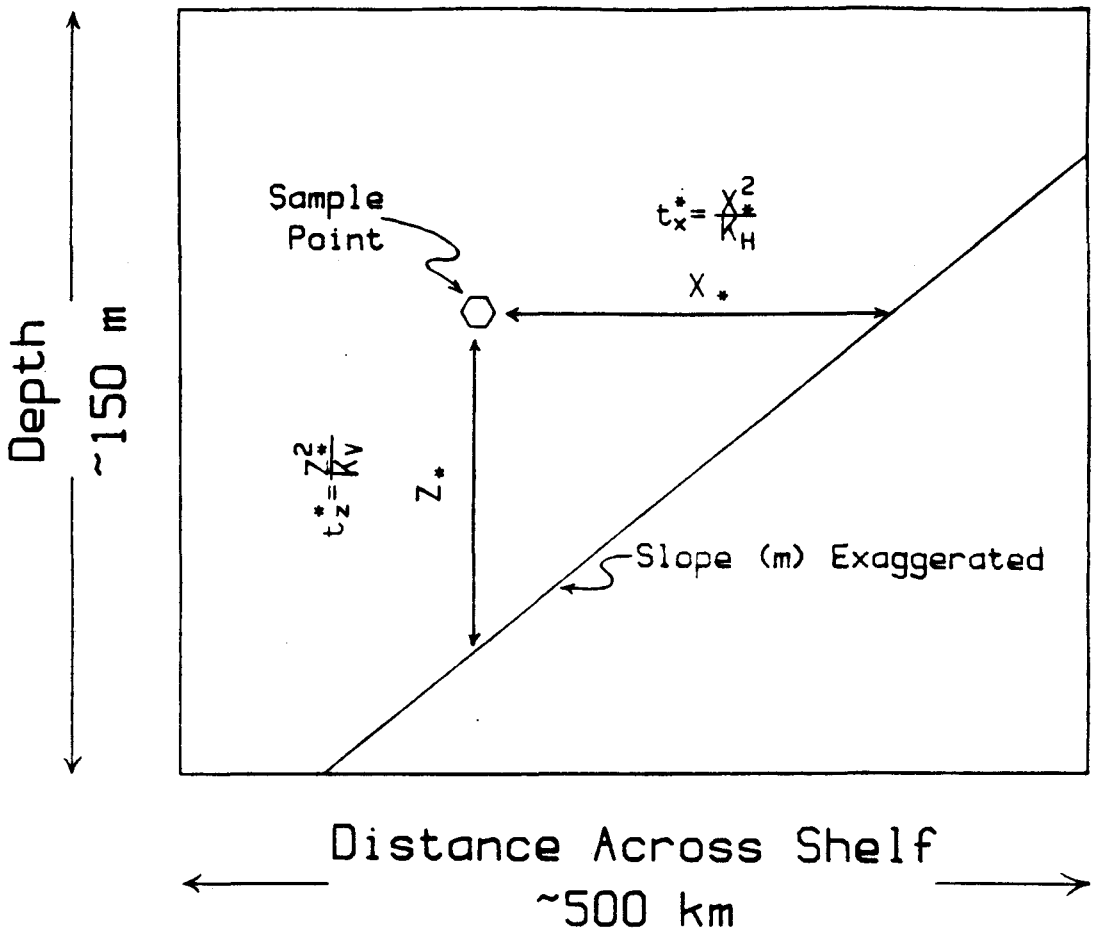

Figure 1-5. Time scaling argument diagram. X_* and t_x^* are characteristic horizontal mixing length and time; Z_* and t_z^* are characteristic vertical mixing length and time. See text for explanation.

of eddy diffusivities $\simeq 9 \times 10^{-8}$ if it were critical. The two-dimensional model (developed in chapter 6) yielded a ratio of eddy diffusivities $\simeq 2 \times 10^{-8}$ implying a critical slope of $\simeq 1.4 \times 10^{-4}$. The two critical slopes are plotted on Figure 1-3 for comparison. All these values and Figure 1-4 imply horizontal fluxes of properties need to be considered on this shelf. The profiles strongly suggest that the simple one-dimensional models of ^{222}Rn distribution will not provide realistic values of vertical eddy diffusivity.

Chapter 2: **DATA COLLECTION**

There is something fascinating about science. One gets such wholesale returns of conjecture out of such a trifling investment of fact.
Mark Twain

In this chapter the three operations involved in the data collection will be discussed. The operations were sample collection, sample analysis and data reduction. Sample collection entails the what, when and where details of the cruises. Sample analysis covers the how of measuring ^{222}Rn and ^{226}Ra. The data reduction includes the calculations and error analysis.

All the methods employed in sample analysis have been described in detail in the literature. Sample collection for water and sediment samples is discussed below. The sample analysis follows those as outlined by Mathieu (1977). The data reduction follows the calculations as outlined by Sarmiento et al. (1976) and Smethie (1979).

Sampling Strategy

The near surface waters, mid-depth waters, near bottom waters and sediments were sampled during October 1980 (cruise HX009), June-July 1981 (cruise TT159) and June 1982 (cruise HX028) using 30-liter Niskin bottles, a Van Veen grab sampler and a Benthos gravity corer. Five water column profiles were measured in 1980, 27 in 1981 and 8 in 1982 for a total of 20 near-surface, 19 mid-depth and 20 near-bottom profiles, several of which were multi-purpose profiles. Fifteen sediment surface grab samples were collected in 1979 (cruise TT138)

and 13 in 1981 (cruise TT159); sediment cores were obtained in 1982 (cruise HX028) and 1983 (cruise HX048). The water column sample locations from 1980 (O), 1981 (+) and 1982 (X) are shown in Figure 2-1a. The sediment core sample (O), 1979 grab sample (+) and the 1981 grab sample (X) locations are shown in Figure 2-1b.

There were four factors affecting sample collection while at sea. First and foremost was a consideration of the weather, the large volume of water necessary (30 liters) required relative sea calmness. The sample spacing in the water column was determined from CTD casts run prior to the ^{222}Rn cast. These CTD casts also provided the temperature, salinity and density data required for later calculations. The sample locations were evaluated according to two opposing criterion. The first was the desire to sample the shelf as fully as possible while the second was the desire to repeat stations to investigate temporal variations. Finally the requirement that the ^{222}Rn extraction gear be ready for analysis was absolute. Once a week the equipment was calibrated and backgrounds checked, making it unavailable for sample collection. The samples were usually taken right after the daily morning productivity cast in 1981, but this was not a universal practice on the other cruises.

Radon-222 Analysis

Radon-222 was extracted from 19-liter seawater samples using the methods outlined by Mathieu (1977). Water samples were transferred through Tygon tubing to evacuated 19-liter glass carboys. The ^{222}Rn was stripped from the sample with a circulating helium stream and

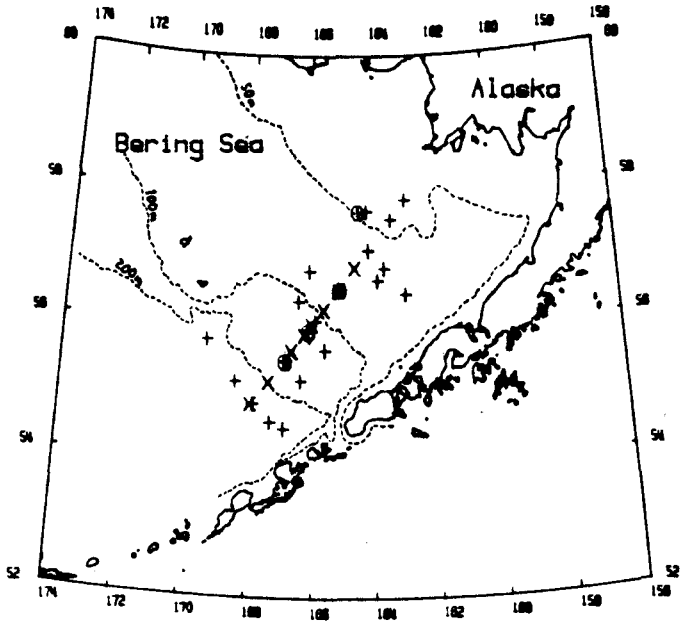

Figure 2-1a. Water column station locations from cruises in 1980 (0), 1981 (+) and 1982 (X). Several station locations overlay each other.

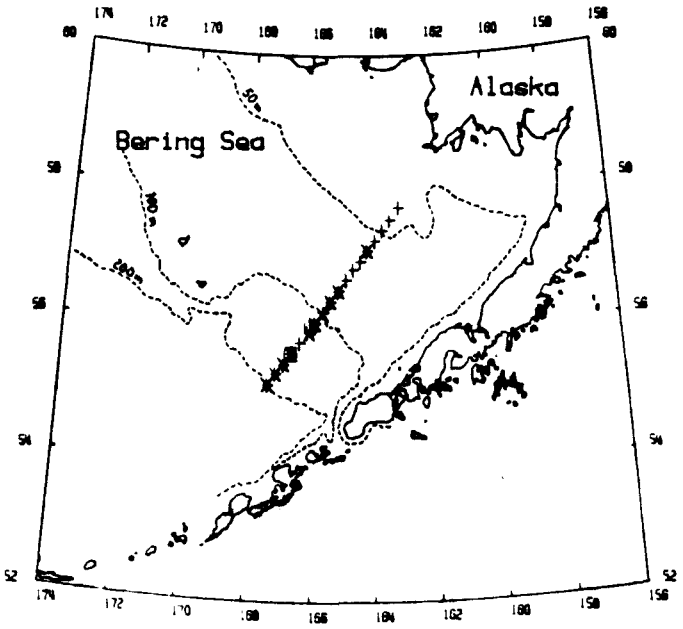

Figure 2-1b. Sediment sampling sites. Benthos corer samples are shown by (0), 1979 grab samples by (+) and 1981 grab samples by (X).

trapped on an activated charcoal column kept at -55° C by a Cryocool unit. The ^{222}Rn was then baked off the trap at 400° C and transferred to an alpha scintillation counting cell. With the stripping and transfer boards (Applied Science of Piermont), four samples could be run simultaneously with a 140 minute turnaround time.

Radium-226 Analysis

Radium-226 was determined by the ^{222}Rn ingrowth method (Key et al., 1979b), so the terminal analysis for ^{222}Rn and ^{226}Ra was identical. Immediately after the ^{222}Rn extraction the water sample was passed through a 15.24 x 2.54 cm PVC pipe packed with Mn-impregnated acrylic fiber (Moore, 1976). These fibers quantitatively remove radium from seawater (Moore, 1976). The fibers were returned to the laboratory and ^{222}Rn was allowed to grow into Mason jars having the metal lids modified with inlet and outlet valves. I compared ^{222}Rn ingrowth from water left standing in the glass carboys and from the untreated fibers in Mason jars and obtained no statistically significant difference at the 95% confidence level. For example, sample HX009-0056-1 yielded 11.5 ± 0.3 dpm/100 kg ^{226}Ra when the sample was stored in the glass carboy and 11.8 ± 0.7 dpm/100 kg when analyzed by the fiber method.

Sediment Radon and Radium Analysis

Sediment samples were stripped in glass Mason jars identical to the ones used for the fiber analysis, but with a known amount of water added to create a slurry. Distilled, deionized water was used to form the slurry in 1982; although it had a very low ^{226}Ra background the

sediment samples did not attain secular equilibrium between ^{222}Rn and ^{226}Ra. In 1983 the slurry was formed with seawater which had been passed through a Mn-impregnated fiber filter to remove ^{226}Ra. The resulting sediment samples did attain secular equilibrium within the accuracy of the ^{226}Ra analysis. The grab samples were collected only for determining ^{226}Ra levels at the sediment surface, so shipboard ^{222}Rn extractions were necessary only for the cores. After the analysis was complete the sediments were dried in an oven at 70^{0} C overnight to determine their dry weight.

Alpha Scintillation Counting

Radon-222 activity was measured using two dual channel alpha scintillation counters Model# DRC-MK6 (Applied Techniques Co). The counting cells were constructed either from Pyrex glass or from quartz tubes and coated on the inside with silver-activated ZnS. The counting cells were counted for 2000 min or 2000 counts, whichever was shorter. Background histories were kept for the counting cells, stripping carboys, extraction boards and ^{222}Rn ingrowth jars. Counting cell efficiencies were monitored by periodically stripping sealed ^{226}Ra standards (480.8 dpm).

Data Reduction and Error Analysis

The calculations and statistics for each sample were determined as in Sarmiento et al. (1976). The calculations were made with an integrated system of programs (in BASIC) on a Hewlett Packard 86A personal computer (the output is compiled in Appendix 1). The activities of ^{222}Rn were found through an application of the Bateman

solution (Friedlander et al., 1981 and Sarmiento et al., 1976) for the decay chain $^{222}Rn \rightarrow {}^{218}Po \rightarrow {}^{214}Bi$. The counting cell background and efficiency histories, bottle blanks, volume errors and counting statistics were used in a propagation of errors analysis to estimate the error associated with each ^{222}Rn and ^{226}Ra determination (see Sarmiento et al., 1976). The overall accuracy and precision (1σ) of the system was approximately $\pm 10\%$.

There were three sources of error in the measured-data: 1) errors that were quantifiable, such as uncertainty from counting, cell backgrounds and efficiencies etc, 2) uncertainty of the depth and time the sample was actually collected and 3) uncertainties that were difficult to quantify, e.g. gas leaks in the extraction system or ^{226}Ra adsorption to sample containers. As mentioned earlier, the first source of error was accounted for in the statistical error calculations as outlined by Sarmiento et al. (1976). The second type of errors had well constrained upper and lower limits. These limits allowed the calculation of their effect and it was found to be negligible. The final type of error undoubtably caused the majority of the error in repeatability. Repeated ^{226}Ra determinations had a relative standard deviation (RSD) of approximately 8%, which also was the average RSD of the statistical error determinations. Given the complexity of making better ^{222}Rn measurements, an uncertainty of $\pm 10\%$ was quite acceptable.

Chapter 3: AIR-SEA GAS EXCHANGE

We are exactly what we pretend to be. Therefore, we should be very careful about what we pretend to be.
Kurt Vonnegut, Jr.

Introduction

The lag between the depletion of CO_2 in the near surface waters by photosynthetic organisms and its invasion from the atmosphere allows the amount of carbon thus fixed to be quantified. A geochemical tracer that could be related to this rate of exchange would be of great value. Broecker (1965) first suggested the near surface distribution of natural levels of ^{222}Rn could be used to quantify this exchange rate. The depth integrated deficiency of ^{222}Rn should be related to the rate at which it escapes into the atmosphere. During this study of ^{222}Rn and ^{226}Ra on the southeastern Bering Sea shelf several near surface profiles were measured. Erroneously low transfer coefficients were found on the inner shelf due to flux of excess ^{222}Rn into the shallow near surface waters. However, some reasonable estimates of the gas exchange on the outer shelf were obtained.

Mathematical Methods

The flux of ^{222}Rn across the air-sea interface can be calculated from the size of the ^{222}Rn deficiency in the upper water column (Peng et al., 1979). The transfer coefficient is determined by a balance of the ^{222}Rn production, decay and evasion to the atmosphere (Emerson et al., 1973). This one-dimensional model considers flux from below or from the side negligible (Broecker, 1965). The flux, F (atoms sec^{-1} cm^{-2}), of ^{222}Rn into the atmosphere is given by:

$$F = -D_w \frac{dC}{dz} \qquad (3\text{-}1)$$

where: D_w = molecular diffusivity of ^{222}Rn in water corrected for temperature ($cm^2\ sec^{-1}$);

C = concentration of ^{222}Rn in the water (atoms cm^{-3});

z = depth in the stagnant boundary layer (cm).

Equation (3-1) can be rewritten in terms of a mass transfer coefficient, J ($cm\ sec^{-1}$), as follows:

$$F = J(C_s - p\alpha) \qquad (3\text{-}2)$$

where $J = D_w/\gamma$;

γ = the thickness of a hypothetical boundary film (cm);

C_s = ^{222}Rn concentration at the surface (atoms cm^{-3});

p = the partial pressure of ^{222}Rn in the atmosphere;

α = the solubility of ^{222}Rn in water.

Implicit in this model is the rate governing assumption of molecular diffusion across a stagnant boundary layer. If the flux of ^{222}Rn across the air-sea interface is set equal to the integrated deficiency of ^{222}Rn with respect to its parent ^{226}Ra then:

$$\int_0^\infty (C_E - C_h)\lambda dh = J(C_s - p\alpha) \qquad (3\text{-}3)$$

where: λC_E = ^{226}Ra surface activity (atoms $sec^{-1}\ cm^{-3}$);

λC_h = ^{222}Rn activity at depth h (atoms $sec^{-1}\ cm^{-3}$);

λ = ^{222}Rn decay constant ($2.1 \times 10^{-6}\ sec^{-1}$);

with the rest as defined above. An application of the mean value theorem of calculus to the integral in equation (3-3) yields:

$$(C_E - C_s)\lambda\bar{h} = \int_0^\infty (C_s - C_h)\lambda dh \qquad (3\text{-}4)$$

where: $\bar{h}$ = the integrated ^{222}Rn deficiency divided by the surface deficiency, i.e. the average integrated depth of ^{222}Rn deficiency (cm);

λC_s = ^{222}Rn activity at the surface (atoms sec^{-1} cm^{-3}).

Substituting equation (3-4) into (3-3) and solving for J gives:

$$J = \frac{D_w}{\gamma} = \lambda\bar{h}\left[\frac{C_E}{C_s} - 1\right], \qquad (3\text{-}5)$$

because C_s >> $p\alpha$ for ^{222}Rn (Emerson et al., 1973 and Broecker and Peng, 1974).

Results

Hypothetical film thicknesses from 1980, 1981 and 1982 are presented in Table 3-1. Immediately noticeable were the anomalously thick values observed at stations TT159-4033, TT159-4068, TT159-4103, HX028-0041 and HX028-0112 compared to the range of values reported in Broecker and Peng (1982). Figure 3-1 shows an apparent decrease in the transfer coefficient in the onshore direction. This was due to flux overlap between ^{222}Rn leaving the water column at the surface and ^{222}Rn leaving the sediments at the bottom of a shallow water column. Excluding these anomalies, the average transfer coefficient ($\pm 1\sigma$) was 2.2 $\pm$ 0.4 m d^{-1} in 1980, 3.0 $\pm$ 1.3 m d^{-1} in 1981 and 1.8 $\pm$ 1.1 m d^{-1} in 1982.

Discussion

The results shown in Figure 3-1 and tabulated in Table 3-1 suggest that the transfer coefficient decreased as the water column

Table 3-1: **GAS TRANSFER COEFFICIENTS**

Station	Depth (m)	Domain	Mixed Layer Depth (m)	$\bar{h}$ (m)	γ (μ)	J (m/d)
HX009-0012	79	middle	51	26	39	1.9
HX009-0031	79	middle	51	151	30	2.4
TT159-3042	101	middle	20	81	38	1.9
TT159-4033	77	middle	17	7	64	1.2
TT159-4068	75	middle	8	34	88	0.9
TT159-4093	72	middle	12	38	25	3.2
TT159-4103	65	middle	15	2	400	0.2
HX028-0041	73	middle	5	5	78	0.9
HX028-0112	93	middle	29	40	64	1.1
TT159-3119	119	outer	16	17	16	4.9
TT159-4083	133	outer	13	26	21	3.8
TT159-3103	1440	off	12	13	34	2.2
TT159-4124	1829	off	12	9	21	3.8
HX028-0030	1550+	off	6	16	27	2.6

$\bar{h}$ is the average integrated ^{222}Rn deficiency depth.

γ is the hypothetical stagnant film thickness (in microns).

J is the transfer coefficient.

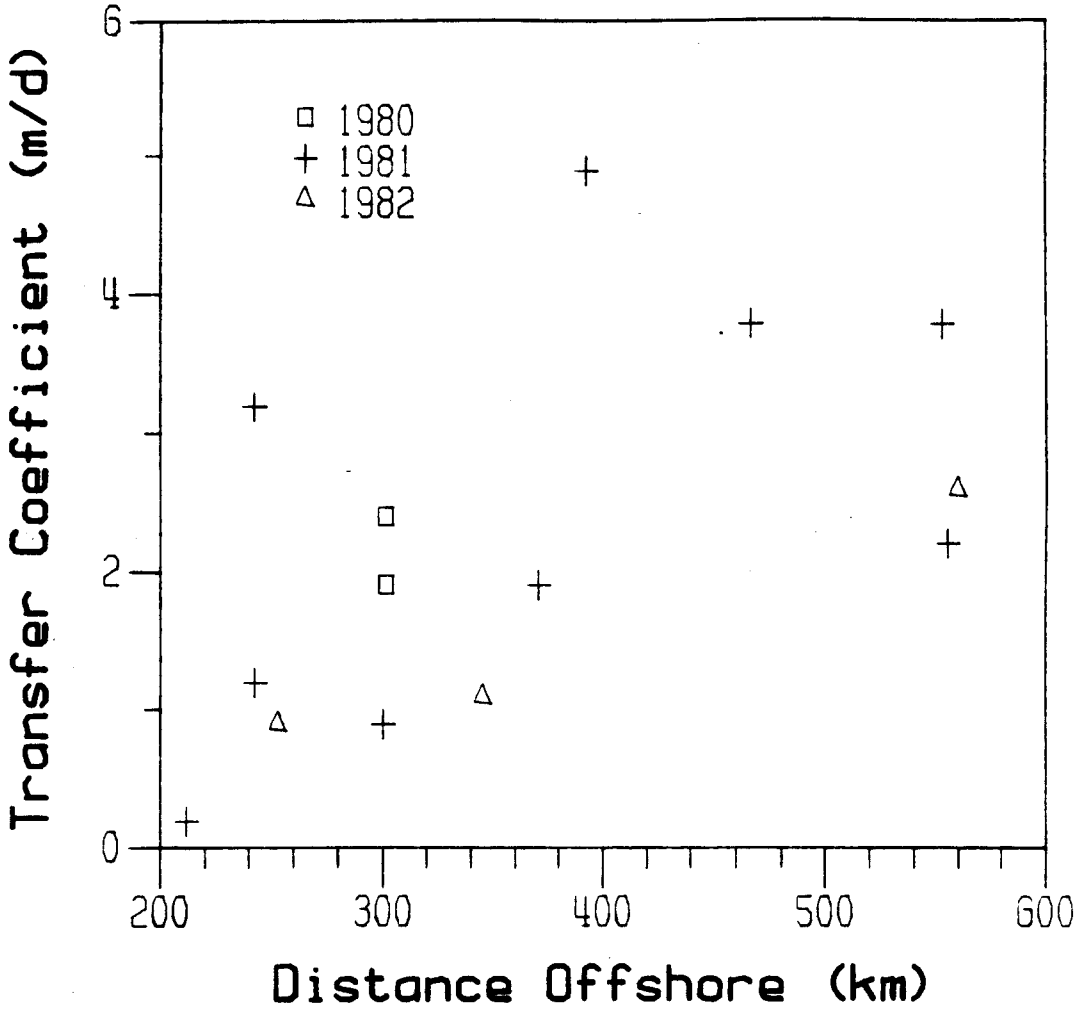

Figure 3-1. Transfer coefficient versus distance offshore calculated from profiles measured in 1980, 1981 and 1982.

shoaled. The wind conditions did not vary appreciably across the study area and there was no other obvious cause for this trend. A question was raised, "Were one of the model assumptions being violated on the inner shelf?". The assumption that there was no lateral net flux of ^{222}Rn into the surface *box* was adequate. The horizontal gradient of ^{222}Rn coupled with the horizontal eddy diffusivity estimate yielded net horizontal fluxes of ^{222}Rn that were an order of magnitude below the vertical integrated ^{222}Rn deficit estimate. The steady state assumption was not violated since no time variable source or sink function of ^{222}Rn was known. The final assumption of no net flux across the bottom of the surface *box* was the most likely candidate to be suspected. Due to the shallowness of the water column and the high sediment ^{222}Rn flux from the inner shelf (see Chapter 4) there was a flux overlap. The flux of ^{222}Rn into the atmosphere was partially overprinted by a flux of excess ^{222}Rn out of the sediments.

Much consideration has been given to the parameters controlling gas exchange at the air-sea interface (Liss, 1983). Theoretical studies have postulated various relationships between wind speed and transfer coefficient. Brtko and Kabel (1978) proposed a square root relationship; Deacon (1977) proposed a linear relationsnip. Laboratory investigations have yielded other possible mathematical relationships between wind speed and transfer coefficient. Kanwisher (1963) obtained a quadratic relationship while Broecker et al. (1978) found a bi-linear relationship in their wind tunnel experiments. Field experience fails to find a consistent relationship between wind speed and

transfer coefficient (Peng et al., 1979; Hasse and Liss, 1980; Broecker and Peng, 1982 and Liss, 1983). However, the empirical approaches of Hartman and Hammond (1984), Wanninkhof et al. (1985) and the time dependent predictive model of Smethie et al. (1985) yield statistically significant linear responses between the wind speed and transfer coefficient. Due to the difficulty encountered by Holmén and Liss (1984) in determining the actual mechanism of gas exchange perhaps these empirical approaches provide the best predictive capabilities at the present time.

The wind velocity (at 10 m elevation) was recorded on the bridge of the *R/V T.G. Thompson* every 2 h during the 1981 cruise. Figure 3-2 shows wind speeds for an 80 d period covering the 1981 field season when ^{222}Rn distributions suitable for calculating gas exchange were measured. An optimization linear regression analysis was conducted to determine the duration for averaging the wind speed that gave the best least-squares correlation between mean wind speed and transfer coefficient. Starting at the time of sample collection this optimization program considered time at 2 h intervals up to 20 d prior to ^{222}Rn sample collection. No statistically significant correlation was found at the 95% confidence level; the optimum averaging period was 3.3 d.

Hartman and Hammond (1984) report a statistically significant linear correlation between wind speed and transfer coefficient. For comparison, Fig. 3-3 shows the optimum averaging period for wind speeds vs. transfer coefficients from the linear optimization

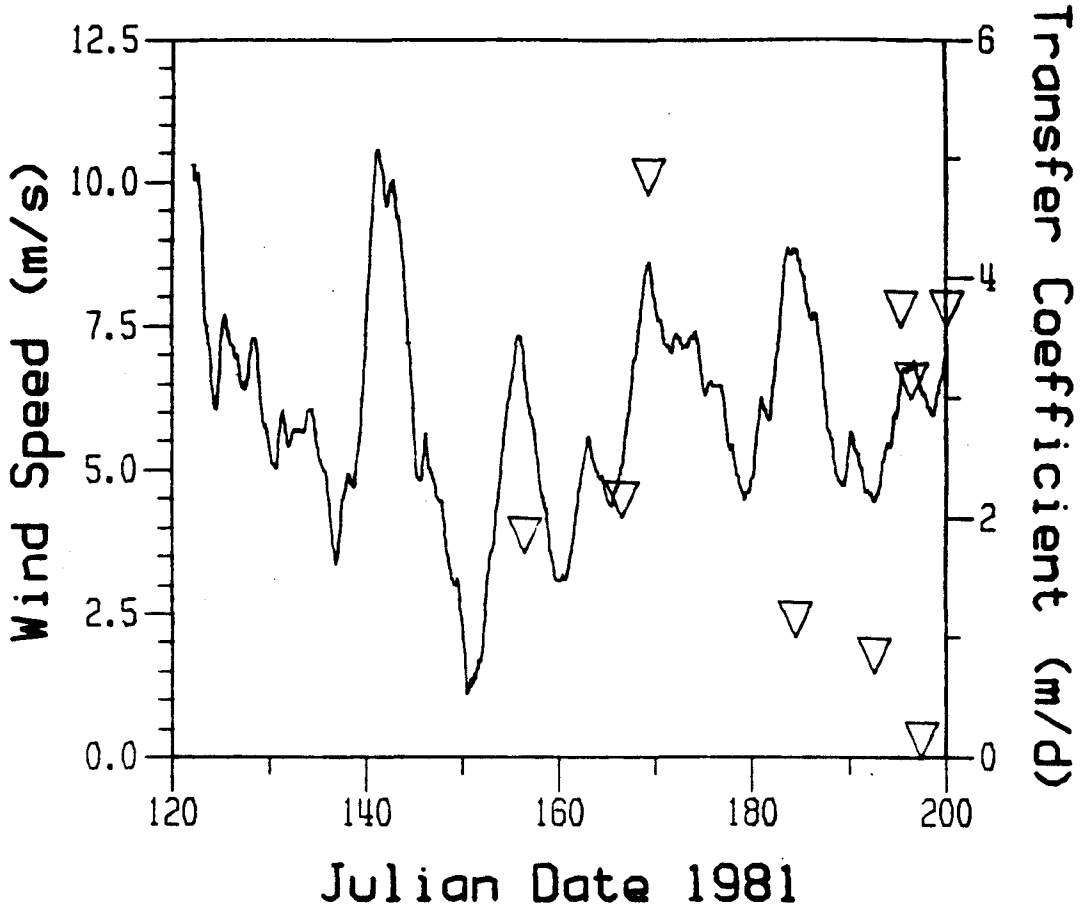

Figure 3-2. Wind speed and transfer coefficient versus day of year, 1981 in the PROBES area. Wind speeds were averaged 96 hours prior to sampling. Wind speed is the solid line; transfer coefficients are the inverted triangles.

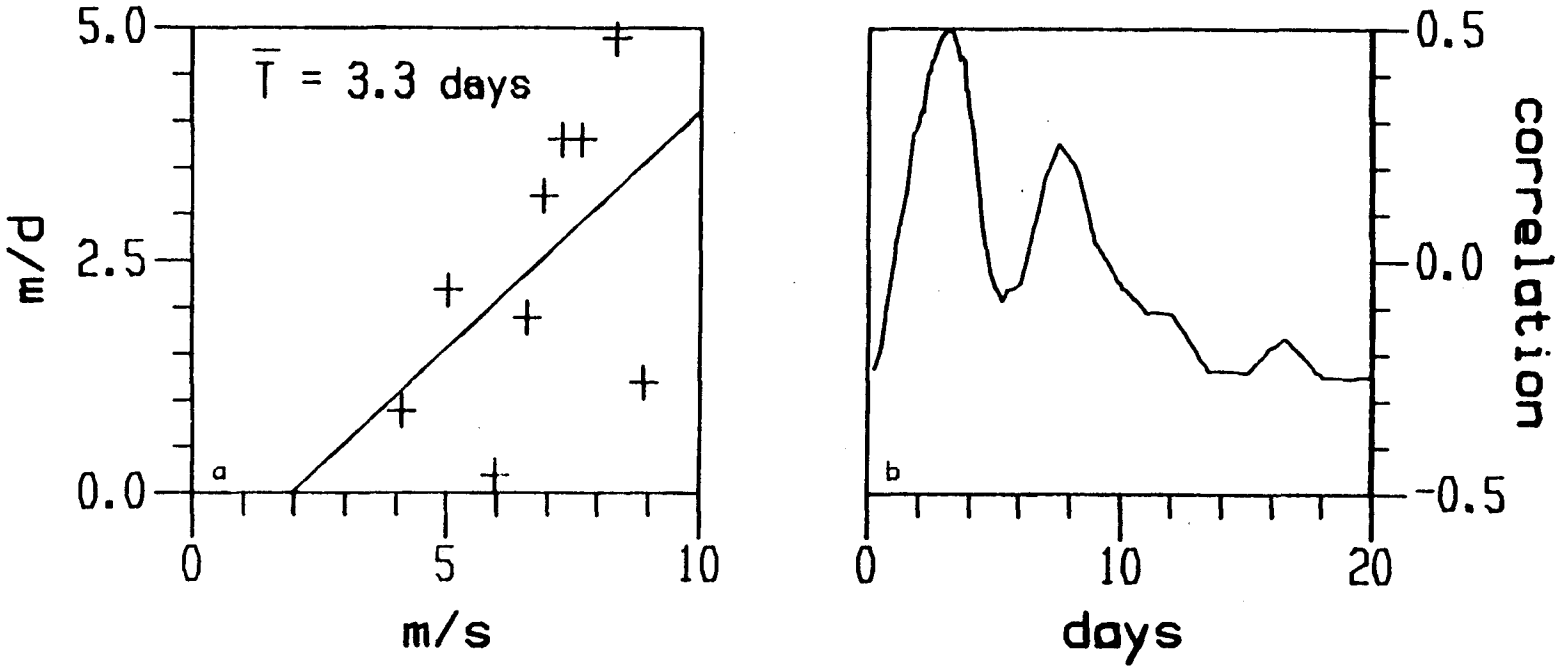

Figure 3-3. Optimum linear regression of averaged wind speed versus transfer coefficient. a) Winds were averaged 3.3 days prior to sampling: this was the optimal averaging period, the line shown is statistically significant at the 80% confidence level ($r = 0.50$, $n = 9$). b) Correlation coefficient spectra of averaging periods from 2 hours to 20 days prior to sampling.

regression and the correlation coefficient spectra for all the averaging periods. As seen in Fig. 3-3b the correlation coefficient has a distinct peak at 3.3 days and becomes weakly negative thereafter; this peak was statistically significant at the 80% confidence level ($r = 0.50$, $n = 9$). An autocorrelation analysis of the raw wind speed data used in this optimization investigation revealed the synoptic time scale was ~3 days. I concluded that longer averaging periods than this did not improve the relationship between wind speed and transfer coefficient.

Although not statistically significant at the 95% confidence level, the results of my optimization regression analysis have some interesting comparisons to the empirical linear regression approaches of Hartman and Hammond (1984), Wanninkhof et al. (1985) and Smethie et al. (1985). These studies, in the field, find statistically significant correlations between wind speed and transfer coefficient; a comparison of the linear regressions is provided in Table 3-2, which also includes the bi-linear wind tunnel results of Broecker et al. (1978). An increase in transfer coefficient is reported beginning between 3 - 4 m sec^{-1} wind speed (Broecker et al., 1978 and Wanninkhof et al., 1985). This increase is associated with the onset of capillary waves and/or a jump in turbulence level beneath the waves (Wanninkhof et al., 1985). The data points above ~2 m sec^{-1} extrapolated to the abscissa yield a wind speed, $U_o \cong 2.0$ m sec^{-1} (Broecker et al., 1978 and Wanninkhof et al., 1985). For these reasons Smethie et al. (1985) forced their regression to have an abscissa intercept of 3 m sec^{-1}.

Table 3-2: **COMPARISON OF LINEAR REGRESSED WIND VELOCITIES VERSES TRANSFER COEFFICIENTS**

Study	Slope	Intercept	r	n	U_o	$\bar{T}$
Hartman and Hammond (1984)	0.35	-0.53 (NR)	0.84	7	1.51	3 days
Smethie et al. (1985)	0.66	--	0.46	29	3*	24 hrs
	0.28	--	0.46	29	-3.9	24 hrs
Wanninkhof et al. (1985)	0.44	-0.89	0.94	15	2.01	variable
Broecker et al. (1978)	1.3	-2.7	--	--	2.1	--
this study	0.51	-0.98	0.50	9	1.92	3.3 days

NR means not reported but calculated from data in report.

U_o is the extrapolated abscissa intercept.

$\bar{T}$ is the averaging period of wind speeds.

* means held constant during regression.

n is the number of data points.

r is correlation coefficient.

-- refers to data missing.

With U_o free, Smethie et al. (1985) obtain U_o = -3.9 m sec^{-1}, which doesn't agree with wind tunnel and *controlled* lake experiments. The value of U_o from my regression was 1.92. The time period the wind speed was averaged over is also shown in Table 3-2. Wanninkhof et al. (1985) used the average wind speed between determinations, but Smethie et al. (1985) used only the preceding 24 hours. Only this study and Hartman and Hammond (1984) used a wind speed averaging period approximately equal to the half life of ^{222}Rn and were the only ones with a U_o approximately equal the values obtained by Broecker et al. (1978) and Wanninkhof et al. (1985) (Table 3-2).

There were at least three possibilities for the lack of a statistically significant relationship between wind speed and transfer coefficient in my work. Liss (1983) has suggested that the *shape* of the ^{222}Rn deficiency profile may change with changing wind conditions. An increase in mixed layer depth with increasing wind speed may cause the ^{222}Rn deficiency to become deeper and narrower. In terms of the model in this thesis, $\bar{h}$ became larger but C_E/C_θ became smaller and the effects tended to cancel each other. This overestimates the gas transfer coefficient so this model might be inappropriate for estimating gas exchange. Second, ^{222}Rn, with a half-life of 3.8 days, may not respond quickly enough to the wind conditions to be useful except in situations with relatively constant wind velocity (see Broecker and Peng, 1971; Peng et al., 1979 or Deacon, 1981). Nevertheless, Smethie et al. (1985) have argued that the radon method is the only method capable of establishing the relationship between

wind speed and transfer coefficient that is applicable to field studies in the ocean. Finally, Holmén and Liss (1984) have presented the results of an experiment designed to distinguish between the stagnant surface film, surface replacement and boundary layer models of gas exchange. They present evidence that the stagnant film model not only seems physically unrealistic, but that it is not the model indicated by the experimentally determined relationship between transfer coefficient and molecular diffusivity. However, they cannot determine whether the film replacement or the boundary layer model is correct due to uncertainties in the molecular diffusivities used in their experiments. Because of the above, the average film thickness reported here can only be considered conceptually and the transfer coefficient was a better measure of gas exchange since it was model independent.

Film thickness, however, was useful for computing annual gas exchange budgets and possibly seasonal budgets. During PROBES, four methods were used to estimate the CO_2 gas exchange rate: 1) ^{222}Rn deficiency measurements and the pCO_2 measurements of Codispoti et al., (1985), 2) net productivity and $^{15}NO_3$ uptake experiments (R. Sambrotto, personal communication), 3) wind speed records and the relationship given by Broecker et al. (1978) coupled with infrared pCO_2 measurements of the atmosphere and seawater (Codispoti et al., 1985), and 4) a floating chamber in which the evolution of pCO_2 was monitored (D. Hood, personal communication). These methods used in PROBES averaged to about the same gas exchange rate over

approximately month-long periods (Table 3-3), suggesting that film thicknesses have long term usefulness.

Table 3-3: **COMPARISON OF METHODS OF ESTIMATING CO_2 GAS EXCHANGE**

	Radon Deficiency	Net Productivity	pCO_2 + Wind	Surface Chamber
		1980 ΔpCO_2 = -169 μatm		
max	1.50	7.90	--	1.8
min	0.18	0	--	0.32
avg	0.46	2.2	0.5	1.03
		1981 ΔpCO_2 = -93 μatm		
max	0.83	2.9	0.57	--
min	0.10	0.59	0.29	--
avg	0.25	1.58	0.43	--

Net productivity values from R. Sambrotto (personal communication).

Surface chamber values from D. Hood (personal communication).

pCO_2 + wind values from Codispoti et al. (1985).

Values reported are CO_2 flux in g C m^{-2} d^{-1}.

Chapter 4: **SEDIMENT RADON FLUX**

Though this be madness, yet there is method in't

William Shakespeare

Introduction

The concentrations of nutrients in the near-bottom waters are mediated by their flux from the sediments. The ^{222}Rn flux out of the sediments is an important source function for the redistribution of ^{222}Rn in the system being examined. Broecker (1965) offered three methods for estimating the flux of ^{222}Rn out of the sediments. Although other workers later improved upon these methods (Smethie et al., 1981; Gruebel and Martens, 1984 and Hartman and Hammond, 1984) it is these three methods that are employed in this chapter. The flux estimates were made from: 1) ^{222}Rn production rate in the surface sediments, 2) standing crop calculations of excess ^{222}Rn in the overlying water column and 3) direct pore water measurements of ^{222}Rn and ^{226}Ra. The basic premise of these estimates was: whatever is missing from the sediments is found in the overlying water column. Direct measurements of the core distributions yielded higher flux estimates than those predicted by purely molecular diffusion based on ^{222}Rn production rate, standing crop estimates gave values between methods 1) and 3).

Mathematical Methods

The basic assumptions in each of the methods employed in this chapter were slightly different. The flux estimates based on the ^{222}Rn production rates, obtained from the sediment surface grab samples,

assumed only molecular diffusion was operative. The flux estimates were a function of the density, porosity and ^{226}Ra concentration of the sediments. The standing crop estimates were a balance between the depth integrated excess ^{222}Rn and the flux out of the sediments. In other words, the extra ^{222}Rn in the water column must have come from the sediments below. The ^{222}Rn flux estimate from the core distributions assumed the integrated ^{222}Rn deficit was equal to the flux of ^{222}Rn out of the sediments. None of these estimations accounted for any horizontal transport of ^{222}Rn.

Given undisturbed sediments, the molecular diffusion of ^{222}Rn from the sediments would be the minimum flux of ^{222}Rn. This molecular diffusive flux, F (atoms cm^{-2} sec^{-1}), is given by:

$$F = -D_T \frac{d\hat{C}}{dz}, \qquad (4\text{-}1)$$

where: $D_T = \frac{D_M}{\theta^2}$;

$\hat{C} = (1-\phi)\rho_s C$;

and C = sediment concentration (atoms g^{-1} dry);

$\hat{C}$ = whole sediment concentration (atoms cm^{-3});

ρ_s = sediment density (2.64 g cm^{-3});

ϕ = sediment porosity (dimensionless);

θ = tortuosity, ~1.3 (Smethie et al., 1981);

D_T = molecular diffusivity of ^{222}Rn, corrected for tortuosity;

D_M = molecular diffusivity of ^{222}Rn, corrected for temperature (4.5×10^{-6} cm^2 sec^{-1}, see Peng et al., 1974);

z = depth in sediment (cm).

This equation becomes, with substitution:

$$F = -(1-\phi)\rho_s D_T \frac{dC}{dz} . \qquad (4\text{-}2)$$

The solution to which (see Imboden and Joller, 1984), using the boundary conditions of $C = 0$ at $z = 0$ and $C = C_E$ at $z = \infty$, is:

$$F = (1-\phi)\rho_s C_E \sqrt{D_T \lambda} , \qquad (4\text{-}4)$$

where: C_E = ^{226}Ra concentration (atoms g^{-1} dry).

The estimates of ^{222}Rn flux from the sediments were given directly from the standing crop depth integration of excess ^{222}Rn in the water column. The profiles of excess ^{222}Rn were integrated point by point and the standing crop, S (dpm cm^{-2}) is given by:

$$S = \int_{\xi}^{z_b} Rn\,dz \qquad (4\text{-}5)$$

where: Rn = excess ^{222}Rn activity (dpm cm^{-3});

z = depth in water column (cm);

ξ = the depth of the top of the excess Rn profile;

z_b = the depth of the bottom.

The integration was done by applying the trapezoidal rule to the data profiles.

A very similar approach was applied to the depth distributions of ^{222}Rn and ^{226}Ra of two sediment cores. However, the assumed monotonic nature of the profiles allowed straight lines to be fitted to the data points thereby smoothing out some of the noise inherent in the ^{222}Rn analysis. The straight lines were fitted using a least squares cubic routine (York, 1966) that accounted for the error in the ^{222}Rn

measurements and the error in the depth. The total flux of ^{222}Rn out of the sediments was set equal to the depth integrated deficiency, ΣD (dpm cm^{-2}):

$$\Sigma D = \int_0^{\xi} Ra\,dz - \int_0^{\xi} Rn\,dz \qquad (4\text{-}6)$$

where: ξ = the depth of intersection between the ^{222}Rn and ^{226}Ra lines;

and all the other terms are the same as above.

Results

The ^{222}Rn production rates vs. distance offshore are presented in Figure 4-1. The ^{222}Rn production (dpm g^{-1}) decreased in an onshore direction. However, the porosity estimates (Table 4-1) also decreased in an onshore direction. The result of these two trends was a ^{222}Rn molecular diffusive flux that slightly increased in the onshore direction (Figure 4-2). This slight increase was statistically significant at the 90% confidence level (for samples stored frozen $n = 18$, $r = -0.41$), these were the lowest ^{222}Rn flux estimates made.

Figure 4-3 shows standing crop vs. distance offshore for all appropriate near-bottom profiles measured. There was a statistically significant linear trend to this data ($n = 20$, $r = -0.70$) at the 99.9% confidence level. These data suggest that the flux of ^{222}Rn from the sediments was increasing in the onshore direction. These fluxes ranged from ~1.5 to ~3 times higher than those estimated from the sediment surface grab samples (compare Tables 4-1 and 4-2).

The profiles of ^{222}Rn and ^{226}Ra for the cores taken in 1982 (HX028-0120) and 1983 (HX048-0014) are shown in Figure 4-4. The

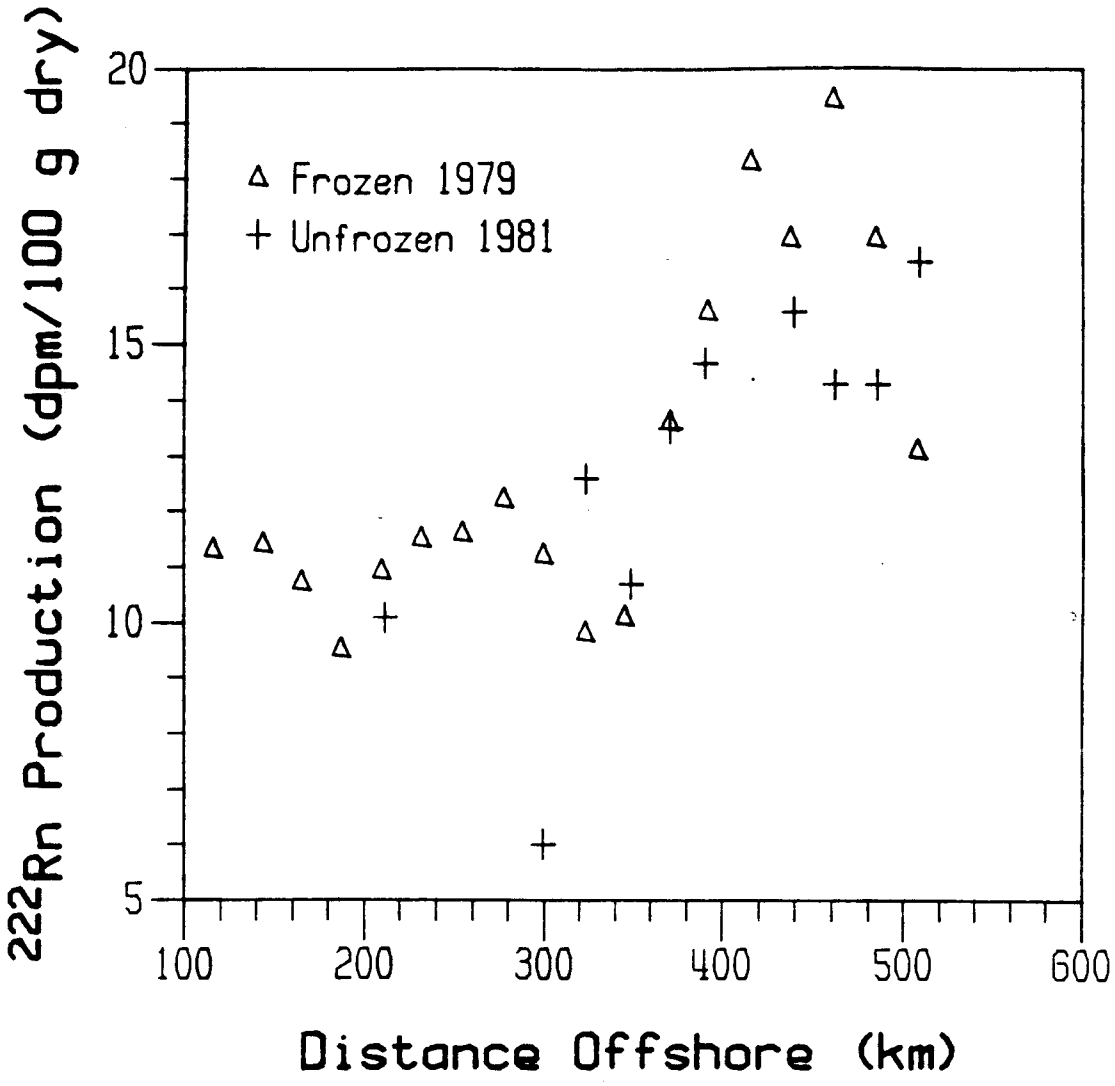

Figure 4-1. Radon-222 production rate versus distance offshore. Radon-222 production rate was determined from ^{226}Ra secular equilibrium activities of sediment grab samples collected in 1979 and 1981.

Table 4-1: **SEDIMENT ^{222}Rn PRODUCTION RATE AND MOLECULAR DIFFUSIVE FLUX**

Station	Porosity	^{222}Rn Prod	F_T
	1979 Grab samples (frozen)		
PRB- 3	0.532	0.131	3.95×10^{-3}
PRB- 4	0.625	0.169	4.08×10^{-3}
PRB- 5	0.651	0.194	4.36×10^{-3}
PRB- 6	0.687	0.169	3.41×10^{-3}
PRB- 7	0.664	0.183	3.96×10^{-3}
PRB- 8	0.613	0.156	3.89×10^{-3}
PRB- 9	0.711	0.136	2.53×10^{-3}
PRB-10	0.512	0.101	3.17×10^{-3}
PRB-11	0.524	0.098	3.01×10^{-3}
PRB-12	0.442	0.112	4.02×10^{-3}
PRB-13	0.470	0.122	4.16×10^{-3}
PRB-14	0.459	0.116	4.04×10^{-3}
PRB-15	0.477	0.115	3.87×10^{-3}
PRB-16	0.393	0.109	4.26×10^{-3}
PRB-17	0.348	0.095	3.99×10^{-3}
PRB-18	0.349	0.107	4.49×10^{-3}
PRB-19	0.347	0.114	4.79×10^{-3}
PRB-20	0.381	0.113	4.51×10^{-3}
	1981 Grab samples (unfrozen)		
TT159-4118	0.458	0.165	5.76×10^{-3}
TT159-4117	0.562	0.143	4.03×10^{-3}
TT159-4116	0.672	0.143	3.02×10^{-3}
TT159-4115	0.691	0.156	3.11×10^{-3}
TT159-4113	0.640	0.147	3.41×10^{-3}
TT159-4112	0.620	0.135	3.31×10^{-3}
TT159-4111	0.384	0.107	4.24×10^{-3}
TT159-4110	0.431	0.126	4.62×10^{-3}
TT159-4109	0.466	0.060	2.06×10^{-3}
TT159-4103	0.449	0.101	3.59×10^{-3}

Molecular diffusive ^{222}Rn flux is reported in atoms cm^{-2} sec^{-1}

Radon-222 production rate is reported in dpm/g dry.

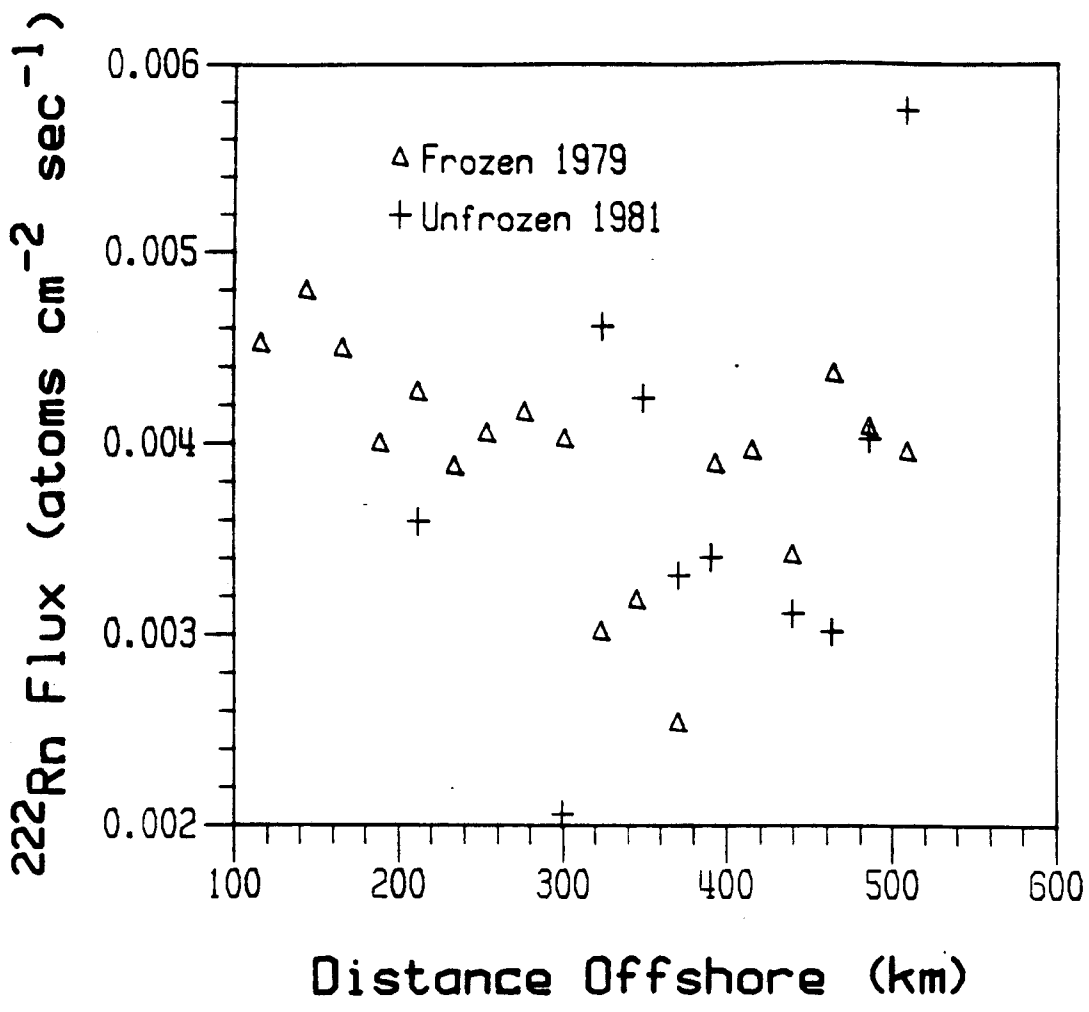

Figure 4-2. Molecular flux of ^{222}Rn from sediment versus distance offshore. Flux was estimated from the grab sample production rates and porosities. The unfrozen 1981 samples may have unreliable porosity estimates due to desiccation.

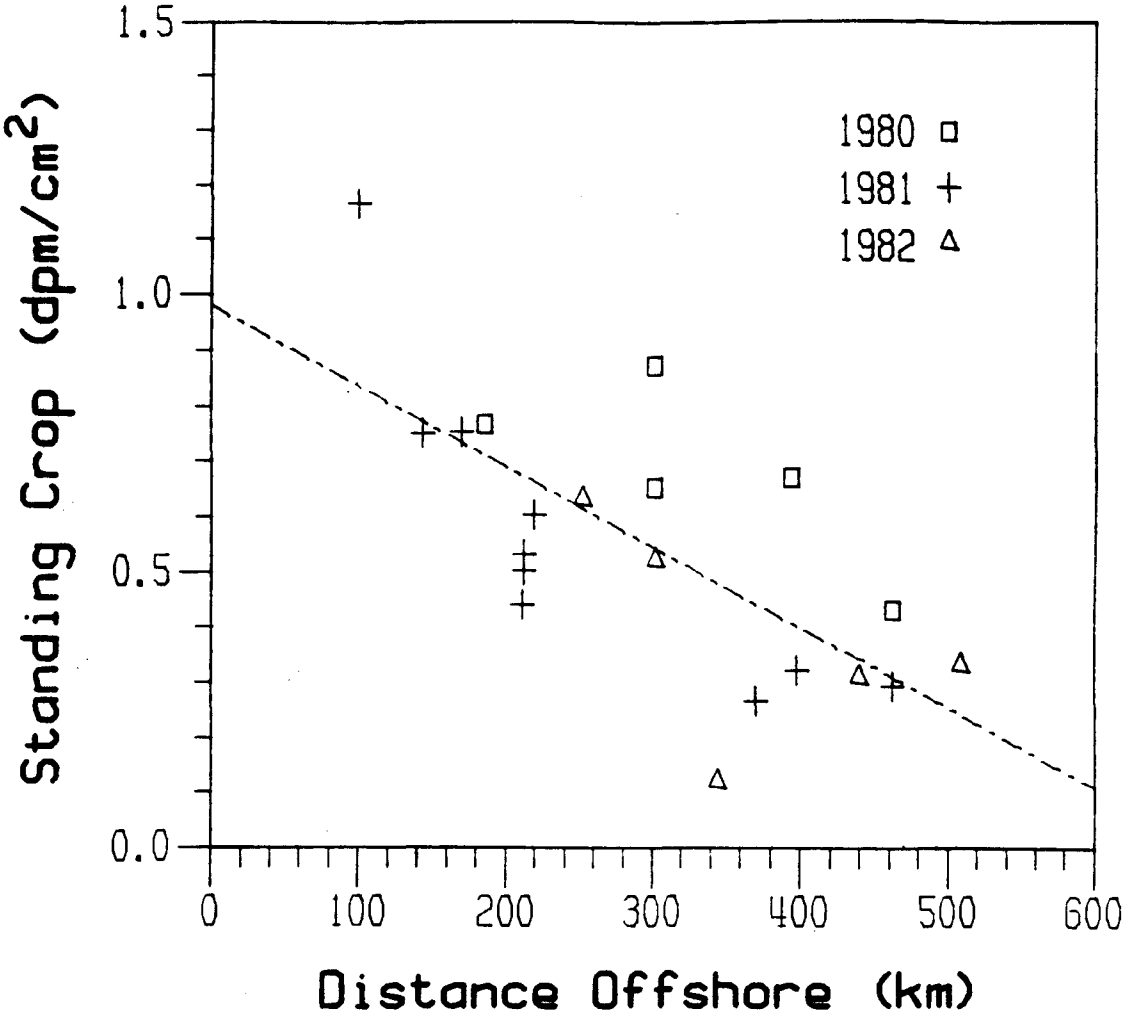

Figure 4-3. Excess ^{222}Rn standing crop versus distance offshore. The line shown is statistically significant at the 95% confidence level ($r = 0.70$, $n = 20$).

Table 4-2: **STANDING CROP OF EXCESS ^{222}Rn AND IMPLIED SEDIMENT FLUX**

Station	Domain	Depth (m)	Standing Crop	Sediment Flux
HX009-0056	inner	50	0.766	1.28×10^{-2}
TT159-3023	inner	44	0.750	1.25×10^{-2}
TT159-3033	inner	48	0.752	1.25×10^{-2}
TT159-4021	inner	40	1.166	1.94×10^{-2}
HX009-0012	middle	79	0.652	1.09×10^{-2}
HX009-0031	middle	79	0.874	1.46×10^{-2}
TT159-3066	middle	67	0.602	1.00×10^{-2}
TT159-3071*	middle	65	0.503	8.38×10^{-3}
TT159-4025*	middle	64	0.531	8.85×10^{-3}
TT159-4103	middle	64	0.439	7.32×10^{-3}
HX028-0010*	middle	80	0.522	8.71×10^{-3}
HX028-0041	middle	73	0.633	1.05×10^{-2}
HX028-0112	middle	93	0.121	2.02×10^{-3}
HX009-0005*	outer	138	0.430	7.17×10^{-3}
HX009-0008*	outer	121	0.671	1.12×10^{-2}
TT159-3058*	outer	112	0.322	5.37×10^{-3}
TT159-3115	outer	134	0.294	4.90×10^{-3}
TT159-4112	outer	104	0.266	4.44×10^{-3}
HX028-0046	outer	160	0.333	5.55×10^{-3}
HX028-0096*	outer	133	0.309	5.15×10^{-3}

Sediment flux is reported in atoms cm^{-2} sec^{-1}.

* means the top of the excess ^{222}Rn profile is missing and its depth is estimated.

Standing crop is reported in dpm/cm^2.

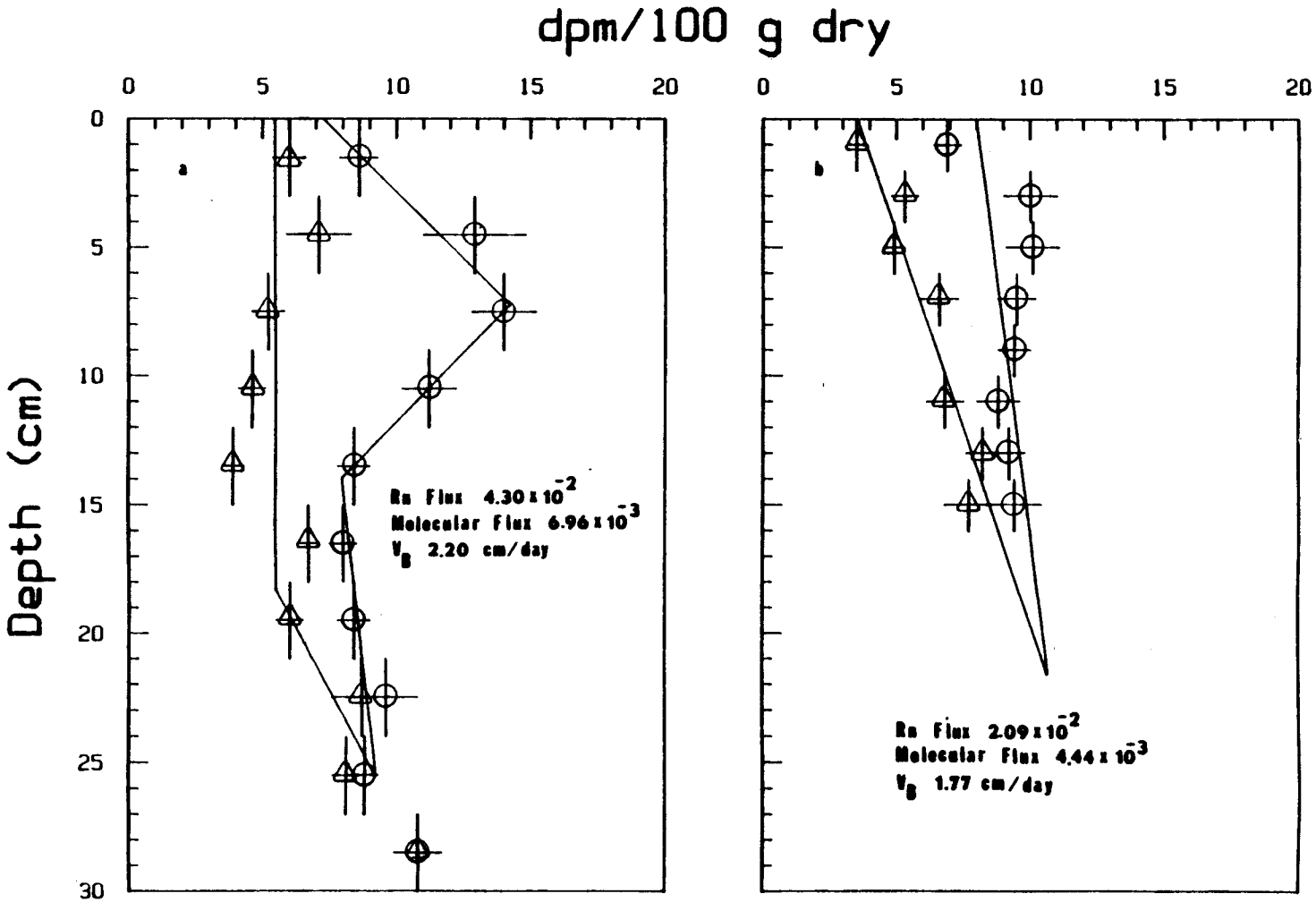

Figure 4-4. Radon-222 and ^{226}Ra depth distributions in sediment cores. The actual flux exceeds the molecular flux (atoms $cm^{-2} sec^{-1}$). a) Station HX028-0120, 110 m. b) Station HX048-0014, 129 m. △ ^{222}Rn. ○ ^{226}Ra.

integrated ^{222}Rn deficiency of these two cores implied a ^{222}Rn flux 2 to 7 times greater than either the grab sample or standing crop estimates above. The difference between the flux calculated from the ^{222}Rn deficiency and the calculated molecular diffusive flux suggested that another process(s) was occurring within the upper sediments on the southeastern Bering Sea shelf.

Discussion

Grab samples

Only the grab samples collected in 1979 were stored frozen, so the 1981 samples were not considered because of possible inaccurate porosities. The decrease in ^{222}Rn production rate onshore is statistically significant at the 99.9% confidence level ($n = 18$, $r = 0.73$) for the frozen samples. The decrease in porosity is also statistically significant at that level ($n = 18$, $r = 0.86$). However, the combination of these two variables is significant at only the 90% confidence level ($n = 18$, $r = -0.41$). A qualitative explanation for the molecular flux increasing onshore might have been the increase in average grain size of the sediments in the onshore direction (Sharma, 1979) allowed a greater permeability to ^{222}Rn.

The molecular diffusive flux of ^{222}Rn from the sediments was an important minimum flux boundary condition for the modeling of ^{222}Rn on the southeastern Bering Sea shelf. Assuming that no other processes were operating, the molecular diffusion of ^{222}Rn would be the minimum flux because ^{222}Rn concentrations in pore waters were much higher than the overlying water column. These molecular diffusive fluxes

compared favorably with those obtained by Smethie et al. (1981) on the Washington continental shelf and Imboden and Joller (1984) from sediments in Baldeggersee, Switzerland. Gruebel and Martens (1984) on the White Oak River estuary and Key et al. (1979a) in the Atlantic Ocean obtained slightly higher values. I assumed that these molecular diffusive fluxes were the lowest possible flux of ^{222}Rn from these sediments.

Standing crop

It was difficult to understand the increasing standing crop of excess ^{222}Rn other than in terms of an increasing sediment ^{222}Rn flux. If the excess ^{222}Rn concentration were equal across the shelf, then as the water depth decreased the standing crop of excess ^{222}Rn would decrease. Instead, the standing crop of excess ^{222}Rn showed a dramatic and statistically significant (at 99.9% confidence level) increase as the water column depth decreased ($n = 20$, $r = -0.70$ for all years, Table 4-2). This suggests that the sediments of the inner shelf were the largest source of excess ^{222}Rn on the southeastern Bering Sea shelf.

Just as the $\int f(x)dx$ is the area underneath the curve $f(x)$, the $\int f(x,z)dz$ is another function $g(x)$ relating g and x. This is essentially what the cross-shelf plot of standing crop is, where g is the mass of excess ^{222}Rn per unit area along x (the distance offshore). Figure 4-3 shows that the mass of excess ^{222}Rn linearly increased in an onshore direction. This mass of ^{222}Rn must have resulted from a larger source in that direction. The only reasonable

and likely candidate was the sediment of the inner shelf.

Core measurements

Several processes could be responsible for the flux of ^{222}Rn out of the sediments: molecular diffusion, bioturbation, physical mixing, bio-irrigation, physical irrigation and chemical processes (Smethie et al., 1981). Molecular diffusion (noted in Figure 4-4) was too small to account for the deficiency seen in the two cores. Bioturbation and physical mixing of sediment particles were disregarded based on the appearance of ^{210}Pb profiles for our sediment cores (Figure 4-5) and other cores from the PROBES area (Banahan, 1983). Bioturbation could be present without homogenizing ^{210}Pb (Kipphut, 1978), but in that case bioturbation would be too slow to affect sediment ^{222}Rn profiles (Imboden and Stiller, 1982). Additionally, physical erosion was unlikely since no large storm had passed over the sampling sites at least 10 days prior to coring. Ten days is the time it takes ^{222}Rn to reestablish a steady state distribution in undisturbed sediments (Smethie et al., 1981). Physical irrigation (wave pumping) can also be disregarded because of the small effect this process has at these depths (>100m). Even under the worse wind-wave conditions encountered on the southeastern Bering Sea, wave pumping is 2 orders of magnitude too small to account for ^{222}Rn deficit (Riedl et al., 1972). The chemical process of ^{222}Rn stripping by methane ebullition (Kipphut and Martens, 1982) can be discounted due to the oxic condition of the sediments. By the process of elimination, bio-irrigation appeared to be the most likely possibility because a rather large community of

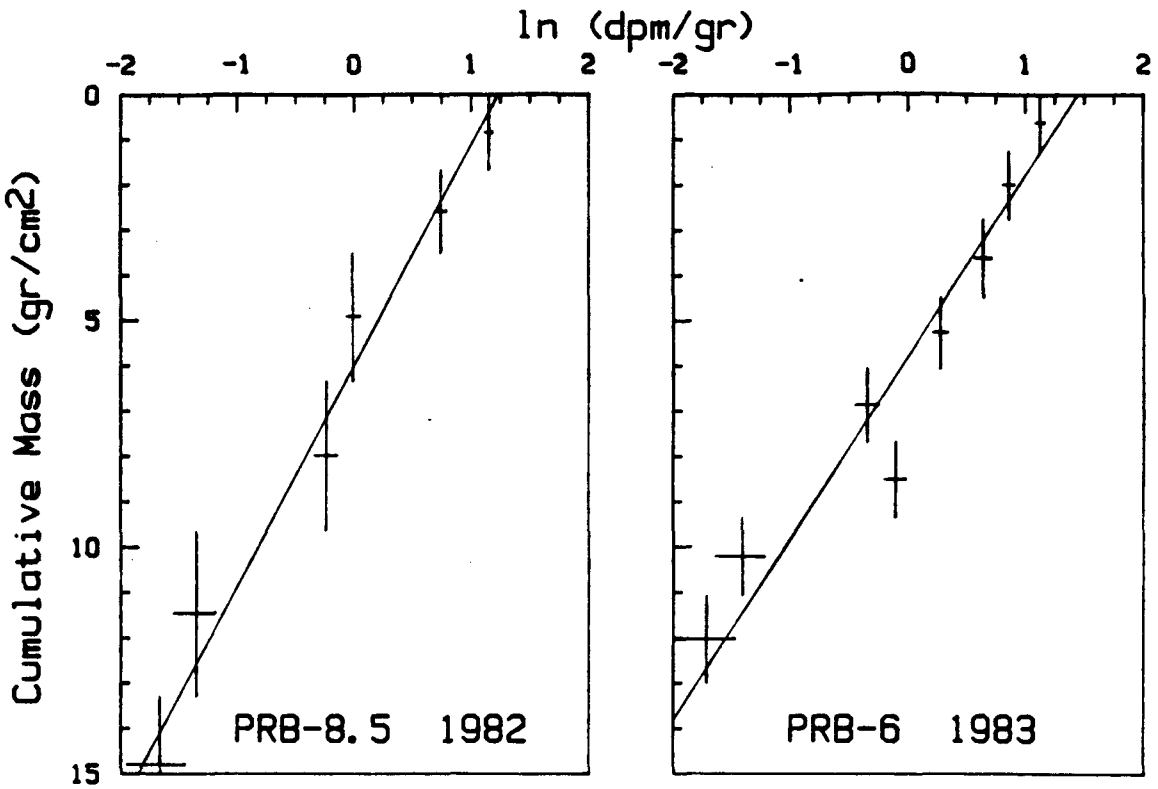

Figure 4-5. ln(^{210}Pb activities) versus cumulative mass. Samples for ^{210}Pb analysis were taken from the same cores in Figure 4-4. PRB-8.5 was station HX028-0120 and PRB-6 was station HX048-0014. Note the lack of an homogeneous ^{210}Pb layer near the surface of the sediments.

suspension-feeding infauna inhabit this shelf (Haflinger, 1978). Bio-irrigation rates (calculated following Smethie et al., 1981) are presented in Figure 4-4.

Biological irrigation rates are calculated for cores from the Washington continental shelf (Smethie et al., 1981) and San Francisco Bay (Hammond and Fuller, 1979); similar rates are presented in Figure 4-4 for cores from the southeastern Bering Sea shelf. The model assumed that the ^{222}Rn flux out of the sediments resulted from molecular diffusion and biological irrigation. Beginning with a simple box model for the sediment column the governing equation for ^{222}Rn can be written as:

$$Flux_{in} - Flux_{out} + production - decay = 0, \qquad (4\text{-}7)$$

which assumes steady state. This equation is solved for the term of interest:

$$Flux_{out} = Flux_{in} + production - decay. \qquad (4\text{-}8)$$

The following substitutions are made:

$$Flux_{out} = V_B C$$

$$Flux_{in} = D_T \frac{\Delta C}{\Delta z} \qquad (4\text{-}9)$$

$$production - decay = \Sigma D = \int_0^{\xi} (Ra - Rn)dz.$$

Solving for biological irrigation, V_B (cm sec^{-1}):

$$V_B = [Rn_{iw}^{\circ}]^{-1}\left[\Sigma D - D_T \frac{\Delta[Rn_s]}{\Delta z}\Big|_o\right] \qquad (4\text{-}10)$$

where $\frac{\Delta[Rn_s]}{\Delta z}\Big|_o$ = ^{222}Rn concentration gradient in wet sediment (atoms cm^{-4}) at the sediment-seawater interface;

$[Rn^{\circ}_{iw}]$ = ^{222}Rn concentration in the interstitial water 1 cm below the interface (atoms cm^{-3}).

All the other terms are the same as above. Unlike the cores examined by Smethie et al. (1981), there was no homogeneous zone of ^{210}Pb in our cores, so only one zone of deficiency was assumed. The line segments in Figure 4-4 were fitted, point by point, with the least-squares cubic routine of York (1966) and their intersection determined the base of the ^{222}Rn deficiency. Another line segment was started when an additional data point changed the slope by ≥2 standard deviations of the previous slope.

These flux estimates from the outer shelf were larger than either the grab sample or standing crop estimates. In addition, the possibile loss of the core top would underestimate the ^{222}Rn deficit in the cores. Underestimating the ^{222}Rn deficits would lead to a low ^{222}Rn fluxes where my flux estimates were already too large. The ^{210}Pb profiles showed no homogeneous surface layer implying that the top of the core may have been lost. The porosity of the top core segment in 1983 (~0.7 compare with porosities in Table 4-1) and the appearance of the sediment surface at the top of the core argued against this possiblity.

The ^{222}Rn deficit could be overestimated by loss of ^{222}Rn from the core during collection and handling. The core segments were extruded directly into He flushed Mason jars on deck immediately after collection. Handling loss was considered minimal because the core segments were in contact with the atmosphere for less than 60 secs.

However, core compaction during sediment penetration may have exuded extra ^{222}Rn from the sediment. The extreme competency of these sandy sediments precluded any significant compaction. These flux estimates must be considered upper limits of sediment ^{222}Rn flux, which was a very important boundary condition on the two-dimensional model (see Chapter 6).

Chapter 5: ONE DIMENSIONAL WATER MASS MIXING MODEL

When the going gets wierd, the wierd turn pro

Hunter S. Thompson

Introduction

The vertical mixing rate of nutrient-rich bottom waters (Reeburgh and Whitledge, 1981) from the southeastern Bering Sea shelf controls the supply of nutrients to the euphotic zone. Broecker (1965) proposed using near-bottom distributions of excess ^{222}Rn to model the vertical eddy diffusivity. This has been the *classic* use of ^{222}Rn in studies of near-bottom waters (see Broecker and Peng, 1982 for a comprehensive overview of this subject). The simple one-dimensional model used in this chapter balances vertical upward mixing of excess ^{222}Rn activity with radioactive decay. The two-dimensional nature of mixing on the southeastern Bering Sea shelf compromised this model seriously by pushing the vertical eddy diffusivities up to 2 orders of magnitude higher than other estimates. A few statistically significant results from this model yielded upper limits of the vertical eddy diffusivity.

Mathematical Methods

The one-dimensional model was applied to excess ^{222}Rn profiles with positive values near the bottom without consideration of the appearance of the profiles. This model fitted a one-dimensional *exponential* decay curve to the excess ^{222}Rn profiles. The only other requirement was the deepest sample must have been within 10 meters of the bottom. The data were selected from Appendix 1.

A steady state model (as outlined by Broecker, 1974) assuming no

lateral transport of ^{222}Rn and no advection was used to calculate the near-bottom vertical eddy diffusivities. The differential equation describing this model is given by:

$$\frac{dC}{dt} = 0 = \frac{d}{dz}\left[K_v \frac{dC}{dz}\right] - \lambda C \qquad (5\text{-}1)$$

where: K_v = the vertical eddy diffusivity ($m^2\ sec^{-1}$);

C = ^{222}Rn concentration;

z = distance above the bottom (m);

λ = ^{222}Rn decay constant ($2.1 \times 10^{-6}\ sec^{-1}$).

Making the assumption that the vertical eddy diffusivity is constant with depth simplified the differential equation to:

$$0 = K_v \frac{d^2C}{dz^2} - \lambda C, \qquad (5\text{-}2)$$

which can be rewritten as:

$$0 = K_v \frac{d^2Rn}{dz^2} - \lambda Rn_z, \qquad (5\text{-}3)$$

where: Rn_z = excess ^{222}Rn activity at distance z above bottom (dpm/100 kg).

Using as boundary conditions, $Rn_z \to Rn_o$ as $z \to 0$ and $Rn_z \to 0$ as $z \to \infty$; the solution is of the form:

$$Rn_z = Rn_o e^{-az} \qquad (5\text{-}4)$$

where: Rn_o = excess ^{222}Rn activity (dpm/100 kg) at the sediment-seawater interface;

$$a = \sqrt{\frac{\lambda}{K_v}}.$$

An exponential decay curve was fitted to the near bottom excess ^{222}Rn

distribution with a non-linear, least-squares cubic regression (York, 1966) performed on log-log transformed data. The equation fitted was of the form:

$$\ln(Rn_z) = \ln(Rn_o) - az, \qquad (5\text{-}5)$$

with the variables as defined above. With this regression routine the error associated with each ^{222}Rn measurement and each depth measurement was incorporated into the calculations. A propagation of errors calculation was used to estimate the uncertainty (shown as σ in Table 5-1) in the vertical eddy diffusivity. A correlation coefficient for each least-squares cubic fit was also calculated (correlation coefficients statistically significant at the 95% confidence level are marked with an asterisk in Table 5-1).

Results

Table 5-1 presents near bottom vertical eddy diffusivities calculated using a one-dimensional model on data from 1980, 1981 and 1982. Of the statistically significant values reported, two were from the inner shelf, three from the middle shelf and two from the outer shelf domain. With propagation of error estimates of standard deviations, the 95% confidence level significant values were 15.9 ± 9.6 $cm^2\ sec^{-1}$ for the inner shelf, 14.0 ± 8.5 $cm^2\ sec^{-1}$ for the middle shelf and 36.0 ± 7.8 $cm^2\ sec^{-1}$ for the outer shelf domain. It should be noted that the model used to obtain these vertical eddy diffusivities does not consider lateral mixing terms and are 1 to 2 orders of magnitude higher than independent estimates (Coachman, 1985) I believe this overestimation resulted from excess ^{222}Rn being

Table 5-1: **NEAR BOTTOM VERTICAL EDDY DIFFUSIVITIES FROM ONE-DIMENSIONAL MODEL**

Station	Depth (m)	Domain	n	K_v	σ	r
HX009-0056	50	inner	5	22.7	5.96	-0.962*
TT159-3033	48	inner	4	1.76	1.43	-0.806*
TT159-4021	40	inner	6	9.14	5.36	-0.878*
HX009-0012	79	middle	3	72.3	18.8	-0.925•
TT159-3066	67	middle	4	3450.	37000.	+0.082
TT159-3071	65	middle	4	126.	283.	-0.551•
TT159-4025	64	middle	5	143.	132.	-0.697*
TT159-4103	65	middle	8	23.6	10.5	-0.737*
HX028-0010	80	middle	6	10.6	5.63	-0.837*
HX028-0041	73	middle	7	7.69	6.17	-0.766*
HX028-0112	93	middle	8	752.	1300.	-0.462•
HX009-0005	139	outer	6	6200.	12700.	-0.455•
HX009-0008	121	outer	6	41.5	58.7	-0.839*
TT159-3058	112	outer	8	35200.	608000.	-0.175
TT159-3115	133	outer	3	69.4	140.	-0.655
TT159-4055	133	outer	7	555.	1690.	-0.379•
TT159-4112	104	outer	7	30.5	14.1	-0.905*
HX028-0046	160	outer	4	17.6	24.9	-0.582•
HX028-0096	133	outer	4	3.41	7.45	-0.469
TT159-3050	1682	off	4	16.1	3.09	-0.916*

* means statistically significant at the 95% confidence level.
† means statistically significant at the 80% confidence level.
@ means statistically significant at the 50% confidence level.

Vertical eddy diffusivity (K_v) is reported in $cm^2\ sec^{-1}$.

n is the number of data points used.

σ is one standard deviation of K_v.

r is the correlation coefficient.

transported horizontally into the water column.

Discussion

Applying the one-dimensional, vertical eddy diffusion model (Broecker, 1965 and Broecker et al., 1968) to the near-bottom excess ^{222}Rn distributions measured in this study gave only seven statistically significant fits (Table 5-1) at the 95% confidence level. In the past horizontal transport of ^{222}Rn has been invoked to explain non-linearities in the transformed data. Smethie (1981) included rapid horizontal mixing of ^{222}Rn from the sides of the fjords to improve the fit to his data. Broecker and Kaufman (1970) found maxima in their near bottom profiles that are explained as horizontal inputs of excess ^{222}Rn from surrounding "hills". Lietzke and Lerman (1975) used a two-dimensional numerical model to describe the distribution of ^{226}Ra on the eastern United States continental shelf. A similar approach for ^{222}Rn in a lake is used by Imboden and Emerson (1978) and in an offshore basin by Berelson et al. (1982). Measured horizontal and vertical gradients of ^{222}Rn in the southeastern Bering Sea waters times the respective eddy diffusivities reported by Coachman (1985) yield horizontal fluxes on the same order of magnitude as the vertical fluxes. This is consistant with what is known about the circulation of the shelf (Coachman, 1982) and tidal excursions on the shelf (Coachman and Charnell, 1979). Small mean flow on the southeastern Bering Sea shelf is significant on the outer and inner shelf and insignificant in the middle shelf regime (Schumacher and Kinder, 1983). Although significant, these mean flows can be ignored

since they are along the isobaths in a northwesterly direction in this study area and not across the shelf. Horizontal and vertical eddy diffusivities are calculated based on salt balance arguments and horizontal eddy diffusivities are found to be 5 to 6 orders of magnitude larger than vertical eddy diffusivities (Coachman and Walsh, 1981). Horizontal mixing is much more rapid than vertical mixing and could therefore be important.

Coachman (1985) determined vertical eddy diffusivities from temperature and salinity data for each of the three hydrographic domains on the southeastern Bering Sea shelf. The one-dimensional model assumed the ^{222}Rn can only be transported vertically in the water column. A comparison of the one-dimensional results with his evaluated the amount of ^{222}Rn in the profile that must be transported into the water column horizontally. If the bottom slope was steep enough, then ^{222}Rn would be transported to a sample location as quickly horizontally as vertically in the water column. This horizontally added ^{222}Rn would tend to cause the one-dimensional model to overestimate the vertical eddy diffusivity. The statistically significant outer shelf values for vertical eddy diffusivity were about a factor of two higher than that of Coachman (1985), implying horizontal flux was important here; the significant middle shelf values were approximately two orders of magnitude higher, indicating that horizontal transport was important in this domain. The inner shelf values I obtained were approximately a factor of two higher than the value reported by Coachman (1985) suggesting that horizontal flux

here was about as important as on the outer shelf. Schumacher and Kinder (1983) suggest that interaction between bottom slope variation and tidal action drives horizontal mixing on this shelf; my data were consistent with this notion.

Consideration of the statistically significant values at less than the 95% confidence level reported in Table 5-1 revealed the presence of horizontal flux of ^{222}Rn. On the inner shelf the 80% significant value was on the same order of magnitude as the 95% significant values implying that perhaps horizontal flux of ^{222}Rn here was not very large. However, further sampling of the near-bottom waters of the inner shelf is necessary before any conclusion can be reached. The 50% and one 80% significant values computed for the middle shelf were all much larger (some indeed were many orders of magnitude larger) than the 95% significant values. The middle shelf was a region of this shelf where the horizontal flux of ^{222}Rn must be present. The outer shelf 50% significant values were a blend of the inner and middle shelf results. Perhaps this is how a more detailed sampling of the inner shelf would appear. Clearly then, a one-dimensional fit to the data was insufficient to accurately assess the vertical eddy diffusivity on the southeastern Bering Sea shelf.

Chapter 6: TWO DIMENSIONAL WATER MASS MIXING MODEL

Raffinert ist der Herrgott aber boshaft ist Er nicht.

Albert Einstein

Introduction

The preceding chapters have shown the abilities and limitations of the traditional one-dimensional models of ^{222}Rn distributions. In this chapter I explain how a two-dimensional model better accounts for the distribution of ^{222}Rn in the Bering Sea waters. The one-dimensional models have assumptions that are violated to various degrees on this continental shelf. Evidence is given that property distributions were quasi-steady state and two-dimensional during the summer of 1981. This model's two-dimensional transport rates of ^{222}Rn in the water column agree with the fluxes out of the sediments and into the atmosphere. Better transport rates of ^{222}Rn in the water column unifies the three transport rates of air-sea gas exchange, water column mixing and sediment-water exchange.

The task this model set out to accomplish was to find a way to interpret the measured-data two-dimensionally. If the governing differential equation of ^{222}Rn could be solved, then a two-dimensional surface could be fit, by least squares, to the measured-data. The non-linear nature of the purely diffusive, two-dimensional governing differential equation of ^{222}Rn on the southeastern Bering Sea shelf made its solution intractable. Instead, a numerical finite difference approximation of the differential equation was fit to a grid of regularly spaced data points. Universal kriging was used to recast the

arbitrarily positioned measured-data into a regularly spaced grid. A χ^2 hypersurface search was used to optimize the horizontal and vertical eddy diffusivities to find the best fit of the numerical finite difference approximation equation to the kriged-data grid points.

The model employed here had four main parts and two major assumptions. The first part was the measured-data, which were collected during June and July of 1981. The second part was the two-dimensional grid of data points estimated from the original measured-data by universal kriging. The third part of the model involved the usage of a numerical finite differencing equation as an approximation of the differential equation that described the behavior of ^{222}Rn in a purely diffusive regime. The final part of the model found the optimal values for the horizontal and vertical eddy diffusivities by a χ^2 hypersurface search. The two key assumptions were: 1) the shelf was in quasi-steady state during the summer season and 2) the majority of the variability of properties on the shelf could be reduced to a two-dimensional section across the shelf.

The measured-data calculations are reviewed in Chapter 2 and the results presented in Appendix 1. The raw data was reduced with a Hewlett-Packard 86A personal computer. The universal kriging was done with the SURFACE-II software package available from the Kansas State Geologic Survey (Sampson, 1978). The measured-data was kriged on a Honeywell dual 66/20B mainframe computer. Additional references to universal kriging are available in Davis (1973), Olea (1974) and Clark

(1979). A comparison of the kriged vs. measured data is provided in Figure 6-1. The kriged data matrix was contoured by a subroutine of SURFACE-II and the results are shown in Figures 6-2 through 6-6. The χ^2 hypersurface searching routine was adapted from a similar, though one-dimensional, routine provided by Bevington (1969). The regularly spaced kriged-data grid was then modeled and the optimal eddy diffusivities obtained with a VAX 785 mini super computer. The eddy diffusivities, predicted transfer coefficients and sediment fluxes are reported in Tables 6-1, 6-2 and 6-3 respectively.

Mathematical Methods

Measured-data

To circumvent interannual variability, only the data collected during the summer of 1981 were used in the model. Nutrients and other properties (temperature, sigma-t) showed only vertical variability along the 70 m isobath (Reeburgh and Whitledge, 1981). Csanady (1976) and Coachman (1982) have argued that, in shallow seas, salt and other property fluxes are decoupled from the mean circulation. Coachman (1982) further argues property transport is accomplished by lateral diffusion across the southeastern Bering Sea shelf. I concluded from this that the cross-shelf variability of properties was much greater than the along-shelf variability and have projected all the 1981 ^{222}Rn profiles along isobaths onto one plane. Radon-222 profiles measured at non-tidal sampling interval showed little variation with time (Figure 6-7). Based upon the limited amount of data available and observed small variation in time I assumed that the shelf waters were in quasi-

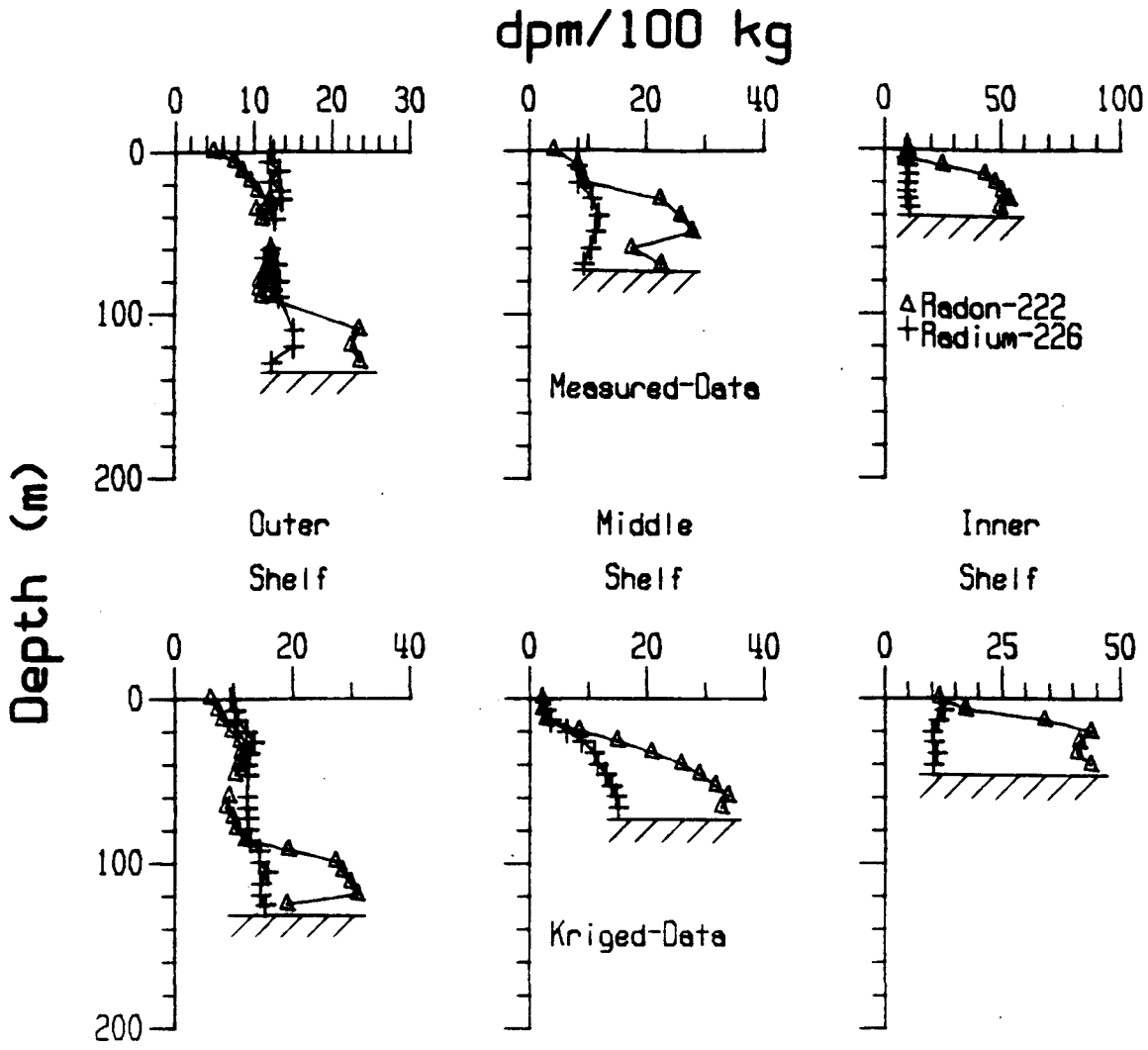

Figure 6-1. Comparison of measured-data and kriged-data profiles. The measure-data profiles were 392.1/462.8, 253.5 and 99.5 km offshore for the outer, middle and inner shelf domains; the kriged-data profiles were 396.05/441.75, 258.95 and 121.85 km offshore respectively. The middle shelf measured-data profile was measured in 1982 and therefore compares poorly with the kriged-data profile, which was based solely on 1981 data.

steady state during the summer season.

Kriged-data

Universal kriging is based on the theory of regionalized variables (see Olea, 1974). Given the problem of estimating a property value Z at a location x, find the optimal interpolation based on the measured data points surrounding x_o (x_o = the grid point). The coordinate system for this problem was oriented with x across the shelf, z positive downward with x = (x,z). The interpolated value of Z is given by:

$$Z^*(x) = \sum_{j=1}^{k} \eta_j Z(x_j) \qquad (6\text{-}1)$$

where: j = 1, k the number of "nearest" measured-data points found by an octant search (see Sampson, 1978);

η_j = the weight given to the measured-data point;

within a radius r around x_o. The optimal value of $Z^*(x)$ is obtained with the following constraints:

$$E[Z^*(x_o)-Z(x_o)] = 0 \qquad (6\text{-}2)$$

and

$$E[(Z^*(x_o)-Z(x_o)]^2] = \min(\eta_j), \qquad (6\text{-}3)$$

where E[ ] has the same meaning as the statistical expected value. These constraints imply that $Z^*(x)$ is an unbiased and best estimate of Z(x). The values for the weights (η_j), coefficients of the trend surface (μ_i) and a constant (ν) are found by Lagrange's method of multipliers on the following set of equations:

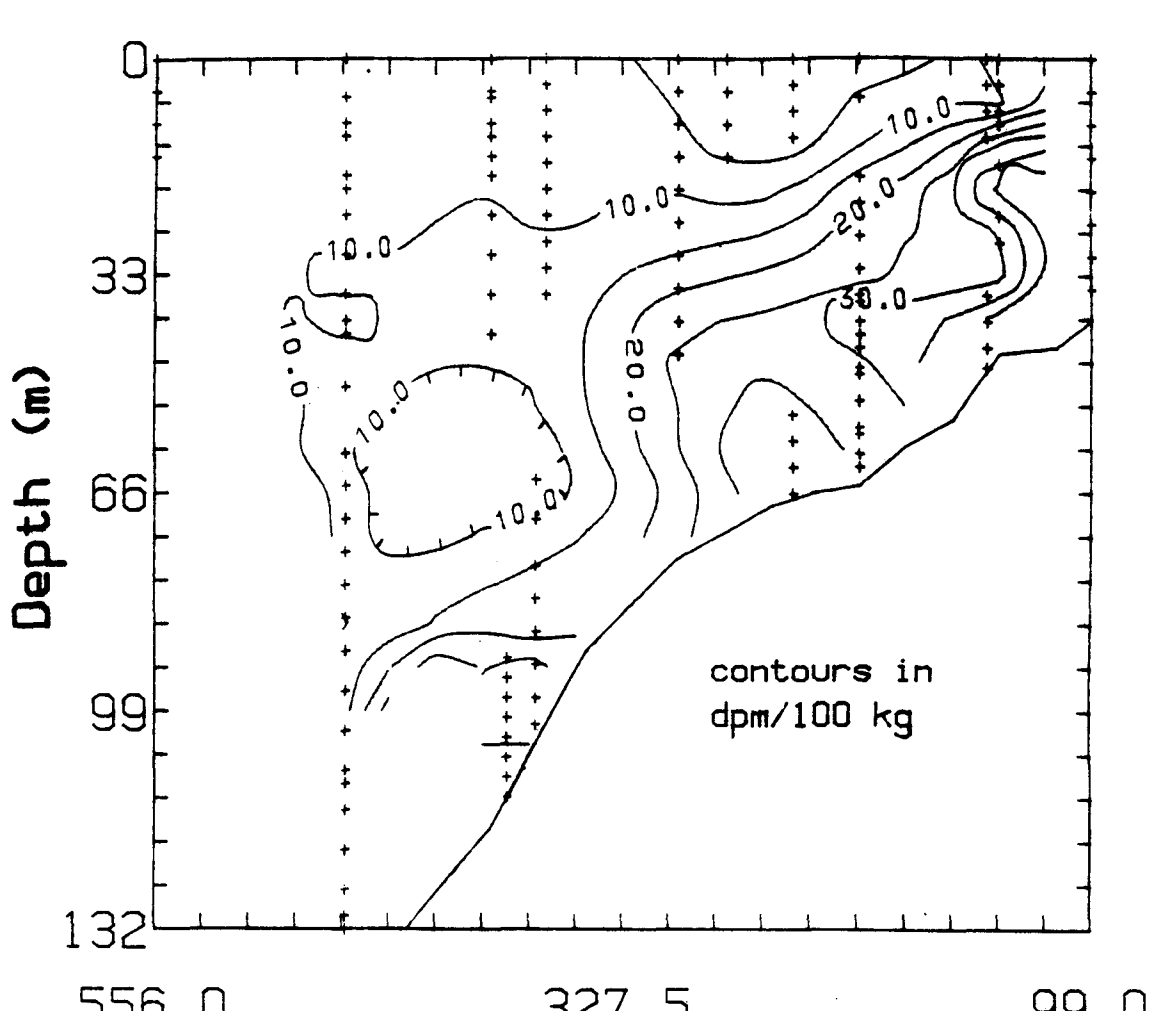

Figure 6-2. Total ^{222}Rn contour plot across the southeastern Bering Sea shelf. Prepared from the kriged-data matrix (see Appendix 2); the actual measured-data points are shown as (+).

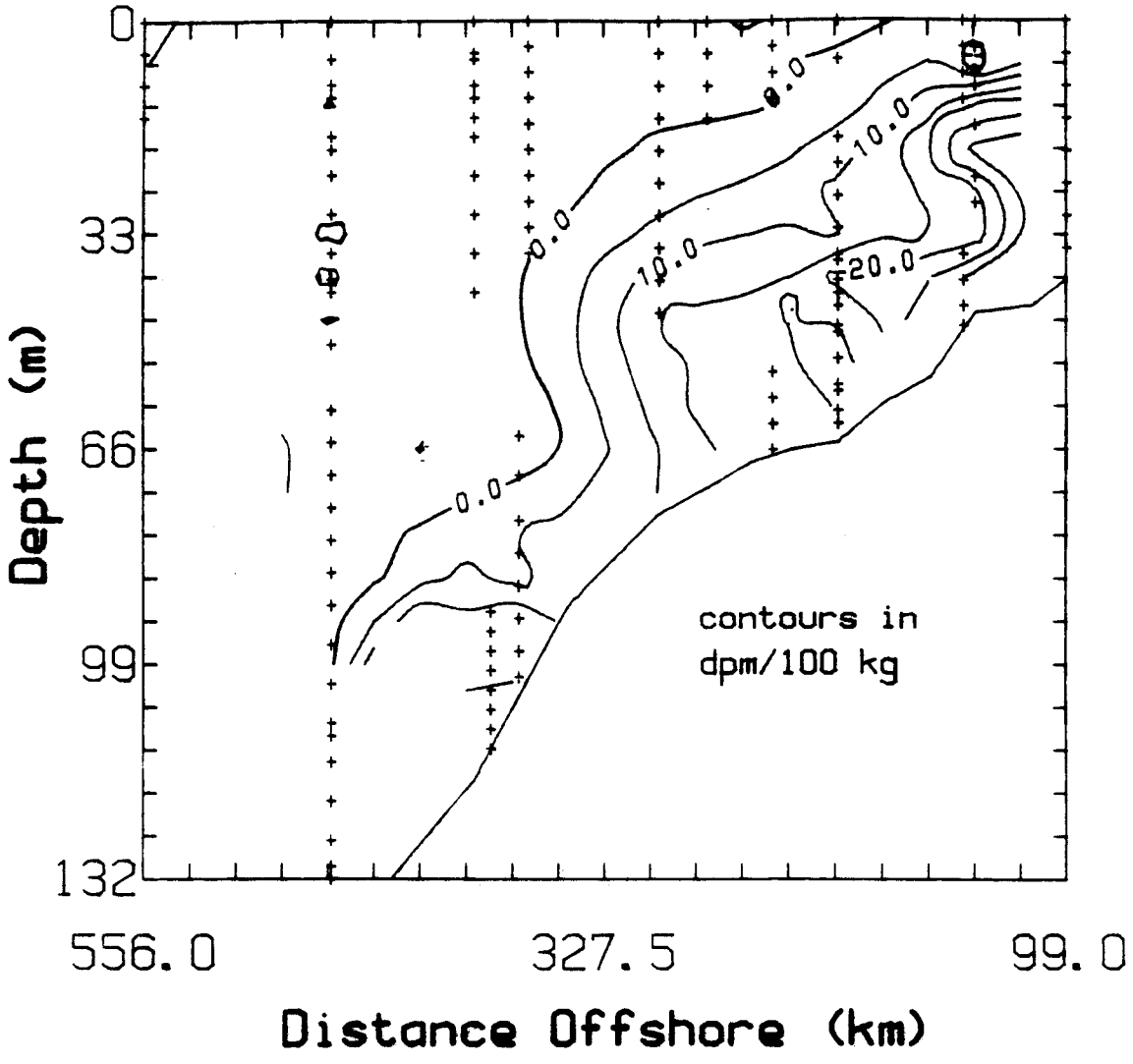

Figure 6-3. Excess ^{222}Rn contour plot across the southeastern Bering Sea shelf. Prepared from kriged-data matrix (see Appendix 2); the actual measured-data points are shown as (+).

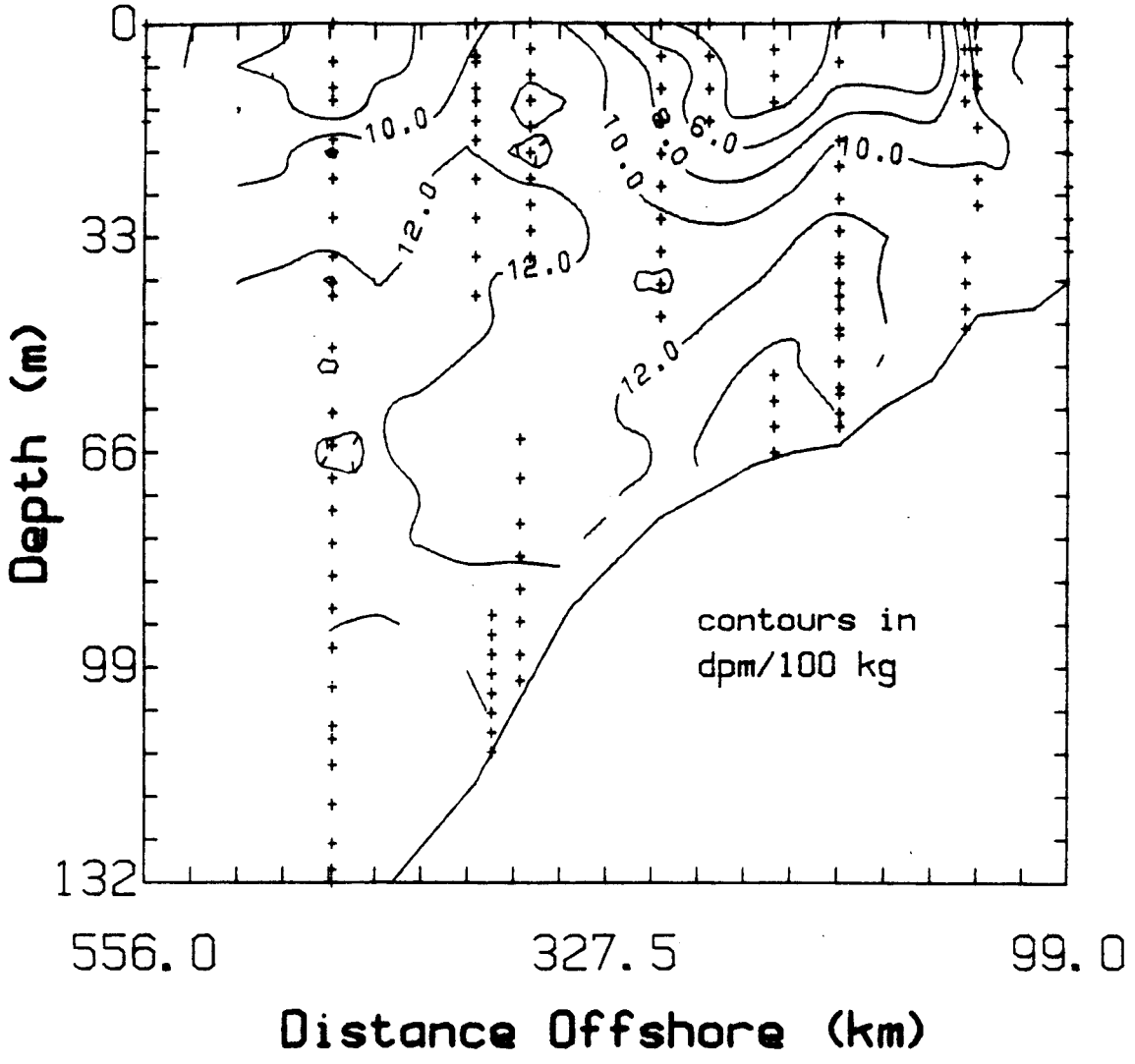

Figure 6-4. Radium-226 contour plot across the southeastern Bering Sea shelf. Prepared from kriged-data matrix (see Appendix 2); the actual measured-data points are shown as (+).

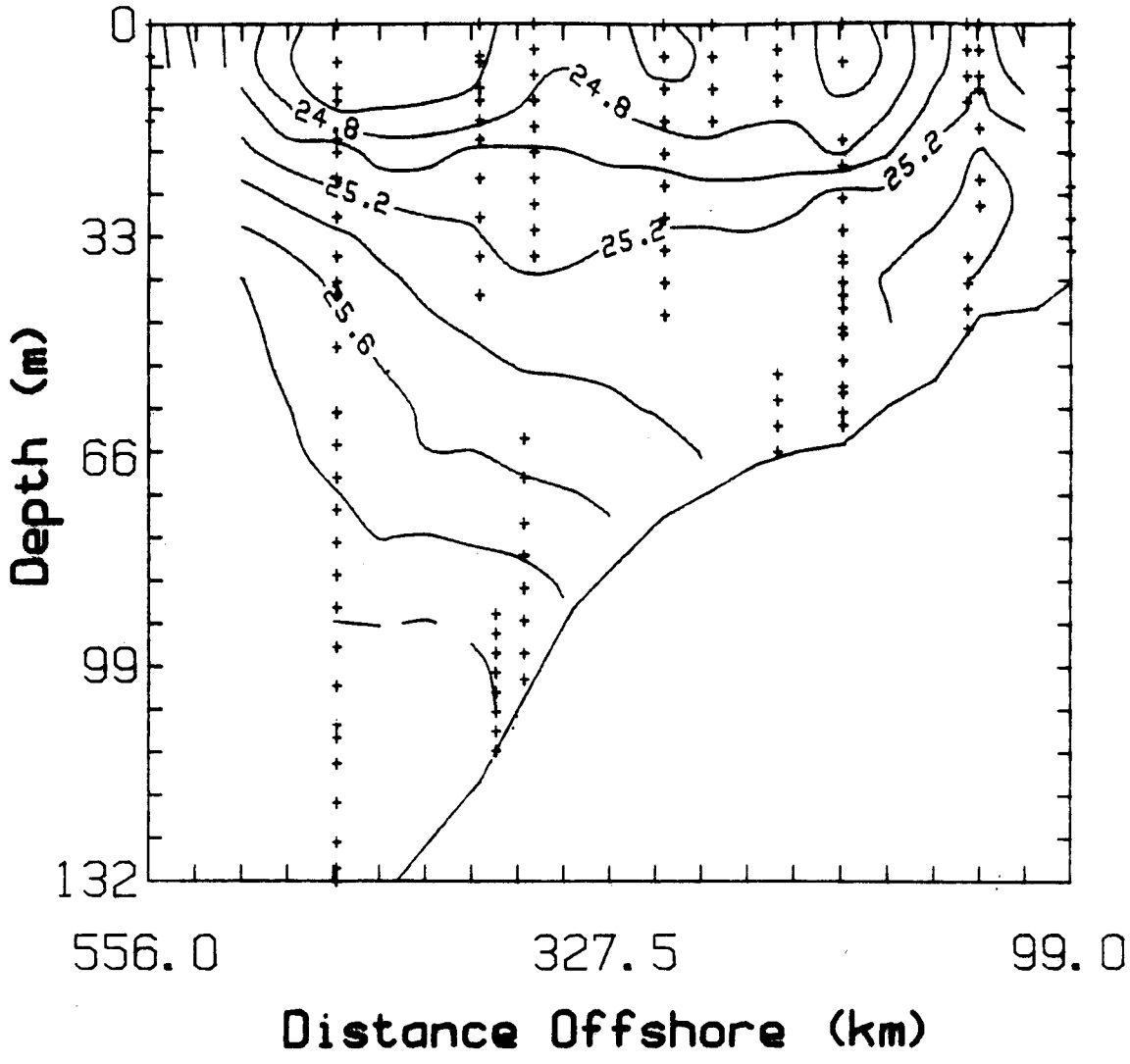

Figure 6-5. Sigma-t contour plot across the southeastern Bering Sea shelf. Prepared from kriged-data matrix (see Appendix 2); the actual measured-data points are shown as (+).

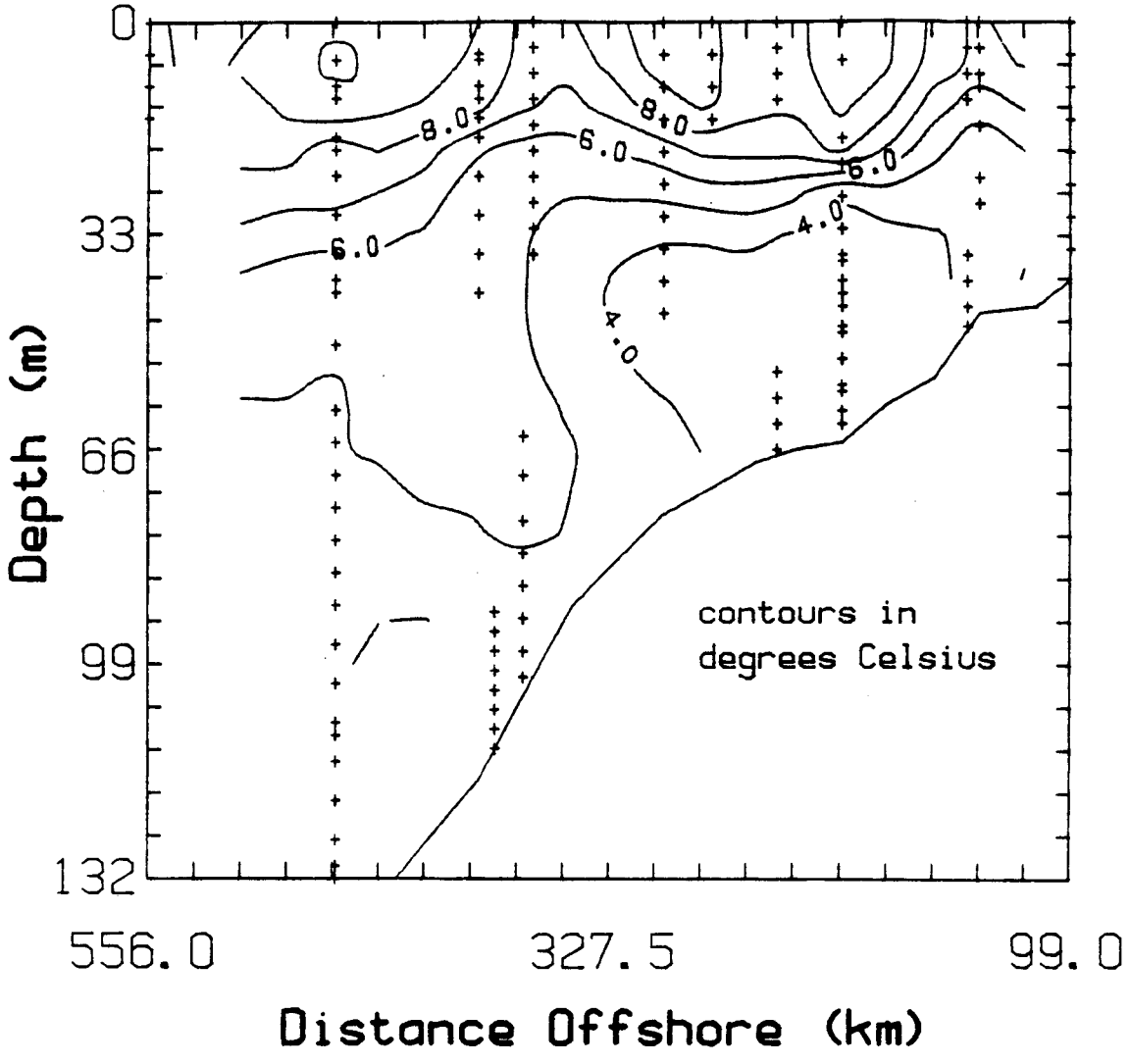

Figure 6-6. Temperature contour plot across the southeastern Bering Sea shelf. Prepared from kriged-data matrix (see Appendix 2); the actual measured-data points are shown as (+).

$$\sum_{jj=1}^{k} \eta_{jj}\gamma(x_1-x_{jj}) + \sum_{i=1}^{N} \mu_i f^i(x_1) + \nu = \gamma(x_1-x_0)$$

$$\sum_{jj=1}^{k} \eta_{jj}\gamma(x_2-x_{jj}) + \sum_{i=1}^{N} \mu_i f^i(x_2) + \nu = \gamma(x_2-x_0)$$

$$\cdots$$

$$\sum_{jj=1}^{k} \eta_{jj}\gamma(x_j-x_{jj}) + \sum_{i=1}^{N} \mu_i f^i(x_j) + \nu = \gamma(x_j-x_0)$$

$$\cdots$$

$$\sum_{jj=1}^{k} \eta_{jj}\gamma(x_k-x_{jj}) + \sum_{i=1}^{N} \mu_i f^i(x_k) + \nu = \gamma(x_k-x_0)$$

$$\sum_{j=1}^{k} \eta_j f^1(x_j) = f^1(x_0) \qquad (6\text{-}4)$$

$$\sum_{j=1}^{k} \eta_j f^2(x_j) = f^2(x_0)$$

$$\cdots$$

$$\sum_{j=1}^{k} \eta_j f^i(x_j) = f^i(x_0)$$

$$\cdots$$

$$\sum_{j=1}^{k} \eta_j f^N(x_j) = f^N(x_0)$$

$$\sum_{j=1}^{k} \eta_j = 1.$$

Here i = 1, N the number of measured-data points and $\gamma(x_j-x_{jj})$ is the semivariogram of the residuals (discussed below) and $f^i(x_j)$ are arbitrary functions of x defined by:

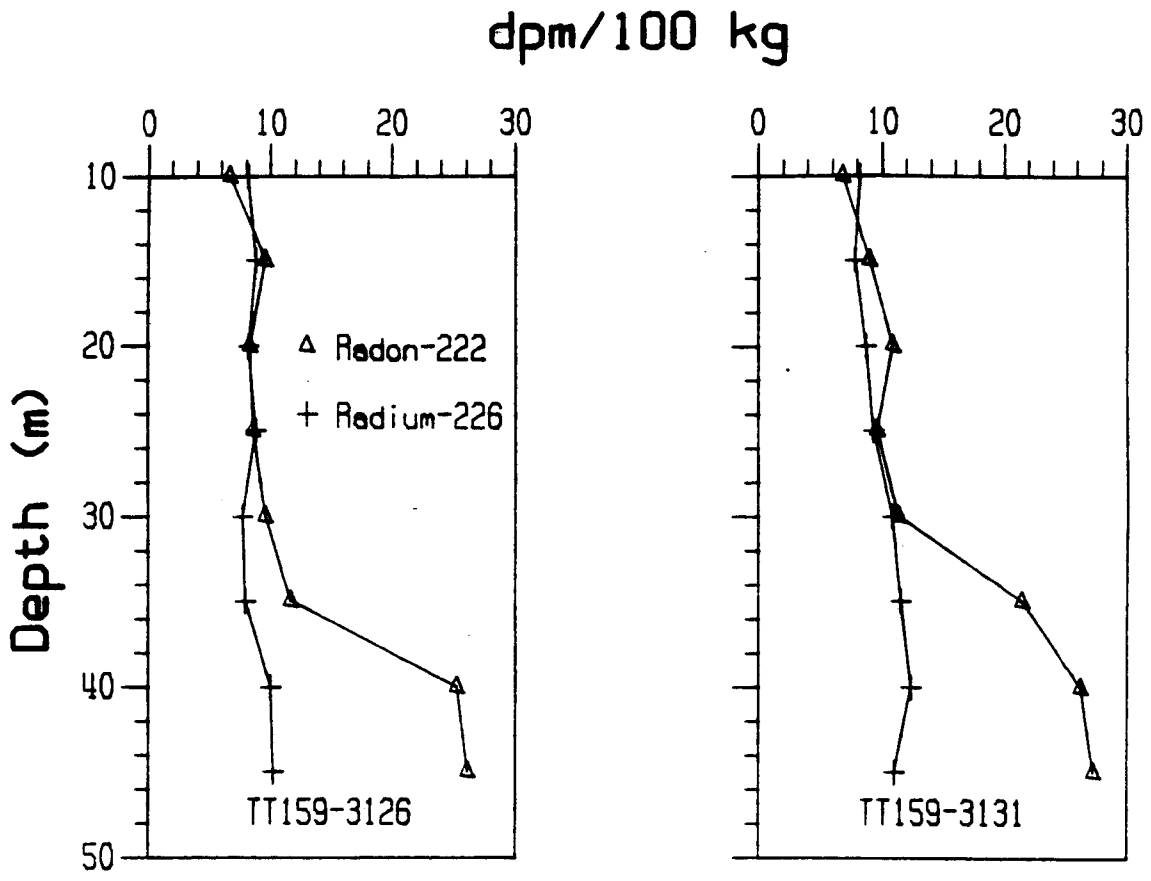

Figure 6-7. Two water column ^{222}Rn and ^{226}Ra profiles measured at non-tidal sampling intervals. The similarity between these two profiles is tcken as further evidence that the southeastern Bering Sea shelf was in quasi-steady state during the summer of 1981.

$$E[Z(x)] = a_0 + \sum_{i=1}^{N} b_i f^i(x), \qquad (6\text{-}5)$$

where $E[Z(x)]$ = the drift determined by a trend surface analysis. Additionally, an estimate of the error associated with each kriged grid point is given by:

$$\mathrm{var}[Z^*(x_0)-Z(x_0)] = \sum_{j=1}^{k} \eta_j \gamma(x_j-x_0) + \sum_{i=1}^{N} \mu_i f^i(x_0) + \nu, \qquad (6\text{-}6)$$

which is based on the geometry of the surrounding measured data points.

The process of kriging the ^{222}Rn data was carried out in seven steps for each property measured. The data was first collated into a data file containing x, z, ^{222}Rn, ^{226}Ra, XS ^{222}Rn, temperature (T) and sigma-t (σ_t). Next the (x,z) coordinates were non-dimensionalized to the range of 0 → 1. A linear trend surface was then approximated to each property field (^{222}Rn, ^{226}Ra, XS ^{222}Rn, T and σ_t). The linear trend surface was subtracted from the original data and the residuals retained. A linear approximation of the semivariogram function was estimated from the residuals. The non-dimensionalized coordinates, original measured property values and the slope of the estimated linear semivariogram were then fed into the SURFACE-II kriging subroutine. Finally, the kriged data grid results were contoured and the kriged data matrix and its associated error matrix were printed out.

SURFACE-II uses an octant search for nearest measured-data points to the point to be kriged (Sampson, 1978). The extremely thin nature

of the shelf waters (width ~500 km, depth ~150 m) resulted in a failure to find sufficient points for kriging estimation of the grid point if x was given in (m,m) or (km,km). The location x was linearly recast into a range of $0 \rightarrow 1$ on a 21 X 21 grid matrix. The result was a kriged data matrix with $\Delta x \simeq 22.85$ km and $\Delta z \simeq 6.6$ m.

Equations (6-2) and (6-3) were used to constrain the optimization of $Z^*(x)$. Equation (6-2) requires that the estimation of the semivariogram be accomplished with data points having no large scale trend. Hence, prior to the estimation of a semivariogram function a linear surface was fitted to the measured-data by the trend surface subroutine of the SURFACE-II package (Sampson, 1978). The semivariogram estimation routine used this linear trend surface to calculate the residuals from which the semivariogram was approximated.

The semivariogram can be estimated by several functions (Davis, 1973). However, the kriging subroutine provided by SURFACE-II can only use the linear estimation model (Sampson, 1978 and Davis, 1973). Consequently, the semivariogram estimation program first removed a linear trend surface from the original measured data, then calculated the discrete semivariances with increasing distance between data points. Finally, the program fit a straight line to the discrete values. This procedure was carried out up to half the range of the data in both the x and z directions. Both directions were considered due to anisotropy in the property fields. The slopes of the straight line fitted to the discrete semivariance vs. increasing distance between data points was the final product of this routine.

The grid points were estimated using the universal kriging subroutine of the SURFACE-II package (Sampson, 1978). The non-dimensionalized x and z, original measured property fields, slopes of the linear estimated function of the semivariogram in both directions and the search radius for the kriging were the inputs to the subroutine subject to the following additional constraints. To avoid overextending the estimation routine, approximately only as many grid points as actual measured-data points were estimated. The dimensions of the grid matrix were arrived at by approximating the number of actual measured-data points with the number of successfully estimated grid points. Blanking of the grid matrix by the topography of the shelf bottom and search failures in the octant searches led to the decision of a 21 x 21 matrix. Additionally, to avoid independent property values inside the search radius the radius was limited to half the total range of the data points (0.5 non-dimensional units). Finally, the resultant grid was contoured and the grid point matrix of estimated property values and the error estimate of each grid point was then printed out. The grid point values of total ^{222}Rn, ^{226}Ra, σ_t and temperature were subsequently used in the χ^2 hypersurface search model.

Functional approximation of ^{222}Rn distribution

Two more assumptions were added to the two key assumptions, given above, to arrive at the governing equation of ^{222}Rn on the southeastern Bering Sea shelf. The results of 30 current meter locations of >1 month duration have led Coachman (1985) to conclude

that there is no significant net advection on the middle shelf. The first additional assumption was: advection had a negligible effect on the ^{222}Rn distribution on the middle shelf. Additionally, within any a priori chosen region of the shelf, I have assumed that the eddy diffusivities were constant. The last assumption had to be made due to our general ignorance of the functional dependence of the eddy diffusivities with depth, velocity shear and density gradient.

The above assumptions led to the following governing equation of ^{222}Rn on the southeastern Bering Sea shelf:

$$\frac{\partial C}{\partial t} = K_H \frac{\partial^2 C}{\partial x^2} + K_v \frac{\partial^2 C}{\partial z^2} + P - \lambda C = 0 \qquad (6\text{-}7)$$

where: C = ^{222}Rn concentration (atoms cm^{-3}),

P = ^{222}Rn production rate (atoms sec^{-1} cm^{-3}),

λ = ^{222}Rn decay constant (2.1×10^{-6} sec^{-1}),

K_H = horizontal eddy diffusivity (cm^2 sec^{-1}),

K_v = vertical eddy diffusivity (cm^2 sec^{-1}).

The analytical solution of equation (6-7) is difficult at best and intractable at its worst. However, the above equation can be approximated by a numerical finite differencing equation.

The numerical finite differencing approximation of the above differential equation is:

$$0 = \frac{K_H}{\Delta x^2}(C_{j,k+1} - 2C_{jk} + C_{j,k-1}) + \frac{K_v}{\Delta z^2}(C_{j+1,k} - 2C_{jk} + C_{j-1,k}) + P_{jk} - \lambda C_{jk} \qquad (6\text{-}8)$$

where: Δx = grid spacing across the shelf (22.85 km),

Δz = grid spacing with depth on shelf (6.6 m),

j,k = 1, 21 the grid point indicies of the kriged data set, and the rest is the same as above. The finite differencing equation can be rearranged and solved for $C_{j,k}$ giving:

$$C^{*}_{jk} = \left[\frac{2K_H}{\Delta x^2} + \frac{2K_v}{\Delta z^2} + \lambda\right]^{-1}\left[\frac{K_H}{\Delta x^2}(C_{j,k+1} + C_{j,k-1}) + \frac{K_v}{\Delta z^2}(C_{j+1,k} + C_{j-1,j}) + P_{jk}\right] \quad (6\text{-}9)$$

where: C^{*}_{jk} = the fitted or estimated ^{222}Rn concentration.

Equation (6-9) provides a means by which each grid point was estimated as a function of the surrounding grid points, K_H, K_v, Δx, Δz, λ and production. When the surrounding grid points and the production rate were taken as knowns, the problem was to find the optimal values of the constant parameters to explain the data distribution. But equation (6-9) is non-linear in K_H and K_v and these parameters in the *normal equations* of the usual least-squares approach cannot be separated into different terms of sums.

χ^2 hypersurface search for optimal K_H and K_v

Any given function can be decomposed into dependent variable(s), indepedent variable(s) and constant parameter(s). Equation (6-9) above has for its dependent variable C^{*}_{jk}; its independent variables are $C_{j+1,k}$, $C_{j-1,k}$, $C_{j,k+1}$, $C_{j,k-1}$ and P_{jk}; and its constant parameters are K_H, K_v, λ, Δx and Δz. The parameters Δx and Δz were set by the constraints mentioned above when the kriged data matrix was calculated. The parameter λ was set by the nature of the isotope under discussion. The problem reduced to finding the optimal values of K_H

and K_v producing the best fit of C^*_{jk} to C_{jk}. This best fit was found by using the minimization of χ^2 as the optimization criterion.

Chi-square is expressed as a measure of *goodness of fit* between C^*_{jk} and C_{jk}:

$$\chi^2 = \sum_j^m \sum_k^n \left[\frac{1}{\sigma^2_{jk}} (C_{jk} - C^*_{jk})^2 \right] \qquad (6\text{-}10)$$

where: σ_{jk} = the standard deviation or error of each grid point,

$j = 1, 21$ the row index of the grid matrix (m rows),

$k = 1, 21$ the column index of the grid matrix (n columns).

Optimal values were found by minimizing χ^2 with respect to K_H and K_v simultaneously, i.e.

$$\frac{\partial \chi^2}{\partial K_i} = \frac{\partial}{\partial K_i} \left[\sum_j^m \sum_k^n (C_{jk} - C^*_{jk})^2 \right] = 0 \qquad (6\text{-}11)$$

where: $i = 1, 2$; $K_H = K_1$ and $K_v = K_2$.

Essentially then, this minimization of χ^2 with respect to K_1 and K_2 was a non-linear, least-squares fit to an arbitrary function (see Bevington, 1969 on this subject).

A straight forward way to find the optimal parameters is a *brute force* search of parameter space and thereby finding the minimum χ^2 (Bevington, 1969). However, a more convenient method was implemented by approximating the χ^2 hypersurface with a parabolic surface and finding the minimum directly. The advantages of this method were 1) there were fewer points on the χ^2 hypersurface to be evaluated hence it was faster, 2) the method chose its own step size and freed the

user from the need to find the optimal step size and 3) this approach was iterated for greater accuracy.

The parabolic approximation starts with a Taylor series expansion of χ^2:

$$\chi^2 = \chi_o^2 + \sum_i \left[\frac{\partial \chi_o^2}{\partial K_i} \delta K_i \right] \qquad (6\text{-}12)$$

where: χ_o^2 = the value at the initial guess of K_1 and K_2,

δK_i = parameter increments of K_1 and K_2.

Then minimizing with respect to K_j yields:

$$\frac{\partial \chi^2}{\partial K_j} = \frac{\partial \chi_o^2}{\partial K_j} + \sum_j^p \left[\frac{\partial^2 \chi_o^2}{\partial K_i \partial K_j} \delta K_i \right] = 0, \qquad (6\text{-}13)$$

where: $j = 1, p$ the number of parameters to be optimized.

This results in a set of p simultaneous equations with respect to δK_i as in:

$$\beta_j = \sum_j^p (\delta K_j \alpha_{i\,j})$$

$$\beta_j = \frac{-1}{2} \frac{\partial \chi_o^2}{\partial K_j} \qquad \alpha_{i\,j} = \frac{1}{2} \frac{\partial^2 \chi_o^2}{\partial K_i \partial K_j}. \qquad (6\text{-}14)$$

Bevington (1969) has shown that the solution to the above set of equations is equivalent to approximating the χ^2 hypersurface with a parabolic surface. After finding χ^2 at three different points in parameter space [ie. $(K_1, K_2)_1$, $(K_1, K_2)_2$, $(K_1, K_2)_3$] a parabolic interpolation of the χ^2 hypersurface is made via:

$$K_i(\chi^2_{min}) = K_i(3) - \Delta K_i \left[\frac{\chi^2(3) - \chi^2(2)}{\chi^2(3) - 2\chi^2(2) + \chi^2(1)} + \frac{1}{2} \right] \qquad (6\text{-}15)$$

and for each K_i, in turn, its value corresponding to the local minimum

on the χ^2 hypersurface is estimated.

An estimate of the error in each parameter optimized was obtained in the following manner. The solution of equations (6-14) involves the inversion of α, the curvature matrix:

$$\delta K = \beta\alpha^{-1} = \beta\epsilon. \tag{6-16}$$

The matrix ϵ is referred to as the error matrix (Bevington, 1969). If the variation of χ^2 is independent of variations in the parameters to be fitted, ie:

$$\frac{\partial^2\chi_o^2}{\partial K_1 \partial K_2} = 0, \tag{6-17}$$

then the off-diagonal elements of α and ϵ are zero and the error associated with each fitted parameter is calculated as:

$$\sigma_{K_j}^2 = \epsilon_{jj}. \tag{6-18}$$

The χ^2 fitting routine was adapted from Bevington (1969) and essentially followed the following steps. A main program passed an initial guess of K_1, ΔK_1, K_2 and ΔK_2 to the χ^2 fitting subroutine. The elements of the curvature matrix, α, are approximated according to the following set of equations:

$$\frac{\partial\chi_o^2}{\partial K_i} \simeq \frac{\chi_o^2(K_i+\Delta K_i, K_j) - \chi_o^2(K_i-\Delta K_i, K_j)}{2\Delta K_i}$$

$$\frac{\partial^2\chi_o^2}{\partial K_i^2} \simeq \frac{\chi_o^2(K_i+\Delta K_i, K_j) - 2\chi_o^2(K_i, K_j) + \chi_o^2(K_i-\Delta K_i, K_j)}{\Delta K_i^2} \tag{6-19}$$

$$\frac{\partial^2\chi_o^2}{\partial K_i \partial K_j} \simeq \frac{\chi_o^2(K_i+\Delta K_i, K_j+\Delta K_j) - \chi_o^2(K_i+\Delta K_i, K_j) - \chi_o^2(K_i, K_j+\Delta K_j) + \chi_o^2(K_i, K_j)}{\Delta K_i \Delta K_j}.$$

The curvature matrix was then passed to another subroutine, inverted

and returned as the error matrix, ε. The parameter increments were calculated with equation (6-16) and the search routine continued in steps of $\delta K_i/5$ until χ^2 started to increase. The last three steps were then used for the parabolic interpolation of the χ^2 hypersurface minimum. The main program then continued the search by resubmitting K_1 and K_2 until: 1) $\Delta\chi^2$ was less than 10^{-10} and 2) ΔK_i dropped below the floating point precision of the computer. The program was run several times from different starting points $(K_1, K_2)_{init}$ to insure the true minimum of χ^2 had been reached.

Results

The output of the kriging exercise has been three fold: the generation of contour plots (Figures 6-2 through 6-6), the estimation of semivariograms (Figures 6-8 through 6-10) and a two-dimensional grid suitable for modeling (Appendix 2). The contour plots of cross-shelf sections are in reality two-month long time exposures of that property. Several features were apparent in these plots: 1) the near surface deficiency layer of excess ^{222}Rn shoaled landward (Figure 6-3), 2) the isopleths of ^{224}Ra were approximately horizontal in the upper water column (Figure 6-4), 3) ^{222}Rn activities near the middle front (~100 m depth) showed a closed contour (Figure 6-2) in the region that has been identified as a fine-structure zone (Coachman, 1985) 4) ^{224}Ra contours implied the presence of a tongue of off-shelf water intruding into the finestructure zone (Figure 6-4), 5) the presence of the middle and inner front (see Iverson et al., 1979) was apparent in the plots of σ_t and temperature (Figures 6-5 and 6-6) and

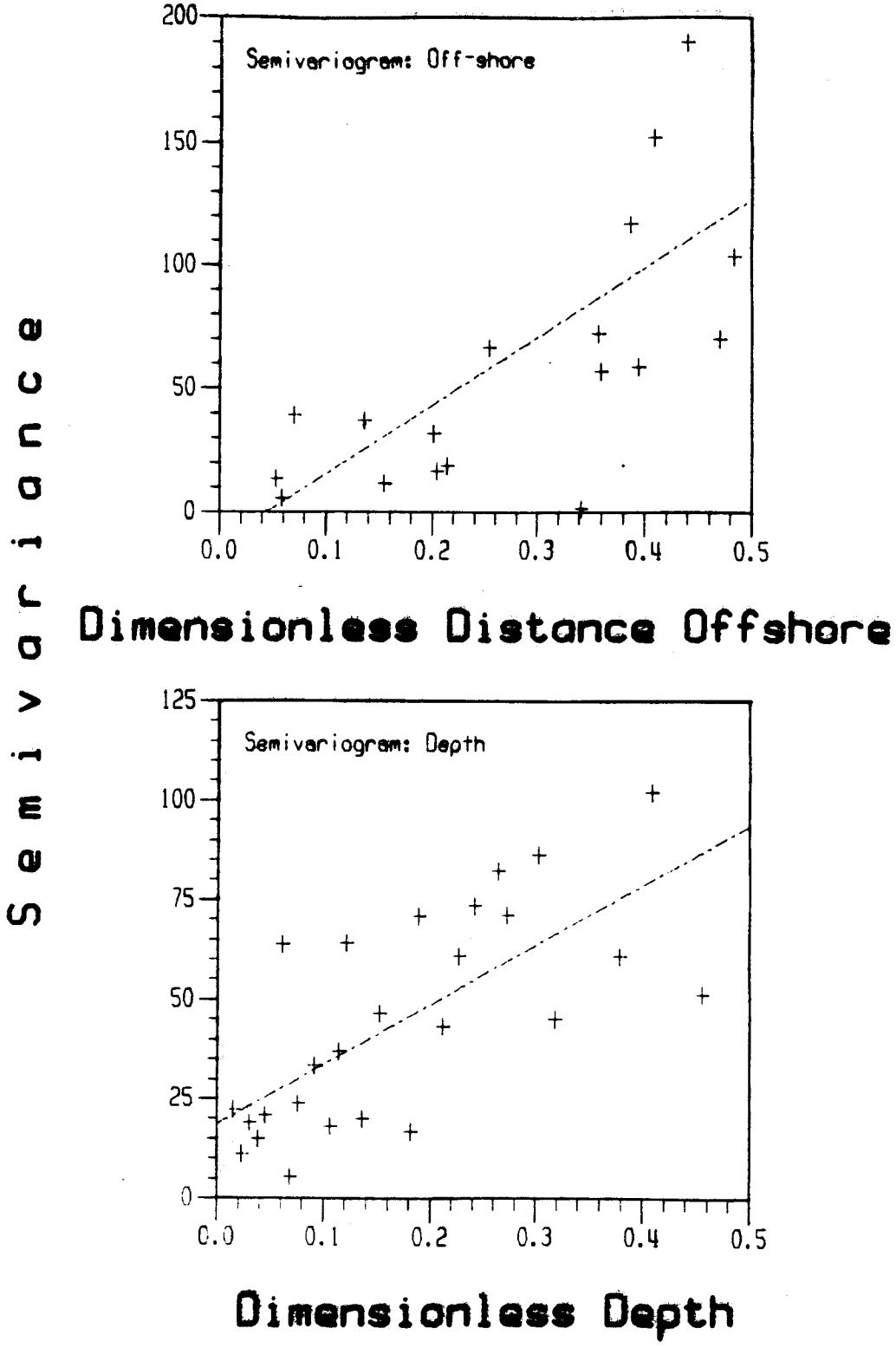

Figure 6-8. Semivariogram of total ^{222}Rn versus distance offshore and depth.

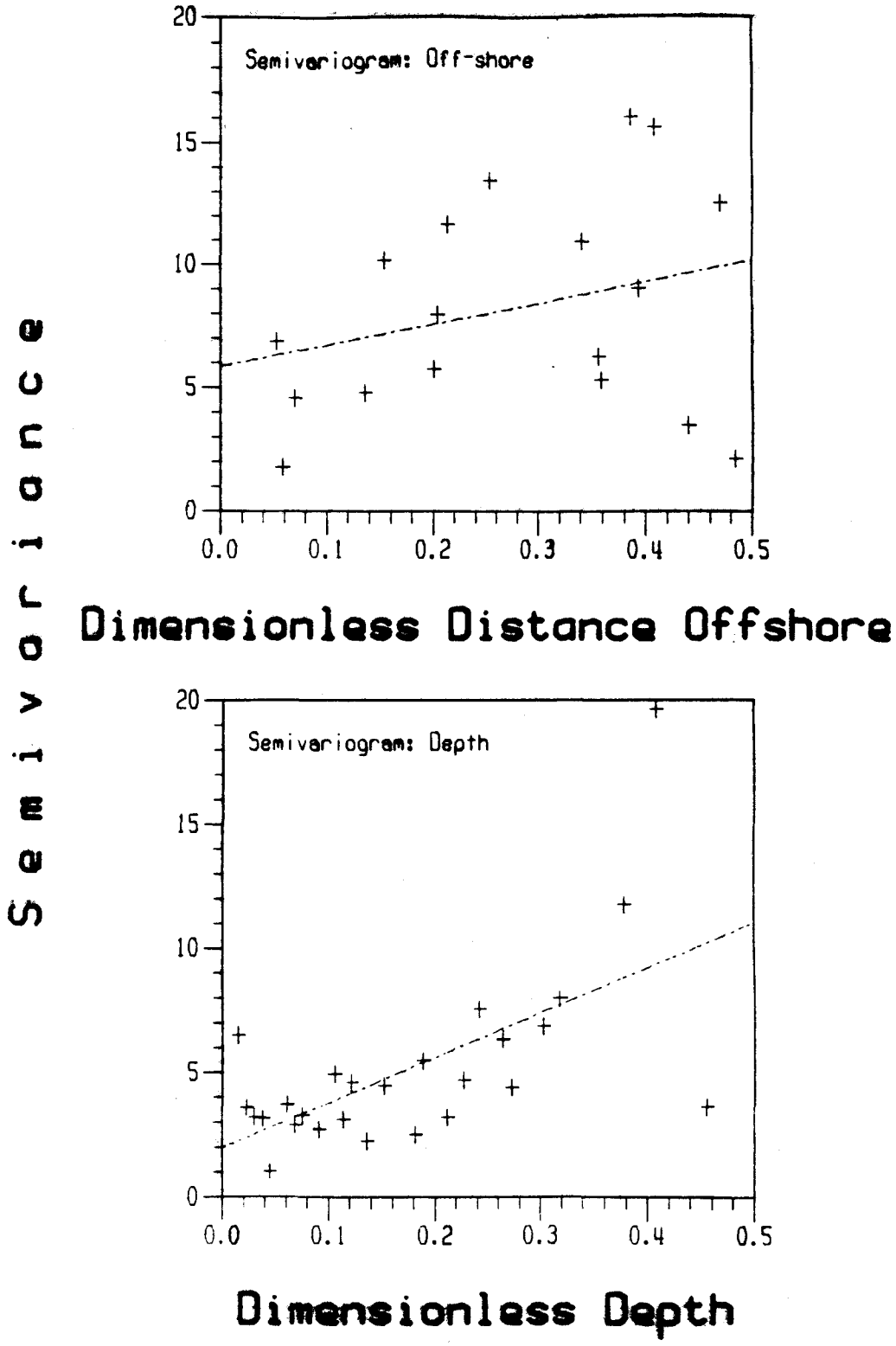

Figure 6-8. Semivariogram of ^{226}Ra versus distance offshore and depth.

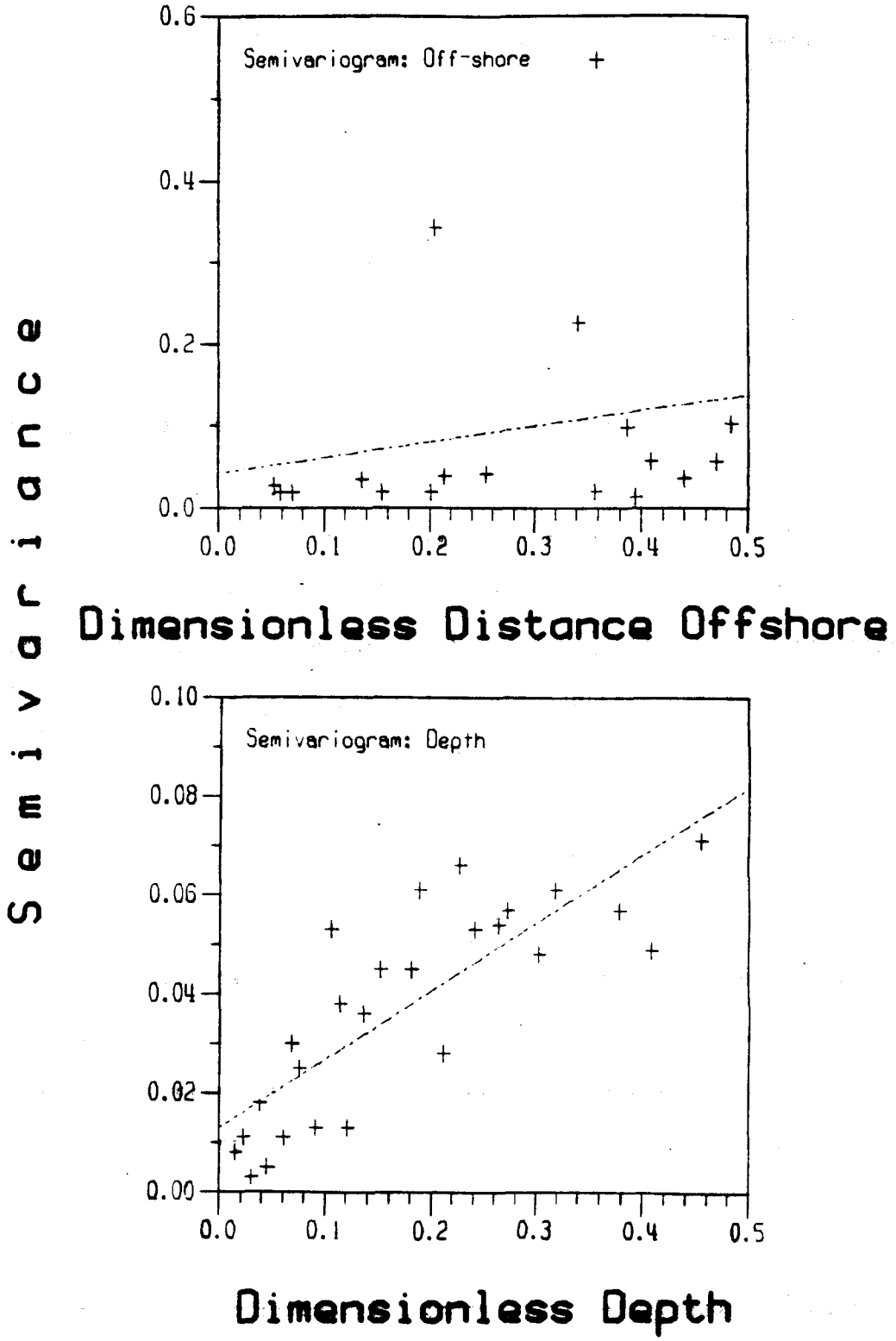

Figure 6-10. Semivariogram of sigma-t versus distance offshore and depth.

6) there was an indication of ^{224}Ra removal from the upper waters of the middle shelf (Figure 6-4).

Local maxima in the horizontal and vertical gradients of σ_t and temperature were used to divide the shelf waters into several subregions, the resultant eddy diffusivities of each subregion are summarized in Table 6-1. The results were grouped loosely into four groups: I) subregions that did not have statistically significant results at the 95% confidence interval even though they were relatively well constrained (had a good measured-data point distribution throughout), II) subregions that either had results not statistically significant (at 95% confidence level) or insufficient or improper distribution of measured-data points, III) subregions that had rectilinear arrangement of grid points and were not suitable for two-dimensional modeling and IV) subregions that gave statistically significant results at the 95% confidence level. Examples of the first type of subregion were the *entire shelf* and *entire middle shelf* zones. The failure of these groups to attain a statistically significant fit was due to the disregard of the water column structure as evidenced by σ_t and temperature. An example of the second type of subregion was the *lower middle shelf* zone. Too few measured-data points actually lie within these zones to properly constrain them or poor arrangement of measured-data points within the zones yielded unacceptably high kriging errors. Examples of the third type of subregion were the *entire thermocline* and *inner front* zones. The rectilinear arrangement of the data points within these zones did not lend themselves to two-

Table 6-1: **TWO-DIMENSIONAL MODEL SUMMARY**

Zone	n	type	K_H	σ_H	K_v	σ_v	χ^2_v
Entire Shelf..	142	I	4×10^8	1×10^8	5×10^0	2×10^0	0.8217*
Entire near-bottom water mass.....	88	I	2×10^8	1×10^8	2×10^0	2×10^0	1.0799*
Entire Middle Shelf.....	48	I	8×10^8	3×10^8	1×10^1	7×10^0	1.0822
Outer Finestructure..	35	II	$\sim 10^{11}$	$\sim 10^{11}$	$\sim 10^3$	$\sim 10^3$	0.5776*
Lower Middle Shelf.....	22	II	5×10^8	2×10^8	1×10^1	4×10^0	2.1009
Entire Thermocline....	16	III	2×10^{12}	$\sim 10^{22}$	1×10^3	$\sim 10^4$	0.4909*
Upper Outer Shelf.....	10	III	1×10^8	$\sim 10^{22}$	2×10^0	$\sim 10^8$	0.0960*
Lower Middle Front.....	9	III	$\sim 10^{10}$	$\sim 10^{21}$	$\sim 10^2$	$\sim 10^2$	0.0213*
Middle Shelf Thermocline.....	8	III	1×10^{12}	2×10^{12}	8×10^4	6×10^3	0.3353*
Outer Shelf Thermocline.....	6	III	$\sim 10^{13}$	$\sim 10^{14}$	$\sim 10^4$	$\sim 10^{17}$	0.0397*
Inner Front.....	5	III	1×10^8	2×10^7	5×10^0	6×10^{-1}	2.5448
Entire Upper Water Column...	29	IV	3×10^7	1×10^7	8×10^{-1}	3×10^{-1}	0.2795*
Upper Middle Shelf.....	8	IV	6×10^4	2×10^7	5×10^{-1}	7×10^{-1}	0.2410*

type	comments
I	not significant at 95% confidence level, sufficient measured-data points, disregarded water structure
II	insufficient or poorly arranged measured-data points
III	points lie in straight line, not suitable for 2-D modeling
IV	sufficient measured-data points and statistically significant at 95% confidence level

* means statistically significant at the 95% confidence level.
† means statistically significant at the 50% confidence level.
n is the number of kriged-data grid points within the zone.
σ_H and σ_v are the uncertainties corresponding to K_H and K_v.

χ^2_v is the reduced chi-squared statistic = $\chi^2/(n-2)$.

K_H and K_v are the horizontal and vertical eddy diffusivities (cm^2/sec) respectively.

dimensional modeling. Examples of the fourth type of subregion were the *entire upper water column* and *upper middle shelf* zones. These zones had distributions of measured-data points sufficient to produce a statistically significant fit at the 95% confidence level.

Boundary fluxes were estimated from the results of the χ^2 optimization and the kriged-data distribution. Fluxes at the surface (transfer coefficients) and at the sediment-water interface are compared to independent estimations in Figures 6-11 and 6-12. A simple two-dimensional box model was used to balance horizontal and vertical fluxes in and out with production and decay, the remainder from steady state was taken to be the flux across the boundary. The surface and sediment fluxes are compiled in Tables 6-2 and 6-3 respectively. Meaningful fluxes were obtained only at grid points where the error estimation was less than 3 dpm/100 kg (Figure 6-13). This points out the usefulness of kriging in that it provides a means of determining where the grid points are too far away from measured data points to give useful estimates.

Discussion

Kriged-data

Universal kriging has quite a number of conveniences as do other types of *objective analysis*. Sarmiento et al. (1982), Freeland and Gould (1976), Bretherton et al. (1976) and Olea (1974) all give explanations and examples of their particular type of objective analysis. All point to the usefulness of an analysis routine that not only yields contour maps of the property's distribution but also the

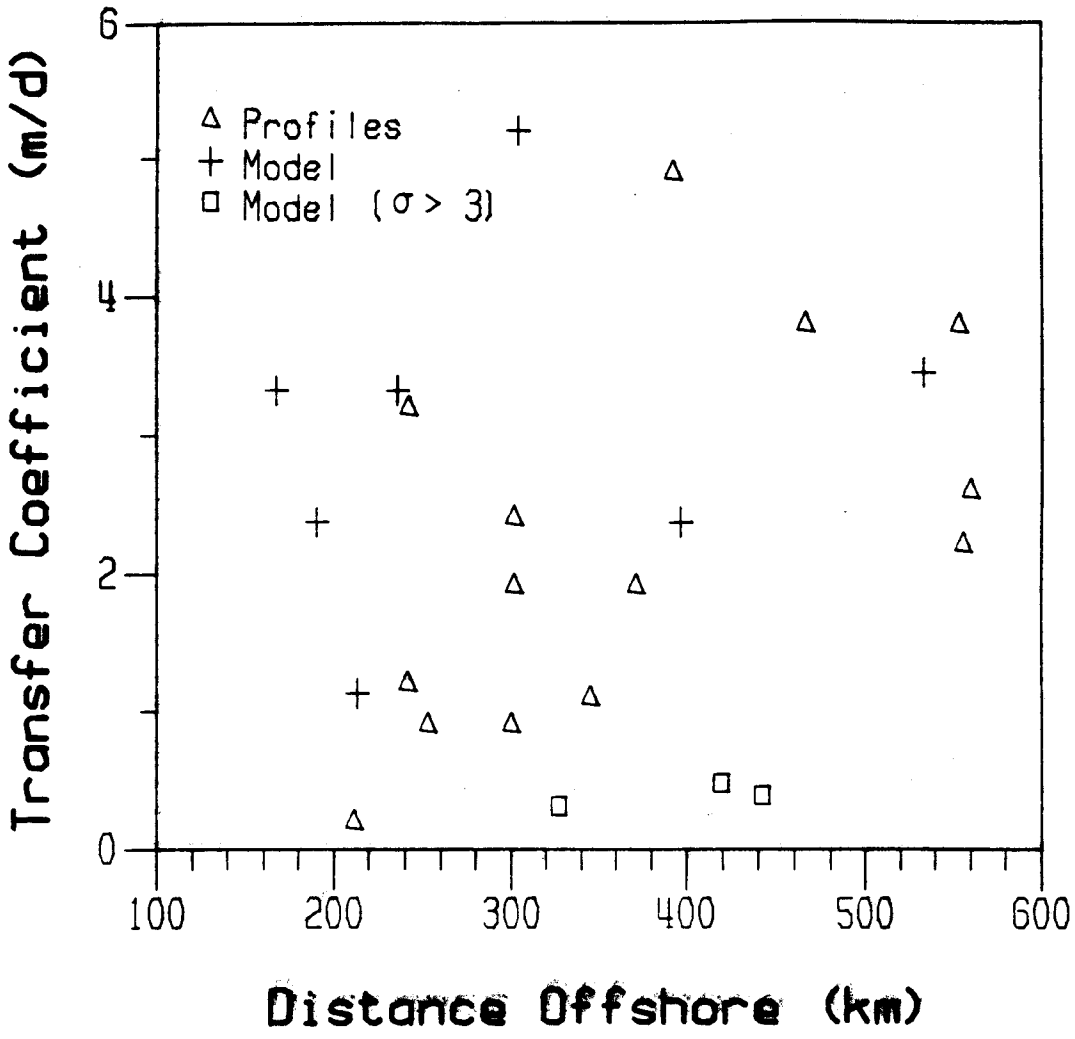

Figure 6-11. Comparison of profile and two-dimensional model estimates of transfer coefficients versus distance offshore.

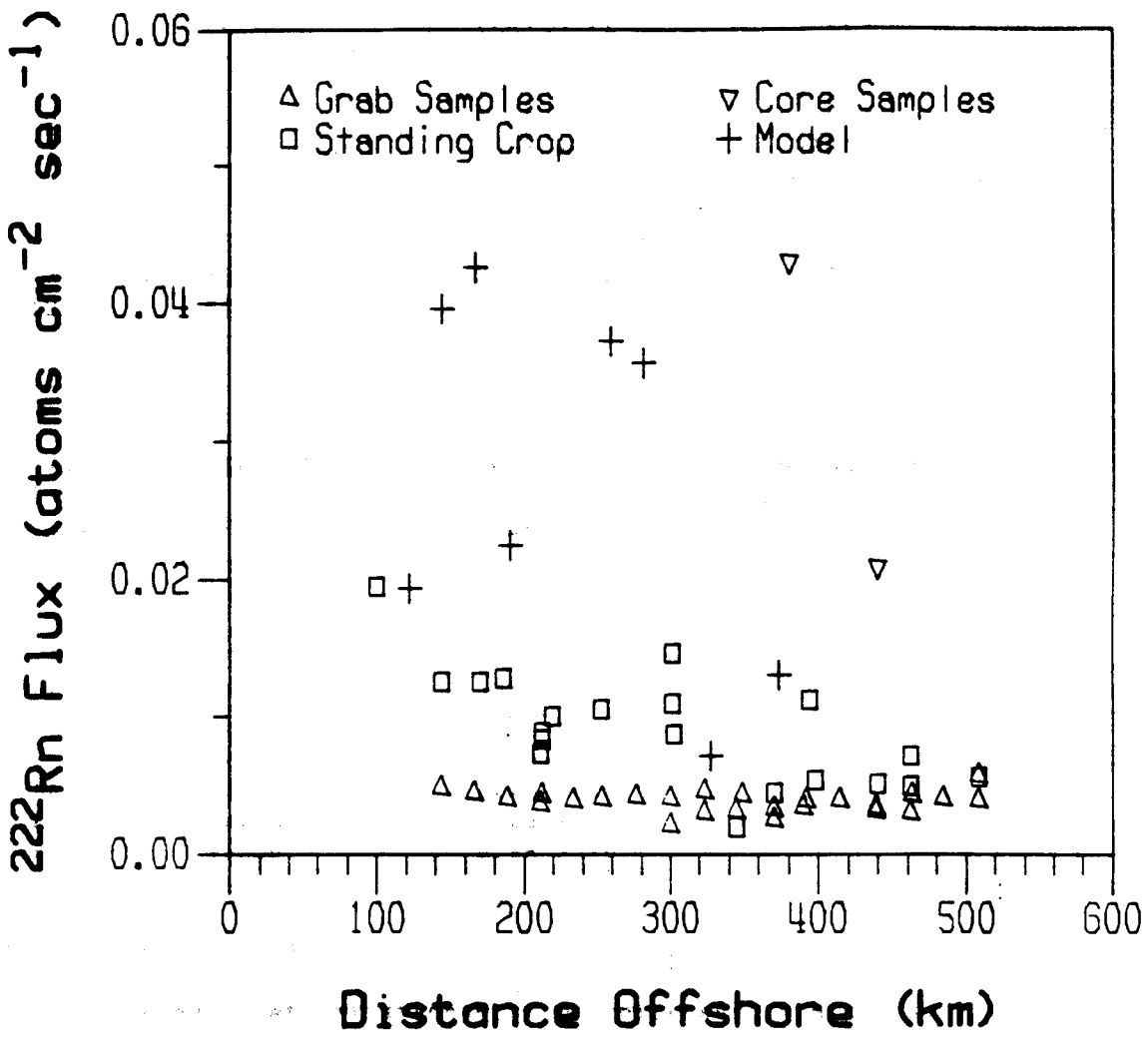

Figure 6-12. Comparison of various estimates of sediment ^{222}Rn flux with two-dimensional model estimates versus distance offshore.

Table 6-2: **TRANSFER COEFFICIENTS SUGGESTED BY TWO-DIMENSIONAL MODEL**

column	Distance Offshore	F (atoms cm^{-2} sec^{-1})	ʃ (μ)	J (m/d)
2	533.15	1.26×10^{-3}	31.4	2.45
6	441.75	2.17×10^{-4}	205.	0.389*
7	418.90	2.70×10^{-4}	167.	0.478*
8	396.05	1.34×10^{-3}	33.0	2.38
11	327.50	1.69×10^{-4}	246.	0.314*
12	304.65	1.36×10^{-3}	15.2	5.22
15	236.10	5.60×10^{-4}	23.0	3.33
16	213.25	3.08×10^{-4}	70.5	1.14
17	190.40	8.03×10^{-4}	33.0	2.38
18	167.55	1.76×10^{-3}	22.5	3.33

Table 6-3: **SEDIMENT FLUX SUGGESTED BY TWO-DIMENSIONAL MODEL**

column	Distance Offshore	F (atoms cm^{-2} sec^{-1})
9	373.20	1.30×10^{-2}
11	327.50	7.18×10^{-3}*
13	281.80	3.57×10^{-2}*
14	258.95	3.73×10^{-2}
17	190.40	2.24×10^{-2}
18	167.55	4.26×10^{-2}
19	144.70	3.96×10^{-2}
20	121.85	1.93×10^{-2}

* means kriged-data grid point uncertainty greater than 3 dpm/100 kg.

ʃ is hypothetical stagnant film thickness in microns.

Distance offshore is in km.

J is transfer coefficient.

F is flux of ^{222}Rn.

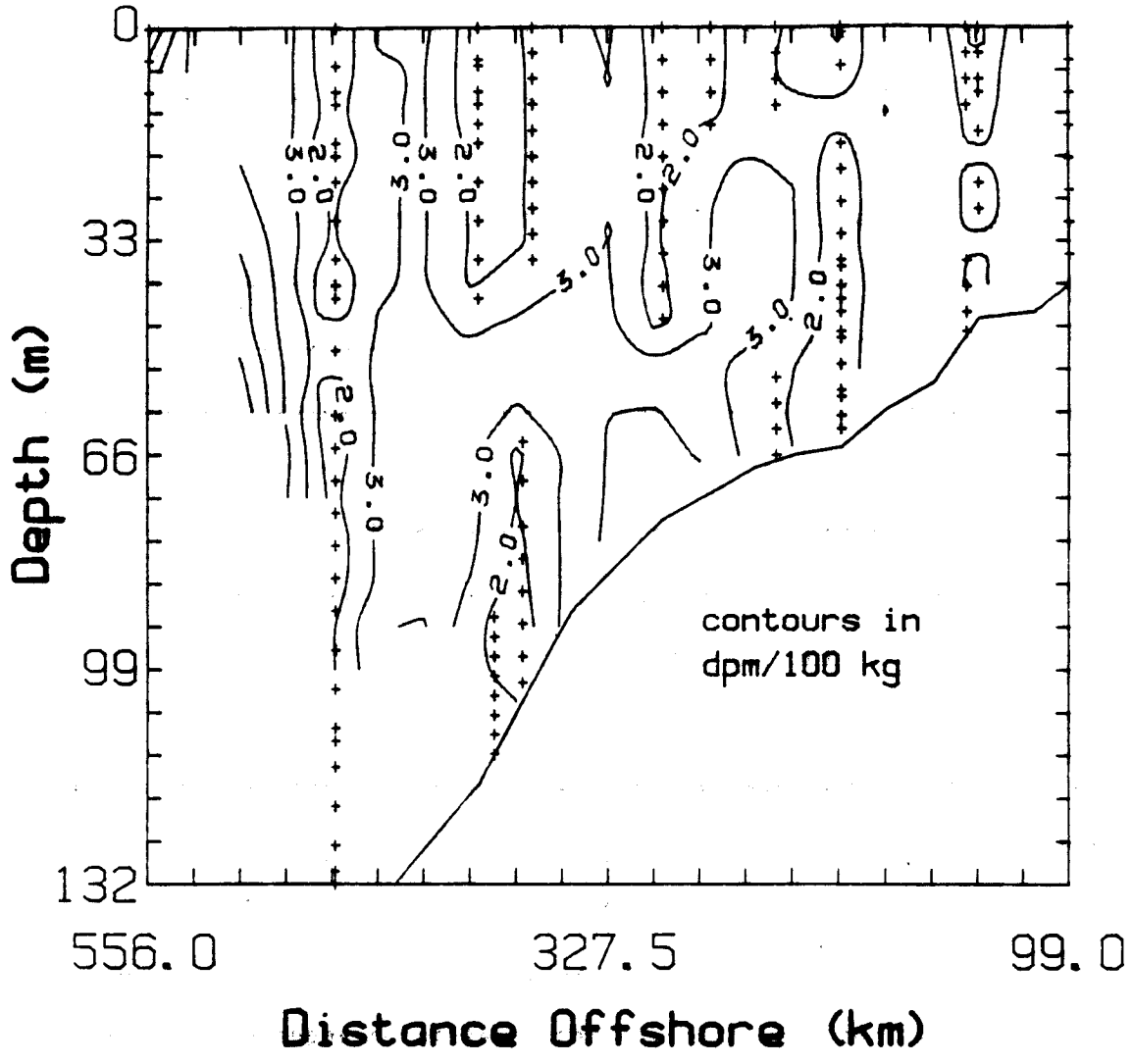

Figure 6-13. Kriging error contour plot across the southeastern Bering Sea shelf. Prepared from kriged-data matrix (see Appendix 2); the actual measured-data points are shown as (+).

error associated with each grid point. For my modeling purposes the finite differencing approximation required a regular grid of data points (with associated error) and universal kriging provided such a grid. Additionally, universal kriging can be expanded to higher dimensions if the problem to be solved requires it.

The bias added to the kriged-data set by an inappropriate straight line fit to the measured-data discrete semivariances was determined from inspection of equations (6-4). These equations are actually 3 sets of simultaneous equations and the effect expected from this error manifested itself in the first set. If the semivariogram was not linear, the semivariance estimate was either too high or too low. For the sake of argument I assume an overestimation. From inspection of equations (6-4), if $\gamma(x_j-x_{j'})$ was an overestimation, the first term of the left-hand side was also overestimated. If $\gamma(x_j-x_o)$ on the right-hand side was also overestimated then the effects canceled and $\hat{\pi}_{j'j}$ was unbiased. This was the case at the extremes of the semivariogram where the direction of deviation was the same on the right-hand and left-hand sides of equations (6-4). At the mid-point of the semivariogram the deviations had opposite signs and the bias of $\hat{\pi}_{j'j}$ was in the opposite sense of the deviation of the semivariance estimate to the true value. Figures 6-8, 6-9 and 6-10 show small deviations with respect to the straight line at their mid-points (dimensionless distance 0.25) and $\hat{\pi}_{j'j}$ had small bias.

The contour plots of ^{222}Rn (both total and excess) reveal some interesting features (Figures 6-2 and 6-3). The shoaling of the near

surface ^{222}Rn deficiency resulted from the overlap of the two exchange fluxes of ^{222}Rn on the shelf. The shallow waters of the shelf allowed the excess ^{222}Rn flux out of the sediments to impinge upon the ^{222}Rn flux out of the water column into the atmosphere. The mid-depth waters of the outer shelf have been identified as a zone of finestructure mixing on the Bering Sea shelf (Coachman, 1985). The presence of a closed contour line surrounding this area implied some sort of interuption to the general from-sediment-to-atmosphere flux of ^{222}Rn on the shelf. Coachman (1982) proposes a weak flow convergence in the middle of this broad continental shelf driving the finestructure mixing, but the physics of this process is still unclear. Along with other data (presented earlier) the contours of ^{222}Rn implied an increasing source of ^{222}Rn from the sediments in the onshore direction. Sharma (1979) reports increasing average grain size and I measured decreasing sediment porosity going onshore. This combination allowed more of the ^{222}Rn produced within the inner shelf sediments to escape into the overlying water column (Figures 4-1 and 4-2 and Table 4-1).

The contour plot of ^{224}Ra also shows some interesting features (Figure 6-4). If ^{224}Ra was derived only from the sediments, then the isopleths of ^{224}Ra would be parallel to the bottom topography. However, the approximately horizontal nature of these isopleths and the appearance of a tongue of ^{224}Ra rich water injecting itself onto the shelf implied that there was another source of ^{224}Ra from off the shelf. The deep off-shelf waters had much higher ^{224}Ra activities

consistent with this idea (station TT159-3050, Appendix 1). A sink of ^{224}Ra was also indicated in the near surface waters of the middle shelf by a depression in activity centered at 247.5 km offshore. This area of the shelf is reported to have high diatom activity (Sambrotto et al., 1985). Figure 6-14 is a plot of silica concentration vs. ^{224}Ra activity for all ^{224}Ra samples measured on the shelf in 1981. The statistically significant linear relationship at the 95% confidence level ($r = 0.66$, $n = 153$) implies an association between silica and ^{224}Ra as found by others (Broecker et al., 1976; Ku and Lin, 1976; Chung, 1980 and Ku et al., 1980).

An important piece of evidence of the quasi-steady state nature of the southeastern Bering Sea shelf waters was provided by the contour plots of σ_t and temperature (Figures 6-5 and 6-6). As stated before, these contour plots are in reality two-month long *time exposures* of these properties. The three-dimensional arrangement of the original profiles was compressed into a two-dimensional slice across the Bering Sea shelf. Nevertheless, the basic structure of the water column was seen (compare Figures 6-5, 6-6 and 1-3). The thermocline, inner and middle fronts are well evidenced in these contour plots (Figures 6-5 and 6-6). Although these properties were smeared out in space and time, the water column structure had sufficient temporal-spatial integrity to claim a quasi-steady state distribution was a reasonable assumption.

χ^2 hypersurface search for optimal K_H and K_v

Sarmiento and Rooth (1980) show a dependence of eddy diffusivity

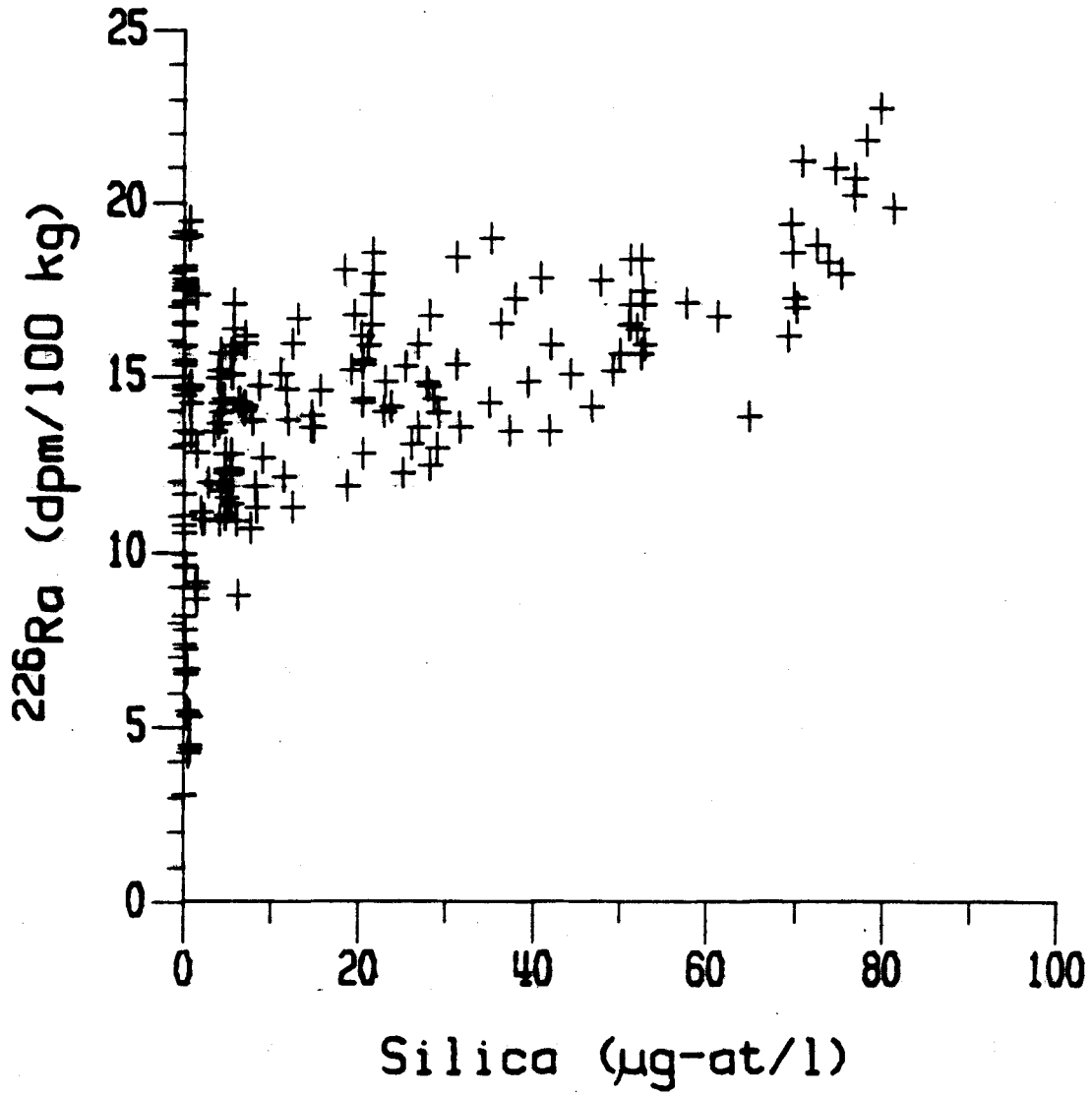

Figure 6-14. Radium-226 activity versus soluble silica concentrations in the PROBES area, 1981. A coefficient of 0.66 obtained from 153 data points is statistically significant at the 95% confidence level.

with density gradient. It seemed reasonable then to divide the shelf waters into subregions bounded by local maximums in σ_t and temperature gradients. Coachman (1985) also makes a similar assumption about the behavior of eddy diffusivity and divides the shelf waters into subregions. For any given row in the kriged data matrix a local maximum in $\Delta\sigma_t/\Delta x$ located either the middle or inner front. For any particular column in the kriged data matrix a local maximum in $\Delta T/\Delta z$ located the thermocline. The names of these subregions (or zones) are descriptive of their orientation to these gradient boundaries (see Table 6-1) and the optimal eddy diffusivities within these bounds were estimated.

From the results of the optimization of K_H and K_v certain characteristics of a statistically significant subregion at the 95% confidence level became obvious. One of the first requirements was that the subregion have approximately as many measured-data points as kriged grid points within its boundaries. However, the existence of type II zones implied that the geometry of these measured-data points was also important. Also the assumption of constant eddy diffusivities within a subregion could not be ignored. If the density structure implied a change of K_H or K_v within a zone, that zone did not yield a statistically significant result at the 95% confidence level (type I). Another requirement was the error estimate from the kriging exercise (based on the geometry of the measured-data point distribution) within each subregion be kept below a certain critical level. The two-dimensional model also required that the grid points being fitted have

a two-dimensional distribution to provide enough sensitivity in both directions. A rectilinear arrangement of grid points did not provide enough information for a fit in the direction perpendicular to the grid point distribution. Only two subregions satisfied all these requirements, the *entire upper water column* and the *upper middle shelf* zones.

The magnitude of the eddy diffusivities in the <95% confidence level statistically significant zones needed to be considered. The estimates of sediment ^{222}Rn flux using the results from the *lower middle shelf* zone (a type II zone) yielded a better result than fluxes estimated with Coachman's (1985) K_H and K_v. Disregarding type III zones and concentrating on type I and II zones (the *lower middle shelf* zone in particular) the K_H estimates were approximately two orders of magnitude higher and the K_v's were approximately one order of magnitude higher than Coachman's (1985) (compare his $K_H \sim 10^4$ and $K_v \sim 10^{-1}$ cm^2/sec with Table 6-1). The K_v estimates were also approximately one order of magnitude less than the one-dimensional model estimates (Table 5-1). Clearly, horizontal flux has been accounted for and these values can be taken as long term upper limits.

The magnitudes of the type IV zone estimates of K_H and K_v agreed reasonably well with those of Coachman (1985) and Coachman and Walsh (1981) (Table 6-1). The vertical eddy diffusivities of these zones were approximately two orders of magnitude lower than the estimates from the one-dimensional model. The inclusion of horizontal flux of ^{222}Rn into the model provided estimates of vertical eddy diffusivity

that were in line with those of Coachman using the model of Joyce (1977). Additionally, the flux of ^{222}Rn to the atmosphere using these zone IV eddy diffusivities and the kriged data yielded very reasonable transfer coefficients at the surface (Figure 6-11).

Simple one-dimensional estimates of the transfer coefficient at the surface were made in the off-shelf waters of the Bering Sea (see Table 3-1). These estimates were considered to be reasonably accurate because 1) the bottom was far enough removed to avoid violation of the *no bottom flux* assumption of Broecker (1965) and 2) the horizontal gradient of ^{222}Rn decreased going off-shelf reducing horizontal flux of ^{222}Rn in the upper water column. These near surface fluxes compared well with those predicted further onshore from the simple two-dimensional box model. This implied that gas exchange across the shelf was fairly uniform but was obscured by overlapping benthic fluxes of ^{222}Rn (Figure 6-11).

The upper and lower limits of sediment ^{222}Rn flux were estimated from core samples and grab samples respectively (Table 4-1). The core samples gave evidence of biological irrigation being important, at least on the outer shelf (Chapter 4). The fluxes calculated from the grab sample ^{222}Rn production rate and porosity assumed that only molecular diffusion was occurring in these sediments. Additionally, estimates of the sediment ^{222}Rn flux made from the standing crop of excess ^{222}Rn fell between these upper and lower limits (Figure 6-12). The 50% confidence level statistically significant K_M and K_v estimates, when used with the kriged near bottom ^{222}Rn grid points

yielded sediment ^{222}Rn fluxes close to the core estimates (Figure 6-12). Coachman's (1985) values for K_H and K_v used in the simple two-dimensional box model, estimate sediment fluxes of ^{222}Rn that were slightly below that of the grab sample estimates (the minimum possible sediment flux). When considered together, these various flux estimates implied that the eddy diffusivities of near-bottom shelf waters were between estimates by Coachman (1985) and my two-dimensional optimization model, possibly closer to the latter.

The sensitivity and robustness of any mathematical model is always of some interest. Sensitive models or models lacking robustness tend to give widely different answers with only slight changes in the initial conditions. I investigated the robustness of this two-dimensional optimization model in two ways: 1) the range of initial guesses over which the model gave the same (and correct) answer was determined and 2) the range of the ratio of the initial conditions was also determined. This model was found to be very robust. The model converged to the same answer over a range of four orders of magnitude in the initial guess of K_H and K_v. Because the solution to some simpler homogeneous differential equations is sensitive to only the ratio of the coefficients, the ratio of the initial guesses was varied as well. The range of the ratios of the initial parameters was only slightly less than that of their magnitudes; yielding a range of three orders of magnitude. Furthermore, a simple sensitivity coefficient (Huson, 1984) was calculated. The 1% sensitivity coefficient was 1.0 and the 2% sensitivity coefficient was 0.0. This implied that when the

initial guess was varied plus or minus one standard deviation (of the final answer) all the resultant eddy diffusivities fell outside ±1% but within ±2% of the eddy diffusivities corresponding to the minimum χ^2. This model, then, was a very robust estimator of eddy diffusivities from the grid of kriged data points.

No mathematical model is without its inadequacies; this one was no exception. The first problem was the lack of type IV subregions found on the shelf. The rectification of this problem was simple: get more type IV groups from the data. One possibility was to increase the number of grid points within each subregion. But better resolution did not necessarily translate to increased precision of the estimations. The error associated with each grid point was a function of the geometric distribution of the measured-data points. More grid points not only gave the illusion of greater resolution than actually exists, but also failed to improve the fit of parameters because the error associated with each grid point did not decrease. As usual, the accuracy and the *goodness of fit* of the model would be increased with more measured-data points. The error map (Figure 6-13) from the kriging exercise can be a valuable guide for either the location of additional data points or a better sampling strategy. This implied that our *best estimate* can always be better.

The second problem with this model had to do with its convergence stability. As noted above, this model was very robust. However, there were a few occasions (type III subregions) when the behavior was distinctly unstable. This does not mean the model did not converge

(blew up) nor does it mean that it converged to a different answer with different initial conditions (non-robust behavior). The instability took the form of very large uncertainty estimates of the parameters fitted and in one case in an upwardly drifting estimate of the eddy diffusivities. This type of instability was due to extreme flatness of the χ^2 hypersurface in the vicinity of the global minimum. The curvature matrix (α), in these cases, had very small elements and when it was inverted to form the error matrix (ϵ) unreasonably large uncertainties were associated with the parameters. The flatness of the hypersurface prevented the search routine from finding the absolute minimum in only one case. The other type III subregions (Table 6-1) had very large uncertainties due to the χ^2 hypersurface flatness. In all but the one case of upwardly drifting eddy diffusivities this type of instability occurred in subregions with rectilinear grid point orientation. The exceptional case had grid points lying in a region of high uncertainty. Again this problem could have been alleviated by more measured-data points which would allow a finer mesh grid to be generated.

This type of model can be extended to other geochemical tracer distributions. Apparently the only absolute requirements are enough measured-data points distributed properly and a governing differential equation that can be approximated by a finite differencing equation. A two-dimensional model would be possible for not only conservative or inert tracers but also bio-active tracers because the zeroth or first order reaction coefficients are optimized rather than guessed.

Additionally, non-linear terms in a differential equation, such as advection, present little problem as long as the finite differencing equation can be solved for the property being fitted. Additional differential equations can be added and the *function* being optimized can be turned into a system of functions allowing for the occasions when the finite differencing equation can not be rearranged directly.

Chapter 7: **CONCLUSIONS**

Well sure I made it, but y'know it was a hell of a trip

John Prine

The flux of ^{222}Rn out of the sediments, the rate it was mixed in the water column and the flux of ^{222}Rn into the atmosphere can be made to balance by a two-dimensional model of ^{222}Rn distribution in the southeastern Bering Sea waters. To my knowledge, this is the first successful application of ^{222}Rn techniques to a continental shelf arriving at a coherent picture of these three transfer processes. The driving force for this environment resulted from the interaction between baroclinic flows, tidal currents and bottom slope variations as proposed by Schumacher and Kinder (1983). The variations in the bottom slope occur approximately beneath the hydrographic fronts and their interaction with tidal currents and baroclinic flows are believed to be generating the fronts that divide the shelf into the three regions (Schumacher and Kinder, 1983 and Coachman, 1985). These fronts allowed ^{222}Rn to be modeled as a purely diffusive system on the middle shelf. The following features were seen in the *time exposure* cross-shelf sections (Figures 6-2 through 6-6): near surface ^{222}Rn deficiency due to gas exchange, two-dimensional mixing of excess ^{222}Rn in the water column, ^{222}Rn deficiency *beneath* ^{222}Rn excess, biological removal of ^{224}Ra and a higher sediment ^{222}Rn flux on the inner shelf. I conclude the following about these features:

1). The loss of excess ^{222}Rn to the atmosphere was obscured in the shallower water column due to overlap of benthic and near surface

fluxes.

2). Like other workers, I found no significant relationship between radon-derived transfer coefficients and wind speed. However, if stations exhibiting benthic flux overlap were omitted, the mean film thickness reflected the average gas exchange conditions as shown from agreement of the four gas exchange rate estimators.

3). The overestimation of the vertical eddy diffusivity by the one-dimensional, vertical flux model was caused by the horizontal flux of ^{222}Rn. This flux resulted from the interaction of the horizontal gradient of ^{222}Rn, tidal action, bottom slope variability and baroclinic pressure field.

4). Molecular diffusion was insufficient to account for the ^{222}Rn deficiency in sediment cores taken on the shelf. The most likely mechanism responsible for the ^{222}Rn deficiency in the sediments was bio-irrigation.

5). ^{226}Ra activity was removed in a region of known high biological activity.

6). ^{226}Ra had nearly horizontal isopleths, and the ^{226}Ra field strongly suggested a flux of ^{226}Ra enriched water from the deep Bering Sea basin onto the shelf. I conclude that the ^{226}Ra on the shelf was not terrestrially derived.

7). The two-dimensional model derived to explain the distribution of ^{222}Rn on this shelf gave reasonable results when provided with a rich enough measured-data field. The results suggested that the K_H of approximately 10^4 cm^2 sec^{-1} and K_v of 10^{-1} cm^2 sec^{-1} (as estimated by

Coachman, 1985) are reasonably good numbers, however, they may be slightly underestimated.

Appendix 1: MEASURED-DATA

In the table that follows I present the output of the BASIC program that analyzes the raw count data and yields ^{222}Rn, ^{224}Ra activities and their standard deviations (sd). Additionally, the depth, sigma-t and temperature for each sample is presented. The excess ^{222}Rn activity was also calculated by the program by subtracting the ^{224}Ra activity from the ^{222}Rn. In each station header the identification, latitude, longitude, date, time of collection and depth of the station is given. Activities are in units of dpm/100 kg and the temperatures are in degrees Celsius.

Appendix 1: Measured-data

Depth (m)	Rn	(sd)	Ra	(sd)	xSRn	(sd)	Sigma-t	Temp
Station: HX009-0005	55.47 N	166.89 W	80/10/ 5	05.34 GMT	Sonic Depth	138 m		
108	25.2	(0.8)	9.4	(0.7)	15.8	(1.1)	26.26	4.340
113	27.8	(0.8)	10.7	(0.0)	17.0	(0.8)	26.27	4.370
118	27.4	(1.1)	12.0	(0.0)	15.4	(1.1)	26.27	4.380
123	27.5	(0.9)	13.3	(0.0)	14.2	(0.9)	26.27	4.390
128	27.3	(2.5)	14.6	(0.0)	12.7	(2.5)	26.28	4.400
133	27.0	(0.9)	15.9	(0.4)	11.1	(1.0)	26.28	4.400
Station: HX009-0008	55.92 N	166.13 W	80/10/ 5	19.52 GMT	Sonic Depth	121 m		
71	17.1	(0.6)	14.5	(0.4)	2.6	(0.7)	25.67	6.810
95	33.1	(0.8)	15.5	(0.3)	17.6	(0.8)	26.07	5.510
100	33.0	(1.1)	16.5	(0.6)	16.6	(1.2)	26.07	5.510
105	32.9	(0.9)	15.7	(0.5)	17.1	(1.0)	26.07	5.510
110	28.6	(2.6)	15.1	(1.2)	13.5	(2.8)	26.07	5.500
115	32.3	(0.7)	16.8	(0.5)	15.5	(0.9)	26.08	5.490
Station: HX009-012	56.54 N	165.14 W	80/10/ 6	16.80 GMT	Sonic Depth	79 m		
1	10.9	(0.3)	15.2	(0.4)	-4.3	(0.5)	24.94	7.660
20	13.8	(0.4)	16.1	(0.0)	-2.4	(0.4)	24.94	7.670
35	20.3	(0.7)	16.8	(0.0)	3.5	(0.7)	24.94	7.670
45	9.5	(0.5)	17.3	(0.0)	-7.8	(0.5)	24.94	7.650
55	37.7	(0.9)	17.8	(0.4)	19.9	(1.0)	25.32	5.280
65	38.2	(3.4)	16.9	(0.5)	21.3	(3.4)	25.51	3.870
75	43.7	(1.2)	15.7	(0.4)	28.0	(1.2)	25.51	3.870
Station: HX009-0031	56.54 N	165.14 W	80/10/ 9	20.02 GMT	Sonic Depth	79 m		
0	10.2	(0.4)	11.1	(0.3)	-1.0	(0.5)	24.98	7.170
20	9.0	(0.3)	15.4	(1.4)	-6.3	(1.5)	24.98	7.190
40	7.5	(0.9)	7.5	(0.5)	-0.0	(1.1)	24.98	7.200
60	46.8	(0.9)	17.4	(0.4)	29.4	(1.0)	25.50	3.910
Station: HX009-0056	57.70 N	164.48 W	80/10/10	04.60 GMT	Sonic Depth	30 m		
0	31.0	(0.7)	10.6	(0.4)	20.4	(0.8)	24.93	6.730
10	19.2	(0.4)	11.9	(0.5)	7.3	(0.6)	24.93	6.750
20	28.8	(0.9)	17.7	(0.4)	11.1	(1.0)	24.93	6.750
30	29.7	(0.7)	12.3	(1.1)	17.3	(1.2)	24.93	6.750
40	29.5	(2.7)	12.2	(0.5)	17.3	(2.7)	24.93	6.740
45	32.6	(1.0)	11.5	(0.3)	21.1	(1.0)	24.93	6.740

Appendix 1: Measured-data (cont.)

Depth (m)	Rn	(sd)	Ra	(sd)	xsRn	(sd)	Sigma-t	Temp
Station: TT159-3023	57.59 N	163.38 W	81/ 6/ 3	15.95 GMT	Sonic Depth	44 m		
0	13.2	(0.7)	11.9	(0.6)	1.3	(0.9)	25.13	6.728
4	13.4	(0.5)	12.2	(1.0)	1.2	(1.1)	25.14	6.726
8	6.9	(0.5)	11.7	(0.8)	-4.7	(0.9)	25.22	6.455
10	16.9	(1.0)	10.4	(0.8)	6.5	(1.2)	25.25	6.275
16	49.4	(4.8)	11.0	(0.5)	38.4	(4.8)	25.41	4.365
24	31.2	(0.9)	8.1	(0.2)	23.1	(0.9)	25.43	4.282
28	30.0	(0.9)	13.3	(0.6)	16.7	(1.0)	25.43	4.274
Station: TT159-3033	57.72 N	164.20 W	81/ 6/ 4	19.00 GMT	Sonic Depth	48 m		
0	8.6	(0.4)	5.9	(0.6)	2.7	(0.7)	25.05	6.982
4	6.0	(0.4)	5.5	(0.6)	0.4	(0.8)	25.06	6.975
8	12.4	(1.2)	6.0	(0.7)	6.4	(1.4)	25.06	6.970
12	17.8	(0.5)	7.8	(0.8)	10.0	(0.9)	25.11	5.865
36	24.7	(1.1)	9.8	(0.7)	14.8	(1.3)	25.41	4.141
40	43.9	(1.5)	10.3	(0.4)	33.6	(1.6)	25.41	4.141
44	48.6	(2.3)	10.0	(0.6)	38.6	(2.4)	25.41	4.140
47	44.1	(4.5)	10.3	(1.3)	33.8	(4.7)	25.41	4.140
Station: TT159-3042	56.37 N	166.45 W	81/ 6/ 5	19.00 GMT	Sonic Depth	101 m		
0	9.8	(0.3)	11.1	(1.3)	-1.3	(1.4)	24.77	7.473
4	9.3	(0.5)	12.3	(0.9)	-3.0	(1.0)	24.77	7.474
8	8.3	(0.8)	11.9	(1.6)	-3.6	(1.8)	24.78	7.466
12	6.4	(0.5)	12.7	(0.7)	-6.3	(0.9)	24.83	7.050
16	9.6	(0.4)	13.1	(0.4)	-3.4	(0.6)	24.94	6.230
20	6.9	(0.4)	6.8	(0.5)	0.1	(0.6)	25.04	5.410
24	6.7	(0.3)	12.9	(1.2)	-6.2	(1.3)	25.06	5.248
28	11.9	(1.4)	13.0	(1.1)	-1.1	(1.8)	25.08	5.086
32	13.4	(0.8)	14.5	(1.6)	-1.1	(1.8)	25.11	5.018
36	11.0	(0.5)	11.7	(0.9)	-0.7	(1.0)	25.14	5.043
Station: TT159-3050	55.17 N	168.45 W	81/ 6/ 6	22.50 GMT	Sonic Depth	1682 m		
225	13.7	(1.2)	16.1	(0.7)	-2.4	(1.4)	26.57	3.625
240	9.4	(0.4)	15.2	(0.4)	-5.9	(0.6)	26.60	3.645
255	13.8	(0.7)	18.3	(0.8)	-4.4	(1.0)	26.62	3.682
1660	20.6	(0.5)	34.3	(1.9)	-13.7	(2.0)	27.60	2.069
1670	39.6	(3.7)	33.5	(1.8)	6.0	(4.1)	27.60	2.061
1674	35.7	(1.8)	36.6	(2.5)	-0.9	(3.1)	27.60	2.056
1678	39.9	(0.9)	31.7	(1.4)	7.3	(1.7)	27.60	2.054

Appendix 1: Measured-data (cont.)

Depth (m)	Rn	(sd)	Ra	(sd)	XSRn	(sd)	Sigma-t	Temp
Station: TT159-3051	54.58 N	167.33 W	81/ 6/ 7	19.50 GMT	Sonic Depth	525 m		
247	6.8	(0.9)	12.9	(1.4)	-6.0	(1.7)	26.47	3.574
249	14.9	(1.0)	17.4	(0.7)	-2.6	(1.2)	26.47	3.589
251	16.2	(0.7)	14.5	(0.4)	1.7	(0.8)	26.48	3.594
253	17.3	(1.1)	14.4	(0.7)	2.8	(1.3)	26.48	3.584
Station: TT159-3058	55.65 N	165.60 W	81/ 6/ 8	19.00 GMT	Sonic Depth	112 m		
91	26.0	(2.7)	12.8	(1.2)	13.2	(2.9)	25.94	4.315
94	27.6	(1.4)	14.1	(0.6)	13.5	(1.5)	25.97	4.301
97	28.5	(1.0)	13.6	(0.3)	15.0	(1.1)	26.00	4.282
100	26.5	(1.6)	13.3	(0.6)	13.2	(1.7)	26.01	4.279
103	30.5	(1.0)	14.3	(0.9)	16.1	(1.4)	26.01	4.278
106	35.3	(3.5)	13.9	(0.9)	21.4	(3.6)	26.01	4.279
109	26.9	(1.6)	15.3	(1.2)	11.6	(2.0)	26.01	4.277
112	27.6	(1.0)	13.2	(0.7)	14.4	(1.2)	26.01	4.278
Station: TT159-3066	56.86 N	163.63 W	81/ 6/ 9	19.00 GMT	Sonic Depth	67 m		
0	1.7	(0.2)	1.6	(0.4)	0.1	(0.4)	24.76	8.100
4	2.1	(0.2)	1.3	(0.2)	0.8	(0.3)	24.76	8.078
8	1.6	(0.1)	2.3	(0.2)	-0.7	(0.2)	24.77	8.056
12	1.9	(0.2)	2.6	(0.3)	-0.6	(0.3)	24.83	7.736
54	31.7	(1.1)	15.2	(1.0)	16.5	(1.5)	25.32	3.853
58	36.7	(3.8)	14.0	(0.9)	22.6	(3.9)	25.32	3.776
62	35.4	(1.4)	16.2	(1.3)	19.2	(2.0)	25.32	3.699
66	32.2	(1.6)	15.6	(0.8)	16.6	(1.8)	25.32	3.622
Station: TT159-3071	57.13 N	164.15 W	81/ 6/11	01.50 GMT	Sonic Depth	65 m		
36	29.7	(1.8)	13.2	(1.0)	16.5	(2.1)	25.37	3.361
40	36.6	(1.0)	14.2	(1.4)	22.4	(1.8)	25.37	3.349
44	33.2	(1.2)	11.4	(0.8)	21.8	(1.4)	25.37	3.349
48	25.3	(2.0)	13.1	(0.8)	12.2	(2.2)	25.37	3.349
52	28.8	(2.4)	12.7	(0.7)	16.1	(2.5)	25.37	3.351
56	28.6	(2.1)	12.5	(0.9)	16.1	(2.3)	25.37	3.354
60	28.1	(2.0)	13.4	(0.6)	14.7	(2.1)	25.37	3.357
Station: TT159-3100	54.35 N	167.88 W	81/ 6/14	16.75 GMT	Sonic Depth	1427 m		
210	12.9	(1.3)	16.3	(1.3)	-4.2	(1.8)	26.61	3.653
220	16.1	(0.8)	18.8	(0.7)	-2.7	(1.0)	26.63	3.679
230	17.1	(0.6)	16.4	(0.4)	0.7	(0.7)	26.66	3.698
240	17.6	(1.0)	19.2	(0.7)	-1.6	(1.2)	26.68	3.727
250	12.7	(1.2)	17.9	(1.0)	-5.3	(1.6)	26.71	3.738
260	15.4	(1.6)	19.5	(1.0)	-4.0	(1.8)	26.73	3.727
270	16.9	(1.4)	20.7	(1.3)	-3.8	(1.9)	26.75	3.718
280	15.7	(1.2)	17.9	(0.8)	-2.2	(1.4)	26.77	3.709

Appendix 1: Measured-data (cont.)

Depth (m)	Rn	(sd)	Ra	(sd)	XSRn	(sd)	Sigma-t	Temp
Station: TT159-3103	54.85 N		167.88 W		81/ 6/15		16.55 GMT	Sonic Depth 1440 m
0	6.3	(0.6)	12.1	(0.9)	-5.8	(1.0)	25.53	7.571
5	5.5	(0.5)	11.6	(0.8)	-6.1	(0.9)	25.54	7.530
10	7.5	(0.6)	10.5	(0.9)	-2.9	(1.1)	25.55	7.489
15	4.5	(0.4)	11.2	(0.6)	-6.6	(0.8)	25.73	7.489
Station: TT159-3115	55.48 N		166.90 W		81/ 6/17		19.00 GMT	Sonic Depth 134 m
60	12.2	(0.9)	12.0	(0.9)	0.2	(1.3)	25.65	5.089
65	12.2	(0.6)	11.3	(1.1)	0.9	(1.3)	25.70	5.069
70	11.7	(1.2)	12.9	(0.6)	-1.2	(1.4)	25.74	4.440
75	11.5	(0.7)	11.8	(0.4)	-0.3	(0.8)	25.80	4.230
80	10.7	(0.5)	13.3	(0.6)	-2.6	(0.8)	25.85	4.555
85	10.7	(0.7)	12.3	(0.9)	-1.6	(1.1)	25.90	4.295
90	11.1	(1.0)	13.2	(0.9)	-2.1	(1.3)	25.95	4.0a4
110	23.6	(2.0)	15.2	(1.2)	8.5	(2.4)	26.09	3.894
120	22.5	(1.8)	15.1	(0.8)	7.3	(1.9)	26.13	3.887
130	23.7	(1.8)	12.3	(1.1)	11.4	(2.1)	26.16	3.887
Station: TT159-3119	55.94 N		166.15 W		81/ 6/18		15.42 GMT	Sonic Depth 119 m
0	4.9	(0.8)	12.5	(1.1)	-7.5	(1.3)	24.64	8.110
6	7.5	(0.4)	11.8	(0.9)	-4.4	(1.0)	24.64	8.104
12	8.6	(0.3)	13.3	(1.3)	-4.7	(1.3)	24.74	7.636
18	9.5	(0.7)	12.0	(0.8)	-2.6	(1.0)	25.01	6.248
24	10.4	(0.9)	13.4	(1.0)	-3.0	(1.3)	25.13	5.634
30	12.1	(1.1)	13.5	(0.7)	-1.5	(1.3)	25.18	5.406
36	10.3	(0.9)	11.6	(0.4)	-1.2	(0.9)	25.23	5.456
42	11.1	(0.9)	12.6	(0.7)	-1.5	(1.1)	25.27	5.483
Station: TT159-3126	56.55 N		165.13 W		81/ 6/20		01.25 GMT	Sonic Depth 76 m
10	6.6	(0.8)	8.1	(1.0)	-1.5	(1.3)	24.66	8.383
15	9.6	(0.5)	8.8	(0.5)	0.8	(0.7)	25.08	5.535
20	8.3	(0.4)	8.2	(0.3)	0.1	(0.5)	25.17	4.766
25	8.6	(0.7)	8.8	(0.5)	-0.2	(0.9)	25.20	4.654
30	9.6	(0.9)	7.7	(0.7)	1.8	(1.1)	25.22	4.541
35	11.6	(1.1)	7.9	(0.8)	3.7	(1.3)	25.30	3.849
40	25.2	(1.8)	10.0	(0.6)	15.2	(2.0)	25.38	3.157
45	26.1	(1.9)	10.2	(0.8)	15.9	(2.0)	25.38	3.152

Appendix 1: Measured-data (cont.)

Depth (m)	Rn	(sd)	Ra	(sd)	XSRn	(sd)	Sigma-t	Temp
Station: TT159-3131	56.55 N	165.14 W	81/ 6/20	20.00 GMT	Sonic Depth	77 m		
10	6.8	(1.6)	8.2	(1.3)	-1.4	(2.0)	24.67	8.308
15	9.0	(0.7)	7.8	(0.6)	1.2	(0.9)	24.67	8.280
20	10.8	(0.7)	8.7	(0.4)	2.1	(0.8)	25.09	5.040
25	9.6	(0.4)	9.3	(0.7)	0.3	(0.8)	25.13	4.773
30	11.3	(1.2)	10.8	(1.1)	0.5	(1.6)	25.17	4.506
35	21.4	(2.0)	11.5	(1.1)	9.9	(2.3)	25.28	3.831
40	26.2	(2.0)	12.3	(1.5)	13.9	(2.5)	25.38	3.155
45	27.3	(2.0)	10.9	(0.9)	16.4	(2.2)	25.38	3.151
Station: TT159-4021	57.88 N	162.89 W	81/ 7/ 1	00.50 GMT	Sonic Depth	40 m		
0	10.4	(1.2)	8.9	(1.3)	1.5	(1.8)	24.15	9.012
5	8.8	(0.7)	9.2	(0.6)	-0.3	(0.9)	24.15	9.002
10	25.0	(0.8)	9.7	(0.4)	15.3	(0.9)	24.17	8.939
15	42.9	(2.2)	10.4	(0.8)	32.5	(2.4)	24.79	7.272
20	47.4	(3.8)	9.6	(1.0)	37.8	(3.9)	25.15	6.132
25	50.3	(4.3)	9.2	(1.1)	41.1	(4.5)	25.16	6.102
30	53.2	(4.0)	9.9	(1.1)	43.3	(4.1)	25.16	6.076
35	49.6	(3.7)	11.0	(1.0)	38.5	(3.8)	25.16	6.075
Station: TT159-4025	57.13 N	164.15 W	81/ 7/ 1	18.50 GMT	Sonic Depth	64 m		
27	22.0	(2.5)	11.2	(1.2)	10.8	(2.7)	25.31	3.744
32	26.0	(1.5)	14.0	(0.6)	12.0	(1.6)	25.33	3.624
37	26.0	(1.0)	9.9	(0.3)	16.2	(1.0)	25.34	3.617
42	26.9	(1.7)	14.2	(0.7)	12.7	(1.8)	25.34	3.613
47	27.7	(2.3)	14.6	(1.0)	13.1	(2.5)	25.34	3.610
52	29.8	(2.5)	14.0	(0.9)	15.8	(2.7)	25.34	3.607
57	28.8	(2.2)	15.7	(1.2)	13.1	(2.5)	25.34	3.606
62	30.4	(2.2)	13.5	(0.7)	16.9	(2.3)	25.34	3.604
Station: TT159-4033	56.47 N	162.92 W	81/ 7/ 3	17.00 GMT	Sonic Depth	76 m		
0	2.0	(0.2)	3.9	(0.7)	-2.0	(0.7)	24.56	9.538
5	2.2	(0.2)	4.4	(0.3)	-2.2	(0.4)	24.56	9.534
10	2.4	(0.3)	-0.8	(0.1)	3.2	(0.3)	24.57	9.533
15	4.5	(1.0)	5.8	(0.4)	-1.3	(1.1)	24.56	9.529
Station: TT159-4040	56.83 N	160.11 W	81/ 7/ 4	18.00 GMT	Sonic Depth	72 m		
0	4.3	(0.4)	3.8	(0.4)	0.6	(0.6)	24.91	8.301
5	5.8	(0.5)	5.5	(0.5)	0.3	(0.8)	24.91	8.403
10	3.6	(0.5)	5.5	(0.5)	-1.9	(0.7)	24.91	8.400
15	4.1	(0.5)	4.3	(0.5)	-0.2	(0.7)	24.83	8.245

Appendix 1: Measured-data (cont.)

Depth (m)	Rn	(sd)	Ra	(sd)	XSRn	(sd)	Sigma-t	Temp
Station: TT159-4040	56.83 N	166.11 W	81/ 7/ 4	18.00 GMT	Sonic Depth	72 m		
0	4.3	(0.4)	3.8	(0.4)	0.6	(0.6)	24.91	8.301
5	5.8	(0.5)	5.5	(0.5)	0.3	(0.8)	24.81	8.403
10	3.6	(0.5)	5.5	(0.5)	-1.9	(0.7)	24.81	8.400
15	4.1	(0.5)	4.3	(0.5)	-0.2	(0.7)	24.83	8.245
Station: TT159-4055	54.48 N	166.90 W	81/ 7/ 8	22.00 GMT	Sonic Depth	133 m		
90	7.7	(0.9)	13.4	(1.2)	-5.7	(1.5)	25.99	4.295
96	16.6	(0.8)	14.8	(0.6)	1.8	(1.0)	26.05	4.115
102	11.0	(0.4)	14.3	(0.3)	-3.3	(0.5)	26.10	4.050
108	19.7	(1.1)	15.2	(1.0)	4.5	(1.5)	26.11	4.047
114	17.0	(1.4)	15.4	(1.0)	1.5	(1.7)	26.13	3.948
120	20.3	(1.7)	15.5	(1.3)	4.8	(1.7)	26.17	3.911
126	12.8	(1.0)	14.6	(0.8)	-2.6	(1.0)	26.18	3.873
132	14.0	(1.1)	13.5	(0.7)	0.6	(1.1)	26.18	3.871
Station: TT159-4064	55.93 N	166.15 W	81/ 7/11	00.42 GMT	Sonic Depth	116 m		
0	7.3	(0.6)	7.2	(0.7)	0.1	(1.0)	24.38	10.039
5	5.8	(0.6)	8.2	(0.7)	-2.3	(0.9)	24.44	9.674
10	8.0	(0.6)	7.4	(0.8)	0.6	(1.1)	24.48	9.451
15	7.2	(0.6)	7.6	(0.6)	-0.4	(0.8)	24.52	9.307
Station: TT159-4068	56.55 N	165.14 W	81/ 7/11	18.25 GMT	Sonic Depth	75 m		
5	6.9	(0.4)	9.8	(0.8)	-2.9	(0.9)	24.49	9.871
10	5.1	(0.2)	9.6	(1.2)	-4.5	(1.2)	24.53	9.777
15	9.2	(0.5)	9.5	(1.0)	-0.4	(1.1)	24.60	9.198
20	8.9	(1.0)	9.4	(1.0)	-0.5	(1.4)	24.63	9.074
25	21.3	(1.6)	10.7	(0.7)	10.6	(1.7)	24.86	6.988
30	17.5	(1.4)	9.7	(0.3)	7.8	(1.4)	25.10	4.902
35	27.1	(2.3)	15.6	(0.6)	11.6	(2.3)	25.24	4.149
40	22.8	(1.8)	15.5	(1.3)	7.2	(2.2)	25.38	3.396
Station: TT159-4083	55.20 N	166.38 W	81/ 7/14	17.50 GMT	Sonic Depth	133 m		
0	4.3	(0.5)	7.8	(0.9)	-3.6	(1.1)	24.48	9.548
10	10.6	(0.5)	12.5	(0.6)	-2.0	(0.8)	24.50	9.485
20	7.5	(0.3)	13.3	(0.3)	-5.8	(0.4)	25.18	7.131
30	13.7	(0.8)	12.1	(0.6)	1.6	(1.0)	25.45	6.076
40	7.3	(0.6)	14.9	(1.0)	-7.6	(1.2)	25.57	5.478
50	12.7	(1.1)	15.0	(1.0)	-2.3	(1.4)	25.67	5.039
60	7.9	(0.6)	12.7	(1.1)	-4.9	(1.3)	25.79	4.801
70	7.4	(0.6)	13.6	(0.8)	-6.3	(1.0)	25.91	4.562

Appendix 1: Measured-data (cont.)

Depth (m)	Rn	(sd)	Ra	(sd)	XSRn	(sd)	Sigma-t	Temp
Station: TT159-4093	**56.68 N**		**163.85 W**		**81/ 7/15**		**18.00 GMT**	**Sonic Depth 72 m**
0	1.5	(0.2)	2.2	(0.5)	-0.7	(0.5)	24.45	10.112
5	1.3	(0.2)	5.5	(0.3)	-4.1	(0.4)	24.46	10.094
10	3.1	(0.3)	3.1	(0.2)	-0.0	(0.4)	24.48	10.034
15	2.2	(0.3)	3.9	(0.3)	-1.6	(0.4)	24.49	9.972
Station: TT159-4103	**57.14 N**		**164.15 W**		**81/ 7/16**		**20.00 GMT**	**Sonic Depth 64 m**
0	2.9	(0.2)	4.4	(0.9)	-1.5	(0.9)	24.49	10.032
6	5.4	(0.4)	4.8	(0.4)	0.6	(0.6)	24.49	10.013
18	14.5	(1.0)	10.5	(0.4)	4.0	(1.0)	24.63	9.355
22	23.7	(5.0)	11.1	(0.7)	12.6	(5.0)	24.94	6.957
32	15.0	(1.7)	12.1	(1.1)	3.0	(2.0)	25.31	3.846
42	27.4	(1.4)	10.9	(0.9)	16.5	(1.7)	25.31	3.856
52	14.0	(0.6)	9.3	(1.1)	4.7	(1.2)	25.31	3.865
62	19.9	(1.2)	11.1	(0.8)	8.9	(1.4)	25.31	3.875
Station: TT159-4112	**56.08 N**		**165.90 W**		**81/ 7/17**		**18.50 GMT**	**Sonic Depth 104 m**
64	4.1	(0.5)	10.5	(1.2)	-6.4	(1.3)	25.52	5.600
70	10.9	(0.6)	10.4	(0.6)	0.4	(0.8)	25.60	5.063
77	15.1	(0.4)	11.8	(0.4)	3.3	(0.6)	25.71	5.356
82	17.6	(0.9)	10.7	(0.7)	6.9	(1.1)	25.79	4.881
87	14.9	(1.2)	13.2	(1.0)	1.7	(1.6)	25.87	4.656
92	27.8	(2.3)	12.2	(0.9)	15.6	(2.5)	25.92	4.572
97	20.0	(1.5)	13.7	(1.2)	6.4	(1.9)	25.92	4.565
101	29.3	(2.1)	11.6	(0.7)	17.7	(2.2)	25.92	4.564
Station: TT159-4124	**55.77 N**		**169.37 W**		**81/ 7/19**		**19.58 GMT**	**Sonic Depth 1829 m**
0	3.4	(0.3)	11.2	(0.9)	-7.8	(1.0)	24.73	9.209
5	7.2	(0.6)	12.6	(0.9)	-5.4	(1.1)	24.74	9.202
10	7.8	(0.6)	10.8	(1.1)	-2.9	(1.2)	24.74	9.195
15	6.2	(0.5)	10.3	(0.7)	-4.1	(0.9)	24.87	8.971
Station: TT159-4131	**55.49 N**		**166.84 W**		**81/ 7/20**		**20.17 GMT**	**Sonic Depth 132 m**
0	7.5	(0.6)	5.5	(1.0)	1.9	(1.2)	24.40	10.270
6	4.1	(0.4)	5.3	(0.5)	-1.1	(0.6)	24.42	10.210
12	6.7	(0.6)	6.2	(0.3)	0.5	(0.6)	24.54	9.888
18	6.9	(0.5)	7.8	(0.6)	-1.0	(0.8)	24.80	9.282
24	5.7	(0.7)	9.8	(1.0)	-4.1	(1.2)	25.07	8.180
30	8.4	(0.5)	9.2	(0.9)	-0.9	(1.0)	25.35	6.839
36	12.5	(0.4)	11.4	(1.3)	1.0	(1.4)	25.48	6.080
42	12.1	(0.7)	9.0	(0.8)	3.1	(1.0)	25.58	5.512

Appendix 1: Measured-data (cont.)

Depth (m)	Rn	(sd)	Ra	(sd)	XSRn	(sd)	Sigma-t	Temp
Station: HX028-0010	56.54 N	165.15 W	82/ 6/21	21.79 GMT	Sonic Depth	89 m		
40	23.3	(2.6)	10.3	(1.5)	13.0	(3.0)	25.73	1.940
45	18.2	(1.1)	10.4	(0.9)	7.9	(1.4)	25.75	1.920
50	14.4	(0.7)	9.4	(0.7)	4.9	(1.0)	25.78	1.920
55	17.5	(1.2)	9.8	(0.9)	7.7	(1.5)	25.80	1.920
60	26.3	(2.2)	13.5	(1.2)	12.8	(2.5)	25.82	1.900
65	29.3	(2.5)	13.0	(1.1)	16.3	(2.7)	25.85	1.900
70	31.7	(3.9)	8.3	(1.2)	23.4	(4.1)	25.87	1.900
75	21.0	(1.4)	6.0	(0.7)	14.9	(1.5)	25.90	1.900
Station: HX028-0018	55.87 N	166.26 W	82/ 6/23	20.15 GMT	Sonic Depth	124 m		
40	12.4	(1.4)	9.6	(1.4)	2.8	(2.0)	25.55	4.720
45	11.5	(0.7)	10.4	(0.9)	1.1	(1.2)	25.57	4.760
50	7.1	(0.4)	9.3	(0.7)	-2.2	(0.8)	25.60	4.370
60	4.0	(0.4)	8.8	(0.9)	-4.9	(1.0)	25.70	4.370
65	6.8	(0.7)	12.1	(1.2)	-5.3	(1.3)	25.72	3.930
70	15.3	(1.3)	11.9	(1.0)	3.4	(1.7)	25.75	3.710
75	13.9	(1.8)	10.8	(1.4)	3.1	(2.3)	25.79	4.180
80	14.6	(0.9)	10.1	(0.9)	4.5	(1.3)	25.84	4.160
Station: HX028-0030	54.84 N	167.96 W	82/ 6/24	20.95 GMT	Sonic Depth	1500 m		
0	5.4	(0.7)	10.6	(1.3)	-5.1	(1.5)	25.86	5.840
8	5.4	(0.4)	12.3	(0.8)	-6.8	(0.9)	25.92	5.410
16	11.1	(0.5)	11.6	(0.6)	-0.4	(0.8)	25.99	5.080
24	11.6	(0.8)	10.2	(0.8)	1.4	(1.1)	25.99	5.070
32	6.4	(0.6)	12.1	(1.1)	-5.7	(1.3)	26.01	4.860
40	16.4	(1.4)	14.5	(1.1)	1.9	(1.8)	26.04	4.790
48	14.4	(1.8)	12.7	(1.6)	1.7	(2.5)	26.05	4.760
56	14.6	(0.9)	14.0	(0.9)	0.6	(1.3)	26.09	4.690
Station: HX028-0041	56.87 N	164.62 W	82/ 6/27	00.07 GMT	Sonic Depth	73 m		
0	4.1	(0.6)	8.3	(1.2)	-4.3	(1.3)	24.82	5.480
10	8.3	(0.6)	8.0	(0.7)	0.3	(0.9)	24.91	5.580
20	9.5	(0.5)	8.3	(0.6)	1.2	(0.8)	25.23	2.520
30	22.4	(1.5)	10.6	(1.0)	11.9	(1.8)	25.44	.120
40	25.9	(2.2)	11.8	(1.2)	14.1	(2.5)	25.45	.090
50	27.8	(2.3)	11.2	(1.0)	16.6	(2.5)	25.47	.160
60	17.4	(2.2)	10.4	(1.4)	7.1	(2.6)	25.49	.290
70	22.6	(1.4)	9.3	(0.9)	13.3	(1.7)	25.51	.550

Appendix 1: Measured data (cont.)

Depth (m)	Rn	(sd)	Ra	(sd)	XSRn	(sd)	Sigma-t	Temp
Station: HX028-0046	55.17 N	167.40 W	82/ 6/28	17.42 GMT	Sonic Depth	160 m		
60	14.9	(1.1)	12.6	(0.8)	2.3	(1.3)	26.11	4.620
70	13.9	(0.7)	12.4	(0.8)	1.5	(1.1)	26.18	4.390
80	8.5	(1.0)	9.6	(1.0)	-1.1	(1.4)	26.23	4.250
90	8.2	(0.6)	10.5	(0.7)	-2.3	(0.9)	26.27	4.070
100	7.5	(0.5)	10.4	(0.6)	-2.9	(0.8)	26.29	3.960
110	7.3	(0.6)	11.3	(0.9)	-4.0	(1.1)	26.32	3.870
120	13.7	(1.2)	12.4	(0.9)	1.4	(1.5)	26.33	3.840
130	25.0	(2.1)	11.8	(0.9)	13.2	(2.3)	26.36	3.820
140	23.6	(3.0)	13.5	(1.4)	10.1	(3.3)	26.36	3.820
150	16.7	(1.1)	11.2	(0.9)	5.5	(1.4)	26.37	3.810
Station: HX028-0063	56.03 N	166.03 W	82/ 6/30	10.54 GMT	Sonic Depth	116 m		
30	7.3	(1.0)	9.9	(1.1)	-2.6	(1.5)	25.39	4.240
35	8.5	(0.6)	9.8	(0.7)	-1.3	(0.9)	25.48	4.150
40	13.0	(0.7)	9.6	(0.5)	3.5	(0.8)	25.51	4.250
45	13.0	(0.9)	10.0	(0.7)	3.0	(1.2)	25.56	4.260
50	11.4	(1.0)	10.6	(0.8)	0.8	(1.3)	25.61	4.200
60	7.7	(0.7)	12.2	(1.0)	-4.6	(1.2)	25.68	3.770
70	11.7	(1.5)	13.8	(1.6)	-2.0	(2.2)	25.79	3.700
80	10.1	(0.7)	12.1	(0.8)	-2.1	(1.0)	25.83	3.720
Station: HX028-0096	55.63 N	166.67 W	82/ 7/ 1	18.04 GMT	Sonic Depth	133 m		
88	21.2	(2.4)	11.4	(1.2)	9.8	(2.7)	25.99	3.820
94	24.2	(1.4)	11.4	(0.7)	12.8	(1.6)	26.03	3.830
100	16.2	(0.8)	10.7	(0.6)	5.4	(0.9)	26.04	3.830
106	12.9	(1.0)	10.2	(0.7)	2.7	(1.2)	26.05	3.830
112	15.2	(1.3)	14.6	(1.1)	0.6	(1.7)	26.05	3.840
118	29.1	(2.4)	13.8	(0.9)	15.3	(2.6)	26.05	3.840
124	19.1	(2.4)	14.0	(1.5)	5.1	(2.9)	26.06	3.840
130	16.4	(1.1)	13.0	(0.8)	3.4	(1.3)	26.06	3.850
Station: HX028-0112	56.25 N	165.63 W	82/ 7/ 3	17.62 GMT	Sonic Depth	93 m		
0	9.5	(0.7)	11.0	(1.2)	-1.5	(1.4)	25.07	6.750
10	7.7	(0.5)	9.4	(0.9)	-1.7	(0.9)	25.07	6.740
20	5.3	(0.6)	9.3	(1.2)	-4.1	(1.3)	25.09	6.660
30	11.5	(0.7)	10.0	(0.7)	1.6	(1.0)	25.21	5.920
40	12.7	(0.6)	9.2	(0.6)	3.6	(0.8)	25.47	3.470
50	10.5	(0.8)	8.5	(0.7)	2.0	(1.0)	25.61	2.060
60	13.3	(1.2)	10.7	(0.8)	2.6	(1.5)	25.62	2.050
70	11.2	(1.1)	10.5	(0.8)	0.7	(1.3)	25.62	2.050
80	10.3	(1.5)	11.2	(1.3)	-0.8	(2.0)	25.62	2.050
87	11.9	(0.8)	9.5	(0.8)	2.4	(1.1)	25.62	2.050

Appendix 2: KRIGED-DATA

This appendix presents the resultant matrices of the SURFACE-II kriging subroutine (Sampson, 1978). These matrices are essentially disassembled 21 X 21 matrices with their rows and columns labeled. In all of the following sets of numbers column one is 556 km and column 21 is 99 km offshore; the distance between columns is 22.85 km. All rows are 6.6 m apart and the first row is at the surface (0 m); row 21 corresponds to a depth of 132 m. The ^{222}Rn, ^{224}Ra and error estimate matrices are in units of dpm/100 kg and the temperatures are in degrees Celsius. The blank value in what follows is zero. Blanks were caused by the bottom topography or search failures during the kriging exercise.

Appendix 2a: Total ^{222}Rn (dpm/100 kg)

row \ col	1	2	3	4	5	6	7
1	6.30	5.47	6.82	6.17	5.85	5.94	6.00
2	6.15	6.18	6.39	5.97	5.17	6.28	6.59
3	5.58	0.00	6.31	6.89	6.71	7.46	7.90
4	0.00	0.00	6.09	6.45	7.30	8.12	9.15
5	0.00	0.00	6.38	7.88	7.78	9.27	10.25
6	0.00	0.00	7.79	9.48	11.69	10.70	10.76
7	0.00	0.00	8.71	10.50	8.16	10.60	10.65
8	0.00	0.00	7.62	10.28	12.33	11.23	10.10
9	0.00	0.00	7.64	9.59	11.82	9.71	9.57
10	0.00	0.00	10.00	9.96	10.27	9.25	8.42
11	0.00	0.00	0.00	6.57	11.70	8.70	6.70
12	0.00	0.00	0.00	8.41	10.45	9.72	8.51
13	0.00	0.00	0.00	0.00	10.84	10.35	12.89
14	0.00	0.00	0.00	0.00	9.76	11.90	15.44
15	0.00	0.00	0.00	0.00	11.60	19.26	28.39
16	0.00	0.00	0.00	0.00	12.62	27.29	28.11
17	0.00	0.00	0.00	0.00	0.00	28.36	29.49
18	0.00	0.00	0.00	0.00	0.00	29.71	0.00
19	0.00	0.00	0.00	0.00	0.00	30.92	0.00
20	0.00	0.00	0.00	0.00	0.00	19.04	0.00
21	0.00	0.00	0.00	0.00	0.00	0.00	0.00

row \ col	8	9	10	11	12	13	14
1	6.00	8.71	8.28	5.73	2.76	2.79	2.25
2	7.21	8.26	8.01	6.62	4.98	3.73	2.14
3	8.03	7.70	7.85	7.20	7.09	3.97	2.82
4	9.65	7.87	8.00	9.30	9.55	8.17	8.49
5	10.98	10.16	10.35	11.70	12.80	13.45	14.86
6	11.10	12.18	13.19	14.97	16.71	19.20	20.79
7	10.73	11.15	13.79	18.25	23.45	24.76	25.95
8	10.21	10.84	14.18	19.34	25.31	27.92	28.98
9	8.61	9.47	13.66	19.01	24.14	28.61	31.80
10	7.08	6.54	11.57	17.69	23.55	29.55	34.00
11	7.55	6.24	10.74	15.81	21.30	27.25	32.78
12	10.45	12.18	14.58	18.35	21.83	28.21	0.00
13	13.98	16.00	18.07	19.13	0.00	0.00	0.00
14	18.73	16.00	19.28	0.00	0.00	0.00	0.00
15	24.59	27.11	21.73	0.00	0.00	0.00	0.00
16	27.26	25.21	0.00	0.00	0.00	0.00	0.00
17	30.76	31.39	0.00	0.00	0.00	0.00	0.00
18	27.25	0.00	0.00	0.00	0.00	0.00	0.00
19	0.00	0.00	0.00	0.00	0.00	0.00	0.00
20	0.00	0.00	0.00	0.00	0.00	0.00	0.00
21	0.00	0.00	0.00	0.00	0.00	0.00	0.00

Appendix 2a (cont.): Total ^{222}Rn (dpm/100 kg)

row \ col	15	16	17	18	19	20	21
1	1.78	2.86	3.59	5.61	12.67	11.54	0.00
2	2.39	5.46	7.10	9.44	8.97	17.05	0.00
3	4.68	9.61	14.45	19.92	30.03	34.12	0.00
4	11.89	18.34	21.64	29.09	40.82	43.96	0.00
5	18.10	21.97	24.49	26.66	30.32	41.30	0.00
6	22.34	22.68	26.40	26.58	28.17	40.99	0.00
7	27.77	34.63	32.08	35.52	41.61	43.92	0.00
8	28.66	29.09	32.91	39.58	0.00	0.00	0.00
9	29.99	25.27	29.95	0.00	0.00	0.00	0.00
10	34.14	28.48	0.00	0.00	0.00	0.00	0.00
11	31.16	0.00	0.00	0.00	0.00	0.00	0.00
12	0.00	0.00	0.00	0.00	0.00	0.00	0.00
13	0.00	0.00	0.00	0.00	0.00	0.00	0.00
14	0.00	0.00	0.00	0.00	0.00	0.00	0.00
15	0.00	0.00	0.00	0.00	0.00	0.00	0.00
16	0.00	0.00	0.00	0.00	0.00	0.00	0.00
17	0.00	0.00	0.00	0.00	0.00	0.00	0.00
18	0.00	0.00	0.00	0.00	0.00	0.00	0.00
19	0.00	0.00	0.00	0.00	0.00	0.00	0.00
20	0.00	0.00	0.00	0.00	0.00	0.00	0.00
21	0.00	0.00	0.00	0.00	0.00	0.00	0.00

Appendix 2b: ^{226}Ra (dpm/100 kg)

row \ col	1	2	3	4	5	6	7
1	12.10	10.03	9.63	8.26	6.67	7.63	8.06
2	11.26	9.75	7.97	7.68	6.41	7.58	8.19
3	10.96	0.00	10.06	8.36	6.60	8.55	9.53
4	0.00	0.00	9.28	9.56	12.28	10.59	10.92
5	0.00	0.00	10.19	10.47	10.14	10.96	12.11
6	0.00	0.00	11.32	11.26	11.03	11.65	12.04
7	0.00	0.00	11.95	12.33	14.22	11.95	12.15
8	0.00	0.00	12.50	12.11	12.15	12.39	12.35
9	0.00	0.00	12.73	13.30	14.22	13.02	12.35
10	0.00	0.00	13.65	12.96	12.51	12.11	11.73
11	0.00	0.00	0.00	12.59	11.77	12.07	11.82
12	0.00	0.00	0.00	13.85	12.40	12.40	11.98
13	0.00	0.00	0.00	0.00	13.08	12.30	11.91
14	0.00	0.00	0.00	0.00	12.34	12.76	12.40
15	0.00	0.00	0.00	0.00	13.90	14.33	13.69
16	0.00	0.00	0.00	0.00	14.56	14.32	14.47
17	0.00	0.00	0.00	0.00	0.00	15.75	15.93
18	0.00	0.00	0.00	0.00	0.00	14.45	0.00
19	0.00	0.00	0.00	0.00	0.00	14.52	0.00
20	0.00	0.00	0.00	0.00	0.00	15.29	0.00
21	0.00	0.00	0.00	0.00	0.00	0.00	0.00

row \ col	8	9	10	11	12	13	14
1	9.43	10.68	10.14	7.59	4.66	3.41	2.12
2	10.14	11.53	11.76	9.90	7.68	5.65	2.82
3	10.59	12.06	12.08	9.94	8.20	5.01	3.46
4	12.20	9.68	10.07	10.26	8.99	6.74	6.35
5	13.41	13.21	12.07	10.75	9.75	8.95	8.87
6	12.58	13.41	12.70	11.58	10.84	10.58	10.91
7	12.18	11.83	11.79	11.56	12.26	11.71	11.63
8	12.37	11.66	11.34	11.37	10.69	11.81	12.99
9	11.81	11.30	11.20	11.24	11.98	12.79	14.00
10	11.29	10.85	10.97	11.81	12.66	13.59	14.74
11	10.90	10.45	10.67	11.27	12.00	14.15	15.14
12	11.07	10.89	11.21	11.71	12.65	13.67	0.00
13	11.51	11.31	11.70	12.25	0.00	0.00	0.00
14	12.33	12.55	12.17	0.00	0.00	0.00	0.00
15	13.39	12.62	12.15	0.00	0.00	0.00	0.00
16	13.93	12.84	0.00	0.00	0.00	0.00	0.00
17	14.74	12.95	0.00	0.00	0.00	0.00	0.00
18	15.06	0.00	0.00	0.00	0.00	0.00	0.00
19	0.00	0.00	0.00	0.00	0.00	0.00	0.00
20	0.00	0.00	0.00	0.00	0.00	0.00	0.00
21	0.00	0.00	0.00	0.00	0.00	0.00	0.00

Appendix 2b (cont.): ^{226}Ra (dpm/100 kg)

row \ col	15	16	17	18	19	20	21
1	2.01	4.26	4.09	4.11	11.21	11.77	0.00
2	2.48	4.77	4.12	4.17	10.36	12.40	0.00
3	4.30	7.30	7.75	7.23	9.81	11.35	0.00
4	7.81	10.65	10.06	9.54	9.60	10.17	0.00
5	10.15	11.16	11.32	10.99	11.24	10.40	0.00
6	11.80	13.07	12.05	11.48	11.18	10.92	0.00
7	12.73	13.53	11.82	11.09	10.22	10.30	0.00
8	13.77	13.75	12.09	10.61	0.00	0.00	0.00
9	14.42	12.21	11.97	0.00	0.00	0.00	0.00
10	14.69	13.94	0.00	0.00	0.00	0.00	0.00
11	15.22	0.00	0.00	0.00	0.00	0.00	0.00
12	0.00	0.00	0.00	0.00	0.00	0.00	0.00
13	0.00	0.00	0.00	0.00	0.00	0.00	0.00
14	0.00	0.00	0.00	0.00	0.00	0.00	0.00
15	0.00	0.00	0.00	0.00	0.00	0.00	0.00
16	0.00	0.00	0.00	0.00	0.00	0.00	0.00
17	0.00	0.00	0.00	0.00	0.00	0.00	0.00
18	0.00	0.00	0.00	0.00	0.00	0.00	0.00
19	0.00	0.00	0.00	0.00	0.00	0.00	0.00
20	0.00	0.00	0.00	0.00	0.00	0.00	0.00
21	0.00	0.00	0.00	0.00	0.00	0.00	0.00

Appendix 2c: Sigma-t

col

row	1	2	3	4	5	6	7
1	25.53	25.11	24.92	24.67	24.45	24.43	24.40
2	25.54	25.19	24.89	24.62	24.43	24.41	24.44
3	25.67	0.00	25.10	24.82	24.60	24.60	24.62
4	0.00	0.00	25.25	25.08	25.12	24.90	24.91
5	0.00	0.00	25.47	25.34	25.21	25.15	25.13
6	0.00	0.00	25.64	25.55	25.45	25.34	25.26
7	0.00	0.00	25.81	25.68	25.57	25.45	25.35
8	0.00	0.00	25.85	25.72	25.63	25.53	25.43
9	0.00	0.00	25.87	25.76	25.69	25.60	25.50
10	0.00	0.00	25.93	25.81	25.72	25.65	25.58
11	0.00	0.00	0.00	25.84	25.73	25.66	25.60
12	0.00	0.00	0.00	25.92	25.81	25.73	25.68
13	0.00	0.00	0.00	0.00	25.85	25.80	25.81
14	0.00	0.00	0.00	0.00	25.91	25.87	25.89
15	0.00	0.00	0.00	0.00	26.00	25.99	26.01
16	0.00	0.00	0.00	0.00	26.07	26.11	26.07
17	0.00	0.00	0.00	0.00	0.00	26.16	26.12
18	0.00	0.00	0.00	0.00	0.00	26.15	0.00
19	0.00	0.00	0.00	0.00	0.00	26.17	0.00
20	0.00	0.00	0.00	0.00	0.00	26.19	0.00
21	0.00	0.00	0.00	0.00	0.00	0.00	0.00

col

row	8	9	10	11	12	13	14
1	24.48	24.69	24.74	24.63	24.56	24.64	24.73
2	24.55	24.71	24.79	24.70	24.57	24.61	24.73
3	24.64	24.80	24.88	24.80	24.69	24.65	24.76
4	25.03	25.02	25.00	24.96	24.95	24.87	24.87
5	25.15	25.10	25.07	25.08	25.09	25.07	25.07
6	25.22	25.14	25.14	25.18	25.23	25.24	25.22
7	25.27	25.21	25.22	25.28	25.36	25.34	25.33
8	25.36	25.31	25.32	25.34	25.38	25.37	25.34
9	25.46	25.39	25.39	25.38	25.38	25.38	25.32
10	25.51	25.47	25.45	25.42	25.39	25.36	25.32
11	25.60	25.55	25.53	25.50	25.46	25.40	25.34
12	25.69	25.65	25.61	25.58	25.49	25.42	0.00
13	25.78	25.75	25.71	25.62	0.00	0.00	0.00
14	25.88	25.86	25.78	0.00	0.00	0.00	0.00
15	25.97	25.93	25.83	0.00	0.00	0.00	0.00
16	26.03	25.94	0.00	0.00	0.00	0.00	0.00
17	26.05	25.96	0.00	0.00	0.00	0.00	0.00
18	26.08	0.00	0.00	0.00	0.00	0.00	0.00
19	0.00	0.00	0.00	0.00	0.00	0.00	0.00
20	0.00	0.00	0.00	0.00	0.00	0.00	0.00
21	0.00	0.00	0.00	0.00	0.00	0.00	0.00

Appendix 2c (cont.): Sigma-t

row \ col	15	16	17	18	19	20	21
1	24.70	24.50	24.65	24.91	25.12	24.73	0.00
2	24.71	24.51	24.62	24.93	25.15	24.88	0.00
3	24.77	24.63	24.77	25.05	25.25	25.08	0.00
4	24.87	24.77	24.96	25.25	25.41	25.34	0.00
5	25.12	25.26	25.25	25.36	25.43	25.39	0.00
6	25.28	25.33	25.37	25.41	25.43	25.37	0.00
7	25.34	25.36	25.41	25.42	25.39	25.32	0.00
8	25.33	25.35	25.39	25.46	0.00	0.00	0.00
9	25.31	25.34	25.38	0.00	0.00	0.00	0.00
10	25.31	25.36	0.00	0.00	0.00	0.00	0.00
11	25.31	0.00	0.00	0.00	0.00	0.00	0.00
12	0.00	0.00	0.00	0.00	0.00	0.00	0.00
13	0.00	0.00	0.00	0.00	0.00	0.00	0.00
14	0.00	0.00	0.00	0.00	0.00	0.00	0.00
15	0.00	0.00	0.00	0.00	0.00	0.00	0.00
16	0.00	0.00	0.00	0.00	0.00	0.00	0.00
17	0.00	0.00	0.00	0.00	0.00	0.00	0.00
18	0.00	0.00	0.00	0.00	0.00	0.00	0.00
19	0.00	0.00	0.00	0.00	0.00	0.00	0.00
20	0.00	0.00	0.00	0.00	0.00	0.00	0.00
21	0.00	0.00	0.00	0.00	0.00	0.00	0.00

Appendix 2d: Temperature (°C)

row \ col	1	2	3	4	5	6	7
1	7.57	8.61	8.72	9.33	9.89	9.77	9.74
2	7.51	8.43	9.21	9.72	10.12	9.89	9.65
3	7.49	0.00	8.51	9.24	9.77	9.24	8.85
4	0.00	0.00	8.37	8.45	7.52	8.08	7.47
5	0.00	0.00	7.55	7.42	7.49	7.00	6.45
6	0.00	0.00	6.81	6.46	6.26	6.15	5.92
7	0.00	0.00	5.92	5.63	5.56	5.69	5.66
8	0.00	0.00	5.10	5.32	5.28	5.39	5.49
9	0.00	0.00	5.37	5.11	5.02	5.21	5.34
10	0.00	0.00	4.92	4.97	4.94	5.12	5.26
11	0.00	0.00	0.00	4.93	4.93	5.10	5.29
12	0.00	0.00	0.00	4.40	4.35	4.83	5.09
13	0.00	0.00	0.00	0.00	4.45	4.73	4.74
14	0.00	0.00	0.00	0.00	4.30	4.63	4.54
15	0.00	0.00	0.00	0.00	4.17	4.01	3.97
16	0.00	0.00	0.00	0.00	4.10	3.88	3.98
17	0.00	0.00	0.00	0.00	0.00	3.69	3.87
18	0.00	0.00	0.00	0.00	0.00	3.81	0.00
19	0.00	0.00	0.00	0.00	0.00	3.78	0.00
20	0.00	0.00	0.00	0.00	0.00	3.77	0.00
21	0.00	0.00	0.00	0.00	0.00	0.00	0.00

row \ col	8	9	10	11	12	13	14
1	9.23	7.94	7.73	8.68	9.46	9.33	8.54
2	8.76	7.86	7.37	8.18	9.31	9.39	8.51
3	8.46	7.24	6.63	7.29	8.33	9.08	8.35
4	6.24	5.71	5.63	6.02	6.38	7.23	7.30
5	5.64	5.20	5.06	5.12	5.19	5.47	5.61
6	5.48	5.14	4.73	4.43	4.23	4.17	4.32
7	5.50	5.12	4.56	4.00	3.40	3.39	3.48
8	5.35	5.14	4.51	3.96	3.32	3.29	3.42
9	5.27	5.22	4.72	4.19	3.77	3.51	3.72
10	5.40	5.42	4.96	4.50	4.14	3.80	3.75
11	5.31	5.43	5.11	4.76	4.38	3.99	3.74
12	5.12	5.18	5.05	4.75	4.58	4.24	0.00
13	4.91	5.13	4.98	4.90	0.00	0.00	0.00
14	4.58	4.68	4.82	0.00	0.00	0.00	0.00
15	4.31	4.51	4.79	0.00	0.00	0.00	0.00
16	4.21	4.50	0.00	0.00	0.00	0.00	0.00
17	4.21	4.45	0.00	0.00	0.00	0.00	0.00
18	4.07	0.00	0.00	0.00	0.00	0.00	0.00
19	0.00	0.00	0.00	0.00	0.00	0.00	0.00
20	0.00	0.00	0.00	0.00	0.00	0.00	0.00
21	0.00	0.00	0.00	0.00	0.00	0.00	0.00

Appendix 2d (cont.): Temperature (°C)

row \ col	15	16	17	18	19	20	21
1	8.53	9.97	9.26	7.84	6.75	7.64	0.00
2	8.45	9.88	9.16	7.63	6.70	7.06	0.00
3	8.17	9.22	8.33	6.53	5.36	6.06	0.00
4	7.38	8.26	6.90	5.29	4.40	5.00	0.00
5	5.26	4.17	4.66	4.42	4.28	4.79	0.00
6	3.92	3.64	3.68	3.94	4.17	4.80	0.00
7	3.44	3.39	3.43	3.78	4.31	5.06	0.00
8	3.44	3.53	3.54	3.59	0.00	0.00	0.00
9	3.71	3.56	3.60	0.00	0.00	0.00	0.00
10	3.70	3.42	0.00	0.00	0.00	0.00	0.00
11	3.65	0.00	0.00	0.00	0.00	0.00	0.00
12	0.00	0.00	0.00	0.00	0.00	0.00	0.00
13	0.00	0.00	0.00	0.00	0.00	0.00	0.00
14	0.00	0.00	0.00	0.00	0.00	0.00	0.00
15	0.00	0.00	0.00	0.00	0.00	0.00	0.00
16	0.00	0.00	0.00	0.00	0.00	0.00	0.00
17	0.00	0.00	0.00	0.00	0.00	0.00	0.00
18	0.00	0.00	0.00	0.00	0.00	0.00	0.00
19	0.00	0.00	0.00	0.00	0.00	0.00	0.00
20	0.00	0.00	0.00	0.00	0.00	0.00	0.00
21	0.00	0.00	0.00	0.00	0.00	0.00	0.00

Appendix 2e: Kriging error (dpm/100 kg)

col

row	1	2	3	4	5	6	7
1	0.00	3.45	3.93	3.41	1.01	3.09	3.25
2	1.57	3.31	3.85	3.29	1.21	2.91	3.07
3	1.62	0.00	3.86	3.26	1.53	2.92	3.06
4	0.00	0.00	3.92	3.25	1.00	2.90	3.07
5	0.00	0.00	4.26	3.31	1.83	2.93	3.08
6	0.00	0.00	4.82	3.42	1.86	2.93	3.08
7	0.00	0.00	5.37	3.49	1.11	2.93	3.11
8	0.00	0.00	5.49	3.64	2.14	3.03	3.35
9	0.00	0.00	6.17	3.85	2.16	3.17	3.64
10	0.00	0.00	6.82	3.89	1.27	3.15	3.75
11	0.00	0.00	0.00	4.23	1.42	3.17	3.82
12	0.00	0.00	0.00	4.08	1.72	3.17	3.79
13	0.00	0.00	0.00	0.00	1.35	3.17	3.63
14	0.00	0.00	0.00	0.00	1.47	3.19	3.52
15	0.00	0.00	0.00	0.00	1.87	3.92	4.11
16	0.00	0.00	0.00	0.00	1.89	3.77	3.59
17	0.00	0.00	0.00	0.00	0.00	4.86	4.13
18	0.00	0.00	0.00	0.00	0.00	3.97	0.00
19	0.00	0.00	0.00	0.00	0.00	4.06	0.00
20	0.00	0.00	0.00	0.00	0.00	4.43	0.00
21	0.00	0.00	0.00	0.00	0.00	0.00	0.00

col

row	8	9	10	11	12	13	14
1	1.56	1.91	2.65	3.16	1.66	1.68	2.24
2	1.54	1.88	2.52	3.01	1.80	1.78	2.17
3	1.57	1.87	2.51	2.99	1.82	1.80	2.25
4	1.85	1.86	2.50	2.98	1.62	2.45	2.96
5	1.92	1.90	2.51	2.99	1.78	2.78	3.39
6	1.95	1.88	2.52	3.01	1.84	2.84	3.49
7	1.92	2.37	2.94	3.10	1.64	2.83	3.51
8	2.80	3.18	3.55	3.36	1.94	2.91	3.27
9	3.59	3.56	3.75	3.78	3.50	3.38	2.74
10	3.50	2.88	3.43	3.98	4.05	3.71	2.63
11	3.30	1.84	3.08	4.06	4.37	3.93	2.83
12	3.28	1.99	3.08	4.10	4.55	4.42	0.00
13	3.22	1.77	3.06	4.21	0.00	0.00	0.00
14	2.96	1.60	3.06	0.00	0.00	0.00	0.00
15	2.38	1.30	3.11	0.00	0.00	0.00	0.00
16	2.36	1.52	0.00	0.00	0.00	0.00	0.00
17	2.40	2.17	0.00	0.00	0.00	0.00	0.00
18	2.94	0.00	0.00	0.00	0.00	0.00	0.00
19	0.00	0.00	0.00	0.00	0.00	0.00	0.00
20	0.00	0.00	0.00	0.00	0.00	0.00	0.00
21	0.00	0.00	0.00	0.00	0.00	0.00	0.00

Appendix 2e (cont.): Kriging error (dpm/100 kg)

row \ col	15	16	17	18	19	20	21
1	1.94	0.88	2.99	2.80	0.64	2.69	0.00
2	1.92	1.21	2.90	2.65	1.39	2.58	0.00
3	2.08	2.48	3.01	2.76	1.60	2.60	0.00
4	2.85	1.52	2.89	2.96	2.12	2.62	0.00
5	3.06	1.18	2.88	2.95	1.48	2.60	0.00
6	3.10	1.35	2.86	2.84	2.14	2.71	0.00
7	3.07	1.03	2.82	2.69	1.70	3.01	0.00
8	2.87	1.21	2.83	2.78	0.00	0.00	0.00
9	2.04	1.26	2.93	0.00	0.00	0.00	0.00
10	1.92	1.12	0.00	0.00	0.00	0.00	0.00
11	2.02	0.00	0.00	0.00	0.00	0.00	0.00
12	0.00	0.00	0.00	0.00	0.00	0.00	0.00
13	0.00	0.00	0.00	0.00	0.00	0.00	0.00
14	0.00	0.00	0.00	0.00	0.00	0.00	0.00
15	0.00	0.00	0.00	0.00	0.00	0.00	0.00
16	0.00	0.00	0.00	0.00	0.00	0.00	0.00
17	0.00	0.00	0.00	0.00	0.00	0.00	0.00
18	0.00	0.00	0.00	0.00	0.00	0.00	0.00
19	0.00	0.00	0.00	0.00	0.00	0.00	0.00
20	0.00	0.00	0.00	0.00	0.00	0.00	0.00
21	0.00	0.00	0.00	0.00	0.00	0.00	0.00

REFERENCES CITED

Banahan, S. (1983) The uptake of silicic acid by diatoms in the Bering Sea. M.S. Thesis, Univ. of Alaska, Fairbanks. 121 pp.

Berelson, W.M., D.E. Hammond and C. Fuller. (1982) Radon-222 as a tracer for mixing in the water column and benthic exchange in the southern California borderland. *Earth Planet. Sci. Lett.* **61**: 41-54.

Bevington, P.R. (1969) **Data Reduction and Error Analysis for the Physical Sciences.** McGraw-Hill Book Co., New York. 336 pp.

Biscaye, P.E., C. Olsen and G.G. Mathieu. (1978) Suspended particles and natural radionuclides as tracers of pollutant transports in the continental shelf waters of the eastern USA. *In* **First American - Soviet Symposium on the Chemical Pollution of the Marine Environment.** Columbia University Press, New York. pp 125-147.

Bretherton, F.P., R.E. Davis and C.B. Fandry. (1976) A technique for objective analysis and design of oceanographic experiments applied to MODE-73. *Deep Sea Res.* **23**: 559-582.

Broecker, H-C., J. Petermann and W. Siems. (1978) The influence of wind on CO_2-exchange in a wind-wave tunnel, including the effects of monolayers. *J. Marine Res.* **36**: 595-610.

Broecker, W.S. (1965) An application of natural radon to problems in ocean circulation. *In* T. Ichiye (ed.). **Symposium on Diffusion in Oceans and Freshwaters.** Lamont-Doherty Geo. Observatory, New York. pp 116-145.

Broecker, W.S., J. Cromwell and Y-H. Li. (1968) Rates of vertical eddy

diffusion near the ocean floor based on measurements of the distribution of excess 222-Rn. *Earth Planet. Sci. Lett.* **5**: 101-105.

Broecker, W.S. and A. Kaufman. (1970) Near-surface and near-bottom radon results for the 1969 North Pacific Geosecs station. *J. Geophys. Res.* **75**, 36: 7679-7681.

Broecker, W.S. and T-H. Peng. (1971) The vertical distribution of radon in the BOMEX area. *Earth Planet. Sci. Lett.* **11**: 99-108.

Broecker, W.S. and T-H. Peng. (1974) Gas exchange rates between air and sea. *Tellus.* **26**: 21-35.

Broecker, W.S. (1974) **Chemical Oceanography.** Harcourt Brace Jovanovich Inc. New York. 214 pp.

Broecker, W.S., J. Goddard and J.L. Sarmiento. (1976) The distribution of ^{224}Ra in the Atlantic ocean. *Earth Planet. Sci. Lett.* **32**: 220-239.

Broecker, W.S. and T-H. Peng. (1982) **Tracers in the Sea.** ELDIGIO press. Lamont Doherty Geo. Observatory. Palisades, N.Y. 690 pp.

Brtko, W.J. and R.L. Kabel. (1978) Transfer of gases at natural air-water interfaces. *J. Phys. Oceanogr.* **8**: 543-556.

Chung, Y.C. (1973) Excess radon in the Santa Barbara basin. *Earth Planet. Sci. Lett.* **17**: 319.

Chung, Y.C. (1980) Radium-Barium-Silica correlations and a two-dimensional radium model for the world ocean. *Earth Planet. Sci. Lett.* **49**: 309-318.

Clark, I. (1979) **Practical Geostatistics.** Applied Science Publishers,

London. 129 pp.

Coachman, L.K. and R.L. Charnell. (1979) On lateral water mass interaction - A case study, Bristol Bay, Alaska. *J. Phys. Oceanogr.* 9, 2: 278-297.

Coachman, L.K. and J.J. Walsh. (1981) A diffusion model of cross shelf exchange of nutrients in the southeastern Bering Sea. *Deep-Sea Res.* **28A**: 819-846.

Coachman, L.K. (1982) Flow convergence over a broad, flat continental shelf. *Continent. Shelf Res.* 1: 1-14.

Coachman, L.K. (1985). Circulation, water masses and fluxes on the Southeastern Bering Sea shelf. *Continent. Shelf Res.* in press.

Codispoti, L.A., G.E. Friederich and D.W. Hood. (1985). Variability in the inorganic carbon system over the SE Bering Sea shelf during spring 1980 and spring-summer 1981. *Continent. Shelf Res.* in press.

Csanady, G.T. (1976) Mean circulation in shallow seas. *J. Geophys. Res.* **81**: 5389-5399.

Danckwerts, P.V. (1970) **Gas-liquid Reactions.** McGraw-Hill, New York. 276 pp.

Davis, J.C. (1973) **Statistics and Data Analysis in Geology.** John Wiley and Sons, New York. 550 pp.

Deacon, E.L. (1977) Gas transfer to and across an air-water interface. *Tellus.* **29**: 363-374.

Deacon, E.L. (1981) Sea-air gas transfer: the wind speed dependence. *Boundary-Layer Met.* **21**: 31-37.

Elsinger, R.J. and W.S. Moore. (1983) Gas exchange in the Pee Dee river based on ^{222}Rn evasion. *Geophys. Res. Lett.* 10; 6: 443-446.

Emerson, S.R., W.S. Broecker and D.W. Schindler. (1973) Gas-exchange rates in a small lake as determined by the radon method. *J. Fish. Res. Board.* 30; 10: 1475-1484.

Emerson, S.R. (1975) Gas exchange rates in small Canadian shield lakes. *Limnol. Oceanogr.* 20: 754-761.

Freeland, H.J. and W.J. Gould. (1976) Objective analysis of meso-scale ocean circulation features. *Deep Sea Res.* 23: 915-923.

Friedlander, G., J.W. Kennedy, E.S. Macias and J.M. Miller. (1981) **Nuclear and Radiochemistry.** 3rd ed. John Wiley and Sons, New York. 684 pp.

Gruebel, K.A. and C.S. Martens (1984) Radon-222 tracing of sediment-water chemical transport in an estuarine sediment. *Limnol. Oceanogr.* 29(3): 587-597.

Haflinger, K.E. (1978) A numerical analysis of the distribution of the benthic infauna of the southeastern Bering Sea Shelf. M.S. Thesis, Univ. of Alaska, Fairbanks. 136 pp.

Hammond, D.E., H.J. Simpson and G.G. Mathieu. (1975) Methane and ^{222}Rn as tracers for mechanisms of exchange across the sediment water interface in the Hudson river estuary. *In* T.M. Church (ed.). **Marine Chemistry in the Coastal Environment.** Amer. Chem. Soc. pp 119-132.

Hammond, D.E., H.J. Simpson and G.G. Mathieu. (1977) Radon-222 distribution and transport across the sediment-water interface in

the Hudson river estuary. *J. Geophys. Res.* 82, 27: 3945-3920.

Hammond, D.E. and C. Fuller. (1979) The use of radon-222 to estimate benthic exchange and atmospheric exchange rates in San Francisco Bay. *In* T.J. Conomas (ed.). San Francisco Bay: the urbanized estuary. AAAS, San Francisco, Calif. pp 213-230.

Hartman, B. and D.E. Hammond. (1984) Sas exchange rates across the sediment-water and air-water interfaces in south San Francisco Bay. *J. Geophys. Res.* 89; C3: 3593-3603.

Hasse, L. and P.S. Liss. (1980) Gas exchange across the air-sea interface. *Tellus.* 32: 470-481.

Holmén, K. and P.S. Liss. (1984) Models for air-water gas transfer: an experimental investigation. *Tellus.* 36B: 92-100.

Huson, L.W. (1984) Definition and properties of a coefficient of sensitivity for mathematical models. *Ecol. Modeling.* 21: 149-159.

Imboden, D.M. and S. Emerson. (1978) Natural radon and phosphorus as limnological tracers: Horizontal and vertical eddy diffusion in Greifensee. *Limnol. Oceanogr.* 23, 1: 77-90.

Imboden, D.M. and M. Stiller. (1982) The influence of radon diffusion on the 210-Pb distribution in sediments. *J. Geophys. Res.* 87; C1: 557-565.

Imboden, D.M. and Th. Joller. (1984) Turbulent mixing in the hypolimnion of Baldeggersee (Switzerland) traced by natural radon-222. *Limnol. Oceanogr.* 29; 4: 831-844.

Iverson, R.L., L.K. Coachman, R.T. Cooney, T.S. English, J.J. Goering, G.L. Hunt Jr., M.C. Macauley, C.P. McRoy, W.S. Reeburgh and T.E.

Whitledge. (1979) Ecological significance of fronts in the southeastern Bering Sea. *In* R.J. Livingston (ed). **Ecological Processes in Coastal and Marine Systems.** Plenum Publishing Corp. New York. pp 437-466.

Joyce, T.M. (1977) A note on the lateral mixing of water masses. *J. Phys. Oceanogr.* 7: 626-629.

Kanwisher, J. (1963) On the exchange of gases between the atmoshere and the sea. *Deep-Sea Res.* 10: 195-207.

Key, R.M., N.L. Guinasso Jr. and D.R. Schink. (1979a) Emanation of radon-222 from marine sediments. *Mar. Chem.* 7: 221-250.

Key, R.M., R.L. Brewer, J.H. Stockwell, N.L. Guinasso Jr. and D.R. Schink. (1979b) Some improved techniques for measuring radon and radium in marine sediments and in seawater. *Mar. Chem.* 7:251-264.

Kinder, T.H. and J.D. Schumacher. (1981) Hydrographic structure over the continental shelf of the southeastern Bering Sea. *In* D.W. Hood and J.A. Calder (eds). **The Eastern Bering Sea Shelf: Oceanography and Resources,** vol 1. University of Washington Press, Seattle, Washington. pp 31-52.

Kipphut, G.W. (1978) An Investigation of Sedimentary Processes in Lakes. Ph.D. Thesis. Columbia University, New York. 180 pp.

Kipphut, G.W. and C.S. Martens. (1982) Biogeochemical cycling in an organic-rich coastal marine basin - 3. Dissolved gas transport in methane-saturated sediments. *Geochim. Cosmochim. Acta.* 46: 2049-2060.

Ku, T-L. and M-C. Lin. (1976) ^{224}Ra distribution in the Antarctic

ocean. *Earth Planet. Sci. Lett.* **32**: 236-248.

Ku, T-L., C-A. Huh and P-S. Chen. (1980) Meridional distribution of ^{226}Ra in the eastern Pacific along Geosecs cruise tracks. *Earth Planet. Sci. Lett.* **49**: 293-308.

Lietzke, T.A. and A. Lerman. (1975) Effects of bottom relief in two-dimensional oceanic eddy diffusion models. *Earth Planet. Sci. Lett.* **24**: 337-344.

Liss, P.S. (1973) Processes of gas exchange across an air-water interface. *Deep-Sea Res.* **20**: 221-238.

Liss, P.S. (1983) Gas transfer: experiments and geochemical implications. *In* P.S. Liss and W.G.N. Slinn (eds.). **Air-Sea Exchange of Gases and Particles.** NATO ASI series #108. D. Reidel, Dordrecht, Holland. pp. 241-298.

Mathieu, G.G. (1977) Radon-222/radium-226 technique of analysis. *Appendix I in Annual Report to ERDA.* **Transport and Transfer Rates in the Waters of the Continental Shelf.** Contract EY76-5-02-2185. 30 pp.

Moore, W.S. (1976) Sampling ^{228}Ra in the deep ocean. *Deep-Sea Res.* **23**: 647-651.

Olea, R.A. (1974) Optimal contour mapping using universal kriging. *J. Geophys. Res.* **79**; 5: 695-702.

Peng, T-H., T. Takahashi and W.S. Broecker. (1974) Surface radon measurements in the north Pacific ocean station Papa. *J. Geophys. Res.* **79**, 12: 1772-1780.

Peng, T-H., W.S. Broecker, G.G. Mathieu, Y-H. Li and A.E. Bainbridge.

(1979) Radon evasion rates in the Atlantic and Pacific oceans as determined during the Seosecs program. *J. Geophys. Res.* **84, C5:** 2471-2486.

Reeburgh, W.S. and T.E. Whitledge. (1981) Nutrient dynamics and distribution in the southeast Bering Sea. Component 2a: PROBES Progress Report 1981, vol 1. pp 95-128.

Riedl, R.J., N. Huang and R. Machan. (1972) The sub-tidal pump: a mechanism of interstitial water exchange by wave action. *Mar. Biol.* **13:** 210-221.

Sambrotto, R.N., H.J. Niebauer, J.J. Goering and R.L. Iverson. (1985). Relationships among vertical mixing, nitrate uptake and growth during the spring bloom in the southeastern Bering Sea middle shelf. *Continent. Shelf Res.* in press.

Sampson, R.J. (1978) **Surface II Graphics System.** Research Associate, Computer Services Section, Kansas Geological Survey, Lawrence, Kansas. 240 pp.

Sarmiento, J.L., D.E. Hammond and W.S. Broecker. (1976) The calculation of the statistical counting error for ^{222}Rn scintillation counting. *Earth Planet. Sci. Lett.* **32:** 351-356.

Sarmiento, J.L. and C.H. Rooth. (1980) A comparison of vertical and isopycnal mixing models in the deep sea based on radon-222 measurements. *J. Geophys. Res.* **85:** 1515-1518.

Sarmiento, J.L., J. Willebrand and S. Hellerman. (1982) Objective analysis of Tritium observations in the Atlantic Ocean during 1971-74. **Ocean Tracers Laboratory Technical Report #1.** Princeton

University. 19 pp.

Schumacher, J.D. and T.H. Kinder. (1983) Low frequency current regimes over the Bering Sea shelf. *J. Phys. Oceanogr.* **13:** 607-623.

Sharma, G.D. (1979) **The Alaskan Shelf: Hydrography, Sedimentary and Geochemical Environment.** Springer-Verlag, New York. 498 pp.

Smethie, W.M. Jr. (1979) An Investigation of Vertical Mixing Rates in Fjords using Naturally Occurring Radon-222 and Salinity as Tracers. Ph.D. Thesis. University of Washington. 248 pp.

Smethie, W.M. Jr. (1981) Vertical mixing rates in fjords determined using radon and salinity as tracers. *Est. Coastal and Shelf Sci.* **12:** 131-153.

Smethie, W.M. Jr., C.A. Nittrouer and R.F.L. Self. (1981) The use of radon-222 as a tracer of sediment irrigation and mixing on the Washington continental shelf. *Mar. Geol.* **42:** 173-200.

Smethie, W.M. Jr., T. Takahashi, D.W. Chipman and J.R. Ledwell. (1985) Gas exchange and CO_2 flux in the tropical Atlantic Ocean determined from ^{222}Rn and pCO_2 measurements. *J. Geophys. Res.* **90;** C4: 7005-7022.

Torgersen, T.G., G. Mathieu, R.H. Hesslein and W.S. Broecker. (1982) Gas exchange dependency on diffusion coefficient: direct 222-Rn and 3-He comparisons in a small lake. *J. Geophys. Res.* **87;** C1: 546-556.

Wanninkhof, R., J.R. Ledwell and W.S. Broecker. (1985) Gas exchange - wind speed relation measured with sulfur hexafluoride on a lake. *Science.* **227;** 4691: 1224-1226.

York, D. (1966) Least-squares fitting of straight lines. *Can. J. Phys.* **44**: 1079-1086.